1. INTRODUCTION

1.1 Thesis rationale

Iron oxide-copper-gold (IOCG) deposits are important sources of copper and gold in Australia with the Olympic Dam, Ernest Henry, Osborne (formerly Trough Tank (Davidson, 1989)) and Selwyn mines all being significant producers. Since the 1975 discovery of the Olympic Dam deposit in South Australia there has been extensive and continued exploration for similar deposits (Porter, 2000). The IOCG class encompasses a wide range of deposits which typically have abundant iron oxides, magnetite and/or hematite, with a characteristic Cu, Au and REE suite of associated elements. The iron oxides, primarily magnetite and hematite, are typically depleted in Ti compared with other types of iron oxide deposits (Hitzman et al., 1992).

Initially these deposits were recognised in Proterozoic terranes (Hitzman et al., 1992), however it has also been asserted that there are large deposits and districts of Phanerozoic age (Barton and Johnson, 1996). Extensive sodic alteration is characteristically present in most districts and is thought to predate mineralisation (e.g. Pollard, 2001).

While the deposits around the world share many of these characteristics there is also considerable variation between deposits, even within a single region such as the Cloncurry District in the Eastern Fold Belt of the Mount Isa Inlier in northwest Queensland (Williams and Skirrow, 2000; Williams et al., 2005). Deposits may occur as veins or breccias or massive bodies although much of the observed variation in

morphology appears to be contributable to local wall rock and structural controls (Hitzman et al., 1992; Adshead-Bell, 1998; Baker and Laing, 1998; Mark et al., 2001).

The origin of IOCG deposits is contentious and three different models have been proposed for the source of the hydrothermal fluids and their acquisition of salinity (Fig. 1.1; Williams, 1994; De Jong et al., 1998; Haynes, 2000; Hitzman, 2000; Barton and Johnson, 2004; Pollard, 2006). One model suggests the dissolution of evaporites by meteoric waters circulating to depth around an intrusion with cooling, wall-rock reactions and fluid mixing proposed as causes of mineral precipitation. A second fluid may have transported the Cu and other metals (Barton and Johnson, 1996; Haynes, 2000). A second hypothesis proposes the involvement of metamorphic fluids derived from devolatilisation reactions with the precipitation mechanisms the same as in the first model. A third model invokes an origin by the exsolution of S-poor metal bearing saline fluids from granitic intrusions (Perring et al., 2000; Pollard, 2000; Mark et al, 2004; Pollard, 2006).

While some researchers look for a single genetic mechanism for all deposits, others believe that different processes operated in different terrains (Barton and Johnson, 2000; Haynes, 2000; Barton and Johnson, 2004). The Eastern Fold Belt of the Mt Isa Inlier in northwest Queensland is one of the world's premier IOCG provinces, with well-exposed and well-described geology and a diverse group of IOCG deposits, and as such provides a good natural laboratory although the deposits do not reflect the entire variety of the IOCG class. Previous researchers have suggested that all the IOCG occurrences in the district are the result of a single ore forming process, with the

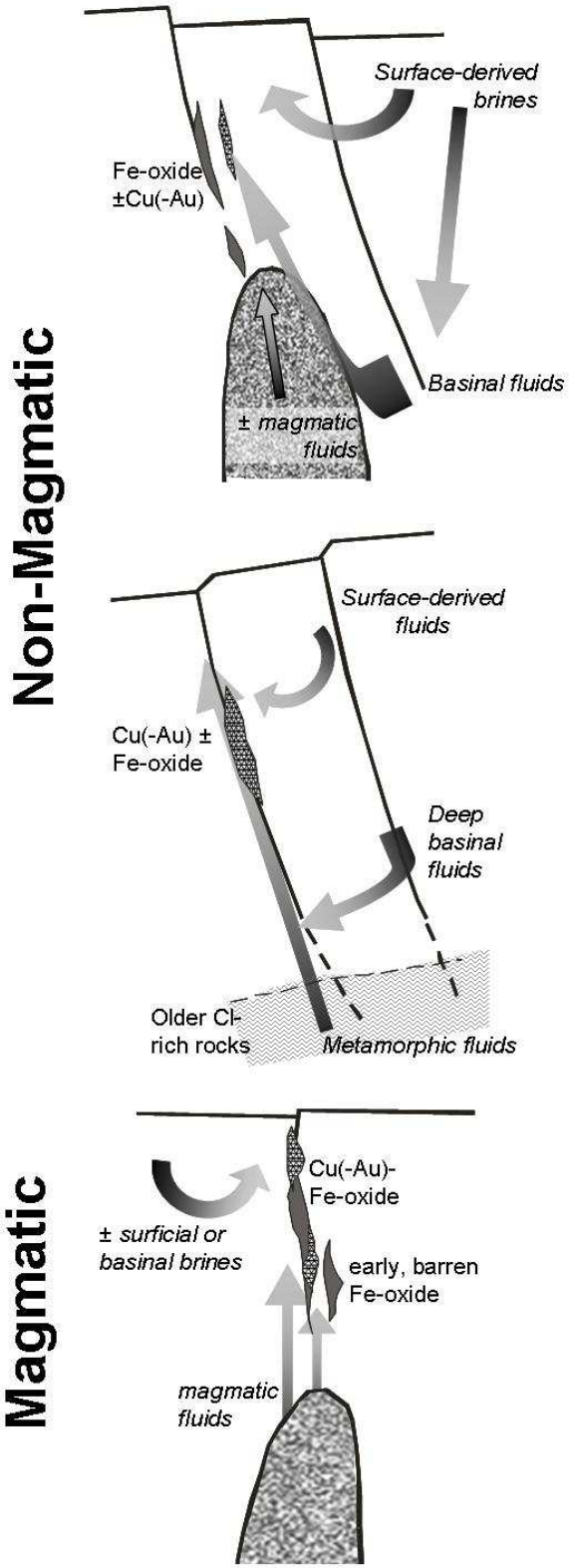

Surface or basin-derived

- Non-magmatic brines
- Thermal convection, most commonly driven by igneous body
- Wall-rock reactions may be source of metals or may be supplied by a second fluid

Metamorphic-derived

- Metamorphic fluids derived from the devolatisation of Cl-rich source rocks
- No necessary association with igneous intrusions but could provide a heat source

Magma-derived

- Fluids derived by exsolution from crystallising magma bodies
- Magmas are high-K, oxidised suites with dioritic to granitic compositions
- Barren Fe-oxides may form in older hydrothermal systems in the same districts.

Figure. 1.1: Schematic diagrams illustrating the three models for the origin of fluids in IOCG ore formation: (1) Surface/basin derived fluids; (2) Metamorphic devolatisation fluids; (3) Magmatic exsolution, after Barton and Johnson (2004).

mineralisation precipitated from fluids exsolved from magmatic intrusions (Lindblom et al., 1996; Pollard, 2006). However, radiometric dating of the Osborne deposit, off the southern tip of the Mount Isa Inlier, suggests ore formation took place more than 50 Ma before the deposition of other major deposits, such as Ernest Henry, in the region and prior to the emplacement of the large granitic batholiths that are usually favoured as a source of ore fluids. The Osborne deposit may therefore have formed by a different process (Gauthier et al., 2001).

The lack of understanding of the genetic processes involved in the formation of IOCG deposits is an impediment to successful exploration. By studying the composition of the ore forming fluids at IOCG deposits the source of the metals and fluids can be determined, defining critical ingredients that can contribute to a terrain scale exploration tool. The Osborne deposit (with proven reserves of 15.2Mt at 3.0% Cu and 1.05 g/t Au (Tullemans et al., 2001)) is one of several mined ore bodies that make the Cloncurry district a significant IOCG province. The source of the ore fluids and timing of formation of the Osborne deposit has been extensively debated (Davidson et al., 1989; Adshead et al., 1998; Gauthier et al., 2001; Rubenach et al., 2001).

The aim of the research presented in this thesis is to contribute to the understanding of fluid events and sources and particularly the role of saline fluids in IOCG deposits and systems through the determination of fluid compositions at the Osborne IOCG deposit in the Cloncurry district of the Eastern Fold Belt. Over the last decade technological improvements have led to the development of microanalytical techniques that allow metals and other elements in ore fluids to be measured at parts per million level or better. Laser ablation inductively coupled mass spectrometry (LA-ICP-MS),

synchrotron-based XRF, proton induced x-ray emission (PIXE) and proton induced gamma emission (PIGE) are all increasingly used to analyse the metal contents of individual fluid inclusions, permitting identification in ore forming systems of the hydrothermal fluid generations that transported and precipitated ore metals. While microanalytical studies of fluid inclusions are increasingly reported they typically utilise only one technique. This study is unique in presenting multiple microanalytical data sets from combined noble gas and halogen analysis, PIXE and LA-ICP-MS studies of fluid inclusions from the same set of samples to produce an integrated model of ore fluid compositions and sources and the evolution of the hydrothermal system at the Osborne IOCG deposit. The use of several analytical techniques on a single set of samples also allows quantification and comparison of analytical artefacts associated with each method.

1.2 Thesis aims

The aims of this study are to provide insight into the origin and nature of the ore forming fluids at Osborne; distinguishing between magmatic, metamorphic and crustal fluid and ligand sources and by doing this defining some of the critical ingredients for IOCG formation as well as identifying metal transport and deposition mechanisms. The study was conducted using laser ablation inductively plasma mass spectrometry, proton induced X-ray emission and combined noble gas and halogen analysis allowing for a comparison of different bulk and micro-analytical methods used in the study of ore forming fluids within fluid inclusions.

1.3 Thesis structure

In Chapter 1 the rationale for the thesis is discussed and the aims and objectives

enumerated. There is a review of the literature pertinent to the study with overviews of IOCG deposits; the regional and local geology of the Osborne deposit; previous fluid inclusion studies and analytical techniques and IOCG fluid studies in the Cloncurry district. The results (chapters 2, 3 and 4) have been written as extended papers. However, to eliminate repetition in introductory sections the relevant information is summarised in the literature review (Section 1.4). Additional descriptions of the analytical methods have been added to each chapter.

In Chapter 2 samples from the Osborne deposit are examined and their ore textures described. A petrographic study of selected samples identifies multiple populations of fluid inclusions and their inter-relationships; further paragenetic constraints are gained using cathodoluminscence studies of the host quartz. Microthermometric results are reported and interpreted giving an overview of the salinity of the fluids and compositions are extrapolated with the main salt systems identified. A Laser Raman spectrometric study of gaseous phases highlights differences between carbonic fluids in different ore environments within the deposit. The fluid inclusion study demonstrates that the mineralised sequence at the Osborne preserves a fluid inclusion assemblage documenting a protracted history of hydrothermal events that encompasses peak metamorphism, anatectic pegmatite intrusion and mineralization and alteration.

In Chapter 3, the source of the ore fluids is further examined using combined noble gas and halogen analysis; a semi-selective bulk analytical technique. Simultaneous measurement of noble gas isotopic composition and elemental halogen ratios are used to identify fluid and ligand sources and, thus, to provide information on the origin of the

fluids and their salinity at the Osborne IOCG deposit. The samples studied overlap with those examined in chapter 4 using PIXE and LA-ICP-MS.

In Chapter 4, the composition of the ore fluids is studied in further detail using two microanalytical techniques: LA-ICP-MS and PIXE. These two methods provide complimentary information on fluid chemistry from which an average ore fluid composition is derived. Element ratios provide information on fluid-rock reactions and on fluid sources. PIXE analyses are from a large number of inclusions in samples representing 3 separate ore lenses and associated pegmatites from the Osborne mine. Fluid inclusions from the same set of samples were additionally analysed using LA-ICP-MS. This unique data set not only provides insight into the composition and origin of the ore forming fluids but also permits direct comparison of microanalytical techniques that are becoming increasingly widely used in the study of fluid inclusions.

In Chapter 5 the accumulated data are combined and incorporated into geochemical models of the ore forming processes. An overall model for ore genesis at the Osborne deposit is described.

1.4 Literature Review

1.4.1 Origin of IOCG deposits

Since the diverse class of Cu-Au- and REE-bearing iron oxide deposits was first proposed (Hitzman et al., 1992) there has been contention over the genesis of these deposits with both the origin of the ore-forming fluids and precipitation mechanisms debated. Many researchers have contended that the IOCG ore forming fluids were exsolved from granitic intrusions and in many districts, including the Eastern Fold Belt,

a temporal and spatial association is observed between granites and IOCG deposits (Hitzman et al., 1992; Wang and Williams, 2001; Pollard, 2006). Studies of the hydrothermal magnetite-hosting Lightning Creek sodic aplite sills associated with the mildly alkalic, K-rich, metaluminous Squirrel Hills Batholith in the Cloncurry district have found they show evidence that Fe- and Cu-rich fluids were produced during crystallisation (Pollard et al., 1998; Perring et al., 2000; Pollard, 2000). Intrusive rocks associated with porphyry Cu-Au mineralisation have dioritic to monzogranitic compositions and the ore-hosting porphyry stocks are calc-alkaline, K-rich calc-alkaline and shoshonites (Sillitoe, 1997). The similarity of the igneous intrusions in IOCG provinces and those associated with Cu-Au porphyry ore deposits has led to speculation that IOCG deposits are part of a spectrum of Cu-Au deposits, the expression of which is dependent on crustal depths and tectonic settings (Pollard, 2000). Smith and Gleeson (2005) used chlorine isotopes and halogen chemistry to examine whether fluid chemistry supported a genetic link between Kiruna-type iron oxide-apatite deposits and IOCG deposits in the Norbotten province of Sweden. Cl/Br ratios in both deposit types were consistent with a magmatic origin for fluids.

However, an alternative hypothesis argues that while some IOCG ore bodies show evidence of igneous derived fluids there are a second group of deposits within the IOCG class which are typified by more oxide-rich, sulphide poor mineralisation and dominantly sodic alteration (Barton and Johnson, 2000). Barton and Johnson, (1996) argue these deposits are the product of hydrothermal processes involving evaporitic ligand sources. This assertion is supported by the lack of correlation in these cases between the composition of mineralisation and alteration and that of intrusive phases.

There is also a spatial association between belts of palaeo-aridity and many of the deposits.

In many types of ore deposits and hydrothermal systems, fluids from varied sources including igneous, metamorphic, sedimentary and meteoric have been found to be significant (Barton and Johnson, 2000). Studies have shown that surface waters can penetrate up to 10km into the crust, particularly in the presence of a flow driver such as an intrusion (e.g. Gleeson et al., 2003).

It has been suggested that more than one fluid may have been active in IOCG systems and that fluid mixing may have triggered mineral precipitation (Haynes et al., 1995). In other cases it has been proposed that the unmixing of a carbon dioxide bearing brine was part of the ore-forming process (Adshead, 1995; Fu et al., 2003). A study of fluid inclusion and stable isotopic data from the Olympic Dam deposit led Oreskes and Einuadi (1992) to argue that while primary magmatic fluids may have precipitated early magnetite, the mineralised hematite rich breccias are the result of an influx of surface derived fluids. The south east Missouri district is host to a number of iron oxide-bearing deposits including the Boss-Bixby IOCG deposit (Seeger, 2000; Day et al., 2001). Studies of non-mineralised iron oxide, silica-rich ore bodies in the same district have concluded they precipitated from saline magmatic-hydrothermal fluids which subsequently boiled, explosively emplacing rare earth element bearing breccias (Nuelle et al., 1992; Sidder et al., 1993). A $\delta^{37}Cl$, $^{87}Sr/^{86}Sr$ and halogen study of a number of IOCG-type deposits in South America, including a magnetite-apatite deposit (El Romeral), found a spectrum of ore fluid origins (Chiaradia et al., 2006). A magmatic hydrothermal fluid that leached evaporites was implicated in the formation of the

Gameleira and El Romeral deposits while mixing between a magmatic fluid and basinal brines was indicated at the Candelaria, Raúl-Condestable and Sossego deposits.

1.4.2 Regional geology

The metamorphosed sedimentary and igneous sequences of the Mount Isa Inlier (Fig. 1.2; 1.3) provide a record of two Palaeoproterozoic and Palaeo-Mesoproterozoic tectonostratigraphic cycles (Etheridge et al., 1987). A Palaeoproterozoic crystalline basement, metamorphosed during the Barramundi Orogeny (ca. 1900-1870 Ma) is unconformably overlain by Palaeoproterozoic and Mesoproterozoic sedimentary and igneous rocks deposited during a prolonged period of intermittent extension between ca. 1800 and 1595 in three stacked basins (Fig. 1.4); the Leichardt, Calvert and Isa Superbasins (Etheridge et al., 1987; O'Dea et al., 1997; Page and Sun, 1998; Jackson et al., 2000).

In the Cloncurry district the metasedimentary and metavolcanic supracrustal cover sequences are estimated to be greater than 25km thick (Blake et al., 1990). The Leichardt Basin (ca. 1790-1730 Ma) was characterised by widespread bimodal magmatism and subsequent clastic fluvial sedimentation with episodic marine incursions (Derrick, 1980; O'Dea et al., 1997). In the Eastern Fold Belt it is represented by the Argylla formation; a synextensional basal felsic volcanic suite interbedded with sandstone and siltstone (Derrick, 1980) which is conformably overlain by the Marraba volcanics and the Mitakoodi Quartzite (Potma and Betts, 2006). The Mitakoodi Quartzites are overlain by the post-rift chemical and carbonate successions of the Overhang Jaspilite, Doherty Formation and the Corella Formation. On the eastern flank

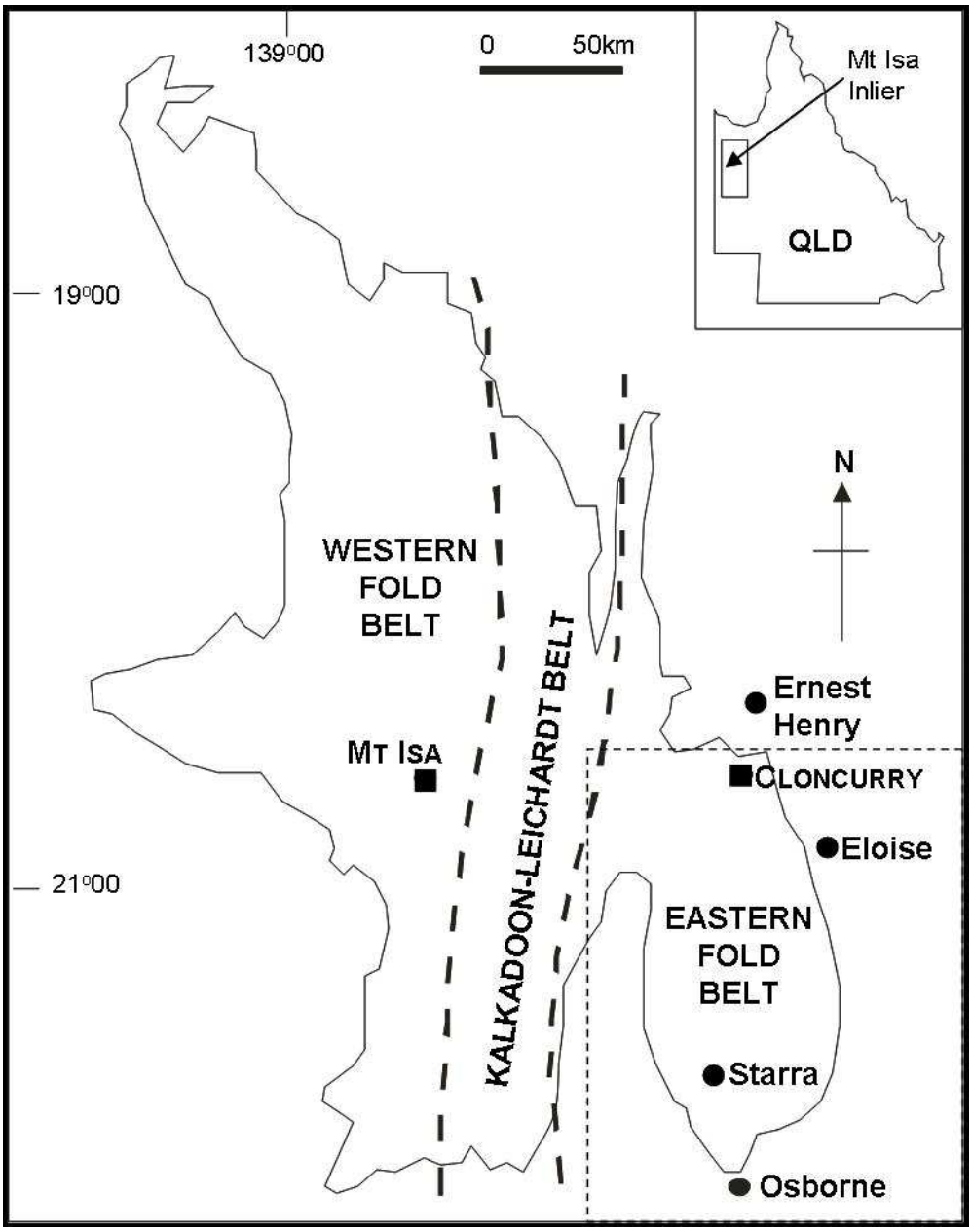

Figure 1.2: Mount Isa Inlier location map. The dashed box denotes the boundaries of the area covered by Fig. 1.3. ■ = towns, ● = IOCG deposits.

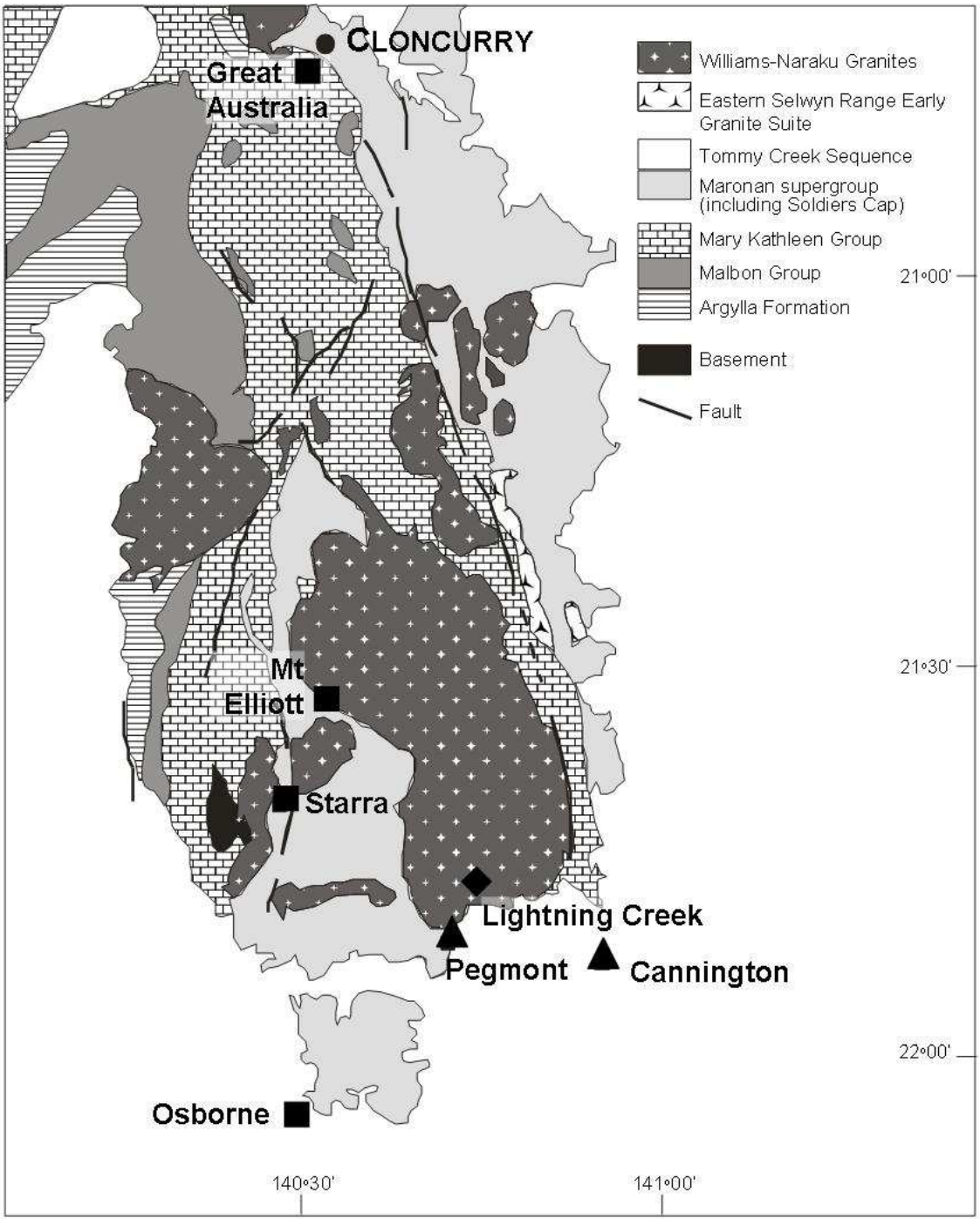

Figure 1.3: Simplified geological map of southern part of the Eastern Fold Belt of the Mt Isa Inlier, showing the location of major IOCG deposits, other base-metal deposits and granitic bodies, (modified after Williams, 1998). Major deposits within the district include ■ IOCG-type, e.g. Great Australia – supergene resource of 1.7 Mt @ 1.2% Cu and undefined hypogene orebody; Cannell and Davidson, (1998); Mt Elliott - 2.9 Mt @ 3.33% Cu, 1.47 g/t Au; Fortowski and McCracken, (1998); Ernest Henry - 167Mt @ 1.1% Cu and 0.55 g/t Au; Ryan, (1998); Starra - 7.4 Mt @ 1.88% Cu and 3.8 g/t Au; Rotherham, (1997a); Osborne - 15.2Mt @ 3.0% Cu and 1.05g/t Au; Tullemans et al., (2001); ▲Pb-Zn-Ag deposits, e.g. Cannington – 43.8 Mt @ 11.6% Pb, 4.4% Zn and 538 g/t Ag; Bailey, (1998); Pegmont – 11 Mt @ 8.4% Pb, 3.7% Zn and 11.5 g/t Ag; Williams et al., (1998) and ♦ the iron-oxide only Lightning Creek prospect.

of the Cloncurry district the Soldiers Cap Group is bounded to the west by the Cloncurry Fault and the Corella Formation of the Mary Kathleen Group.

The Corella Formation consists of thin-bedded calcareous, dolomitic, pelitic and quartzo-feldspathic metasedimentary rocks. It has been interpreted as having been deposited in a near-shore, evaporitic carbonate shelf environment and contains extensive meta-evaporite horizons with halite casts observed at a few localities in the Selwyn region (Derrick et al., 1977; Blake, 1982). While some researchers have considered the Doherty Formation to be a distinct unit, Williams and Phillips (1992) interpreted it as extensively metasomatised portion of the Corella Formation.

In the Calvert Basin (ca. 1730-1670 Ma) the earliest stages of sedimentation in the Eastern Fold Belt are marked by rift-related turbidite and quartzite successions and basalt and dolerite of the Kuridala and Llewellyn Creek Formations and the Mt Norna Quartzite. The latter two units form part of the Soldiers Cap Group, the upper parts of which extend into the Isa Basin (ca. 1670-1590 Ma) and contain the 1654 ± 4 Ma Mt Norna Quartzite (Page and Sun, 1998). The Soldiers Cap Group, a sequence of metamorphosed clastic rocks, amphibolites and banded iron formations, hosts the Osborne deposit and some of the other IOCG deposits in the district.

The basinal sequences were deformed during the prolonged and multi-phase (Table 1.1) Isan orogeny (ca. 1600 – 1500 Ma). In the Eastern Fold Belt the first stages of orogenesis are characterised by N-S or NNW-SSE shortening and N-NW directed thrusting in a thin-skinned tectonic environment (Betts et al., 2006; Betts and Giles,

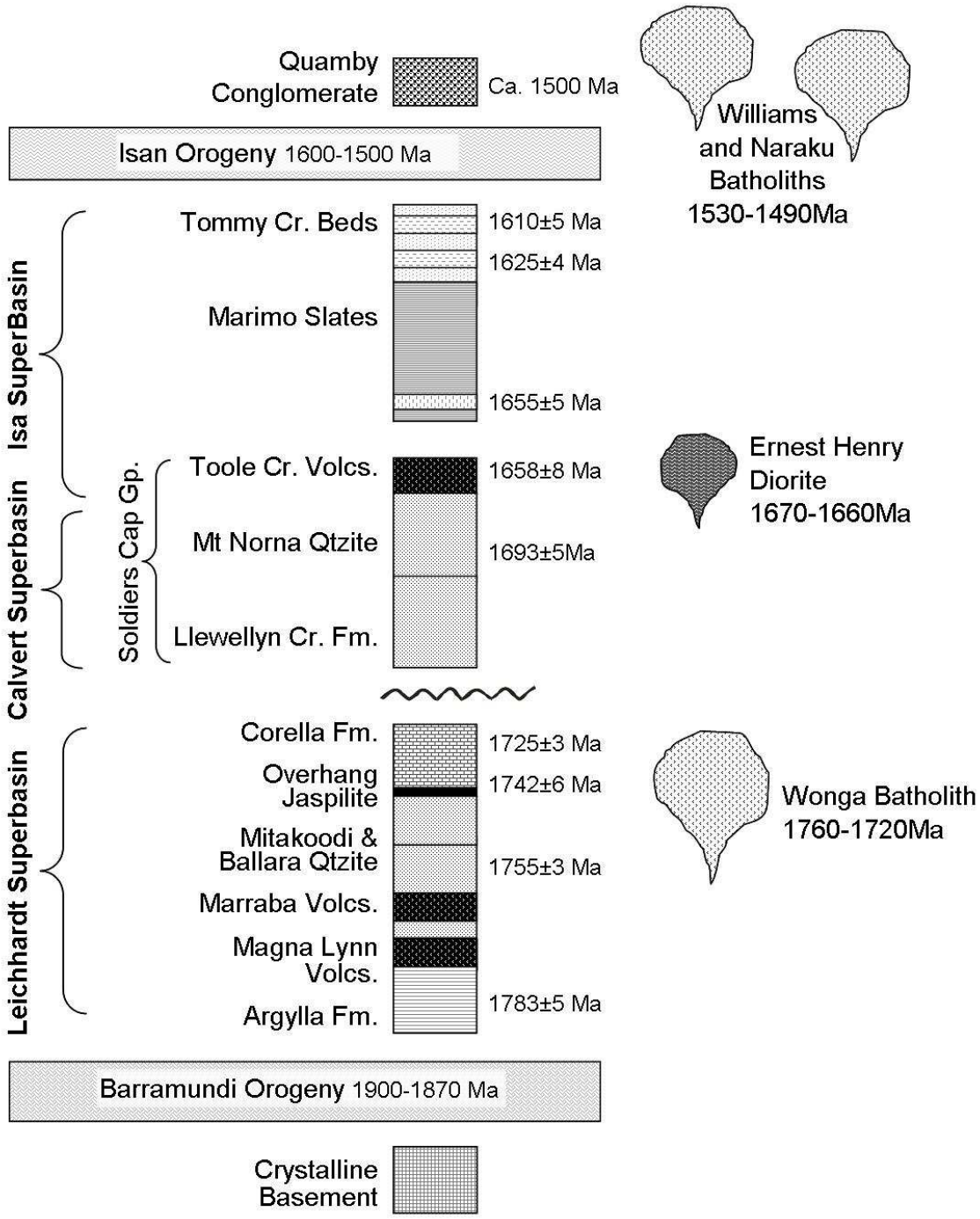

Figure 1.4: Stratigraphic and geochronological framework of the Mt Isa Eastern Fold Belt (modified after McLaren and Sandiford, 2001 and O'Dea et al., 2006, with ages from Pollard and McNaughton, 1997; Page and Sun, 1998; Idnurm and Wyborn, 1998).

2006). A second phase of deformation occurring from 1550 to 1500 Ma, involved thick-skinned east-west crustal shortening (Page and Sun, 1998; Betts et al., 2006; Betts and Giles, 2006). Peak metamorphism is thought to have been associated with the earlier phase of deformation (Foster and Rubenach, 2006) and peak metamorphic assemblages have been dated to between 1600-1580 Ma (Page and Sun, 1998; Giles and Nutman, 2002; 2003; Hand and Rubatto, 2002; Foster and Rubenach, 2006).

Regional		**Osborne**
Event	**Structure and Metamorphism**	**Geological Expression**
Pre D1	Albitisation	Dating of early albitisation suggests prolonged metasomatism between 1680-1640 Ma (Rubenach, in press)
D1 N-S shortening	Prograde metamorphism – large F1 folds	Prograde metamorphism to upper greenschist facies, early metasomatism and albitisation. 1640-1600 Ma
D2 E-W shortening	Peak metamorphism, F2 folding with N-S striking axial planes	Peak metamorphism, reaching amphibolite facies, albitisation (Page and Sun, 1998; Gauthier et al., 2001), pegmatite anatexis (e.g. Mark et al., 1998), silica flooding, Cu-Au deposition (Gauthier et al., 2001). 1595 ± 5 Ma
D3	Retrograde metamorphism, upright F3 folds and crenulations	Retrograde metamorphism in greenschist assemblages.
Post D3	Reactivation of D2/D3 faults	
D4	Gentle folding of F3 fold axes producing upright, W-plunging folds	Late carbonate veining and pyrite vein brecciation (Adshead, 1995).

Table 1.1: Regional and local Osborne deformation and geological history. (The regional structural data are taken from Beardsmore et al., 1988 and Laing, 1996)

Metamorphic grade varies from upper greenschist to amphibolite facies across the Eastern Fold Belt and increases to the southeast where partial melting of the host metasedimentary rocks near Osborne occurred (Mark et al., 1998; Rubenach et al., 2001; Foster and Rubenach, 2006). U-Pb dating of titanites at Osborne identifying the timing of migmatite formation suggest local peak metamorphic conditions were attained at 1595 ± 5 Ma (Gauthier et al., 2001), a finding which is supported by monazite and metamorphic zircon analyses at the nearby Cannington Pb-Zn deposit which record a 1585 ± 5 Ma thermal event (Giles and Nutman, 2002; 2003).

Predominately potassium rich, 'A-type' granitoids were intruded during the later phases of the Isan Orogeny (ca. 1550-1490) forming the regionally extensive Williams and Naraku Batholiths (Fig 1.3; Pollard et al., 1998; Wyborn, 1998). Many of the IOCG deposits in the Eastern Fold Belt, including Ernest Henry and Eloise, have been dated as forming at the same time as the emplacement of the Williams and Naraku batholiths (Perkins and Wyborn, 1998; Pollard et al., 1998; Mark et al., 2006). This, however, is not necessarily the case at Osborne, where mineralisation has been suggested to predate granitoid emplacement (Gauthier et al., 2001).

Regionally extensive sodic and sodic-calcic alteration is found across the Eastern Fold Belt and represents the preserved remnants of massive hydrothermal systems (De Jong and Williams, 1995; Oliver et al., 2004; Mark et al., 2006). Intense sodic alteration is a common feature of many IOCG systems (Hitzman et al., 1992; Barton and Johnson, 1996; Pollard, 2001) and is recognised at deposit scale (Rotherham, 1997a; Adshead et al., 1998). The majority of albitisation in the Eastern Fold Belt is thought to have developed synchronously with the emplacement of the Williams and Naraku Batholiths

(Oliver et al., 2004; Mark et al., 2006) although zones of albitisation around the Osborne deposit have been dated to ca. 1595 ± 5 Ma (Adshead, 1995; Perkins and Wyborn, 1998; Gauthier et al., 2001) and 1630-1650 Ma (Rubenach et al., in press). The earliest albitisation is considered to have formed concurrent with the D1 regional metamorphism that formed E-W foliation, while the 1595 Ma albitisation formed during the D2 event (N-S folding) during which, peak metamorphic conditions were reached (Rubenach et al., in press).

1.4.3 Cloncurry IOCG deposits

The Cloncurry district contains numerous base metal and precious metal deposits and prospects including Cannington (43Mt @ 11.6% Pb, 4.4% Zn and 538 g/t Ag), Ernest Henry (167Mt @ 1.1% Cu, 0.58 g/t Au), Eloise (3.2Mt @ 5.8% Cu; 1.5 g/t Au); Mount Dore (26Mt @ 1.1% Cu, 5.5g/t Ag); Osborne (15.2 Mt @ 3.0% Cu and 1.1 g/t Au) and Starra (7.6Mt @ 1.65% Cu, 4.8 g/t Au), and the region has been widely studied (e.g. Beardsmore, 1992; Rotherham, 1997a; Adshead et al., 1998; Bailey, 1998; Baker, 1998; Williams, 1998; Williams et al, 1998; Perring et al., 2000; Williams and Skirrow, 2000; Mark et al., 2006). The deposits share a number of characteristics including (1) a shear zone or fault structural control on mineralisation; (2) early regional albitisation; (3) high temperature K-Fe-(Ca-Mg) pre- to syn-mineralisation alteration mineral assemblages; (4) hypersaline brine and carbonic fluid inclusion assemblages; (5) ore emplacement at depths exceeding 5km (Williams and Skirrow, 2000). However, while the deposits share these basic characteristics considerable variation is observed between deposits, particularly in size, grade, Cu:Au ratios; host rock age, lithology and metamorphic grade.

The majority of IOCG deposits in the Cloncurry district are temporally, and in some cases spatially, associated with I-type granitic intrusions (Rotherham, 1997a; Pollard et al., 1998; Wang and Williams, 2001) however a direct genetic link has not been proven.

1.4.4 The Osborne deposit

The Osborne iron oxide-copper-gold deposit is situated 130km south of Cloncurry in northwest Queensland and has proven reserves of 15.2Mt at 3% Cu and 1.05g/t Au (Tullemans et al., 2001). The ore bodies are hosted within a dominantly metasedimentary sequence believed to be equivalent to the Soldiers Cap Group.

The source of the ore fluids and timing of formation of the Osborne deposit has been debated (Davidson et al., 1989; Adshead et al., 1998; Gauthier et al., 2001; Rubenach et al., 2001; this study). The origin of both the ore-forming fluids and precipitation mechanisms is uncertain in many IOCG deposits and several models have been proposed for the genesis of the Osborne deposit. Initial studies of the deposit based on textural and environmental features of the ironstones concluded that the ore bodies were syngenetic, exhalative deposits (Davidson et al., 1989; Davidson, 1992). However, these studies were based on examination of weakly mineralised ironstones from early drilling, before it was recognised that the high grade ore is hosted by extensive coarse grained hydrothermal quartz, termed ‘silica flooding’ (Adshead et al., 1998).

Other researchers preferred an epigenetic model but debated the age of the deposit with Adshead et al. (1998) using ^{40}Ar-^{39}Ar data to interpret it as part of a retrograde assemblage. ^{40}Ar-^{39}Ar from actinolite hornblende and biotite in a metamorphic assemblage in the hanging wall of the ore body give dates of ca. 1595 ± 2 Ma and 1568

± 3 Ma while metasomatic hornblende and biotite associated with mineralisation give ages of 1538 ± 2 Ma (Perkins and Wyborn, 1998). Gauthier et al. (2001) used Re-Os dating of two ore-associated molybdenite samples to conclude that the deposit formed between 1600 and 1595 ± 5 Ma.

1.4.4.1 Host rocks

Metasedimentary and meta-igneous rocks are predominant in the host rock sequence at Osborne. Although no direct correlations have been made, the Osborne host rock sequence has similar rock types and metamorphic grade to parts of the Soldiers Cap Group (Beardsmore et al., 1988) with the psammitic and ironstone bearing sequence considered to resemble the Mt Norna Quartzite (Adshead et al., 1998). The main host rock types present in the Osborne sequence are:

Feldspathic psammite and pelite: Pale pink to grey, albite rich feldspathic psammites with locally developed pelite bands and migmatite. They comprise >95% albite and/or sodic oligoclase and quartz with minor biotite. Rare pelitic bands occur only more than 200 metres above banded ironstones (Adshead et al., 1998).

Banded ironstone and associated schist: Banded magnetite-quartz-apatite ironstones that are continuous for over 1.3 km along strike are a significant host rock at Osborne and occur as two stratiform units that strike north west, and dip at 25-60^{o} to the north east. The upper ironstone is 10-45 metres thick while the lower ironstone reaches thicknesses of 8-15 metres. The two ironstones are separated by 6-40 metres of feldspathic psammites. A gradational contact with

several metres of interleaved magnetite-quartz and feldspathic psammite is observed where the contacts of the ironstones with the host rock sequence are unaltered by mineralisation, whereas the upper contact of the lower ironstone is delineated by strongly foliated anthophyllite schist (Adshead et al., 1998).

Metabasic intrusions: Sheeted tholeiitic amphibolite and a discrete pod of amphibole peridotite predate the amphibolite grade metamorphism of the host rock sequence (Adshead et al., 1998). The amphibolitic peridotite body is located structurally above weakly mineralised silica flooding to the north east of the Osborne deposit and is bounded by phlogopite-rich shear zones. Relative age relationships of the tholeiitic dykes and the peridotite have not been determined but their relative geochemistry indicates they are not the product of a single magmatic episode (Adshead, 1995).

Pegmatitic intrusions: These comprise 2-3% by volume of the host rock sequence. Adshead (1995) recognised three types of pegmatitic sheets at Osborne: (i) quartz poor porphyritic syenite; (ii) non-porphyritic, biotite poor alkali feldspar granite and (iii) coarsed grained pegmatite (Adshead, 1995). All three types are dominated by sodic plagioclase, microcline and quartz. Adshead (1995) suggested they may represent fractionated portions of a single magmatic intrusion. However, Kennedy (2000) observed that all three varieties may occur in separate zones of the same intrusion.

Adshead et al., (1998), considered the pegmatite dykes to post-date the peak of metamorphism while observing cross-cutting relationships that suggest the pegamatites

were emplaced pre- and post-ore. Kennedy, (2000), interpreted their emplacement as syn-post tectonic with some being synchronous with the peak of metamorphism. Similar pegmatites at the nearby Cannington deposit, which also reached amphibolite conditions during metamorphism, are the products of anatexis during peak metamorphism (Mark et al., 1998). Large bodies of pegmatite are present in the Osborne mine, forming part of the host rock assemblage in the eastern domain. It has been shown that these pegmatites are larger equivalents of the partial melts in migmatites and they are thought to have been emplaced synchronously with foliation-development (Kennedy, 2000). Magmatic microcline rims are observed on albite within pegmatites; this is interpreted as evidence of anatectic melting of already albitised gneisses during the peak of metamorphism (Rubenach, 2005a).

1.4.4.2 Metamorphism and structure

While the host rocks at Osborne have a complex structural history limited orientated drill core and the absence of outcrop has precluded development of a detailed structural history for the deposit. Tight to isoclinal folding is observed within the banded ironstones which has been suggested to have formed during the early stages of the Isan Orogeny; D1 (1600-1630 Ma) during which an E-W foliation developed and D2 (1595 ± 5 Ma) which was a N-S compressional event (Adshead et al., 1998; Rubenach et al., in press). The earlier events were ductile in nature while the later D_3 and D_4 (1540-1520 Ma) events were characterised by the formation of brittle structures and features such as brecciation.

Rubenach et al., (in press) identified an early group of albitised samples from Osborne which have age dates between 1680-1640 Ma suggesting a major albitization event

occurred at that time. In the centre of the main albitite zones, "calc-silicate" albitites with pyroxene and grandite garnet are reported (Rubenach, 2005a). The peak of metamorphism, which is thought to have been synchronous with D_2, has been dated at 1595 ± 5 Ma – i.e. broadly syn-mineralisation (Gauthier et al., 2001). Peak assemblages in the gneisses include biotite, microcline, albite, and (in some) sillimanite. Garnet is not common. Cordierite is rare and only occurs with garnet in albitic gneisses free of microcline (Rubenach, 2005a). During peak metamorphism, upper amphibolite conditions were reached locally around Osborne (Foster and Rubenach, 2006). Geothermometic and geobarometric studies of pelite assemblages and migmatites in the Osborne host rock sequence indicate peak metamorphic conditions of 650-700 ^{o}C and ~3-7kb (Adshead, 1995). A study of the albitites refined the interpretation to 640-719 ^{o}C and 3-5kb (mean 700 ^{o}C, 4kb) using garnet-cordierite and garnet-biotite thermometers (French, 1997). A P-T-t study by Rubenach, (2005a) indicated that the anatectic melting which formed pegmatites probably would not have occurred unless albite was present.

Rubenach (2005a) interpreted the metamorphic assemblage at Osborne as evidence for an anticlockwise P-T-t path for the region based upon a positive slope for cordierite to sillimanite (Spear, 1995). However, a study of the metamorphosed sequence in the Selwyn Range, north of Osborne, proposed a clockwise P-T-t path with initial N-S shortening driving metamorphism into the kyanite stability field, followed by isothermal decompression from kyanite to andalusite via staurolite (Sayab, 2006).

1.4.4.3 Ore lodes and assemblages

The Osborne mine is subdivided into Western and Eastern Domains, based on host rock

lithology. Economic mineralisation in the Western Domain occurs along the contacts of the upper and lower ironstones with the psammitic units whereas in the Eastern Domain the ore is not associated with ironstones but is hosted by albitites and pegmatites (Fig. 1.5; 1.6; 1.7). In both domains there is an association of the ore with the massive coarse-grained quartz, termed 'silica flooding' (cf. Adshead et al., 1998). This abundant hydrothermal quartz is a feature not generally observed in IOCG deposits in the region (Rotherham, 1997a; Mark et al., 2004) or elsewhere, although there are siliceous lode rocks at Eloise which can be considered similar (Baker, 1998).

Within the Western domain ore are the 1S, 1SS, 2M and 2S ore bodies. The 2M ore body is to the north of the Western domain with the 2S ore body located south along strike; these ore bodies are associated with the upper ironstone. The 1S orebody and its southern extension, the 1SS ore body, form the largest ore body at Osborne and are located in the lower ironstone. The Eastern domain hosts the 2N and high grade 3E ore bodies. The 2N ore body is situated to the east of the Upper Ironstone while the north-south trending 3E body is located 100 to 200 metres east of the 2M and 2N bodies (Fig 1.5; 1.6; Tullemans et al., 2001).

1.4.4.4 Paragenesis

Early hydrothermal activity at Osborne resulted in pervasive albitisation (French, 1997; Adshead et al., 1998; Rubenach et al., 2001; Rubenach et al., in press). Albitised feldspathic psammites (albitites) are spatially associated with replacive vein stockworks of sulphide-poor quartz + magnetite ± biotite rocks. The presence of relict albite-rich clasts within the quartz-magnetite assemblage has been taken to indicate that albitisation pre-dates the mineralisation (French, 1997).

Quartz crystals in the silica-flooding rarely have euhedral terminations against other phases such as chalcopyrite. It is more common to find relict and altered mineral inclusions suggesting the majority of silica-flooding is formed by replacement rather than infill. Locally the coarse-grained quartz contains interstitial sulphides and minor quartz which suggests that the majority of silica-flooding predates the main period of Cu-Au deposition (Adshead, 1995). The main phase of Cu-Au deposition produced an assemblage of chalcopyrite, magnetite ± hematite ± pyrite ± pyrrhotite ± Fe-hornblende ± biotite ± siderite ± ferropyrosmalite (Table 1.2).

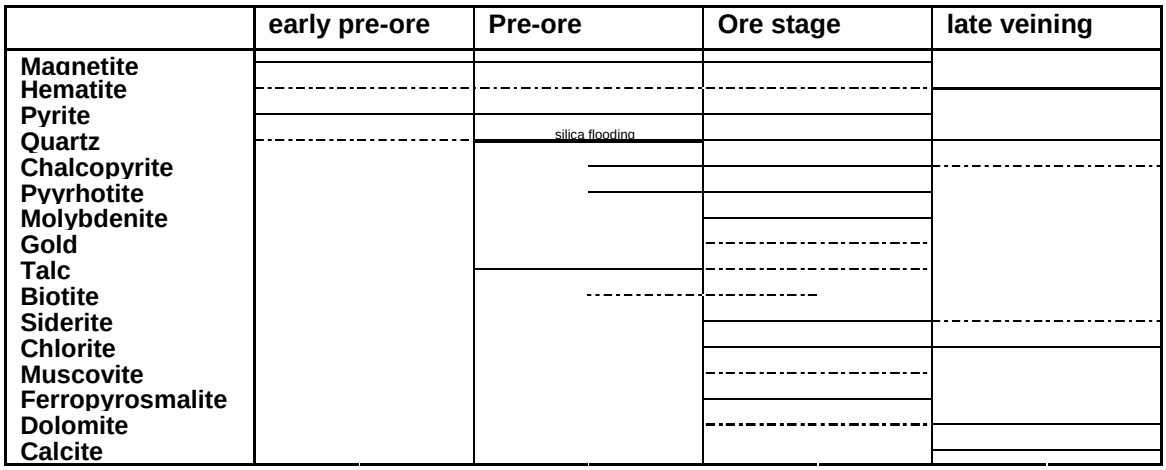

Table 1.2: Paragenesis of Osborne ore assemblage (after Adshead, 1995).
Solid lines indicate major phases, whereas dashed lines indicate minor phases.

The high-grade Cu-Au ore is hypogene and chalcopyrite is the only Cu-sulphide phase. Cu-Au mineralisation is hosted by hydrothermal quartz (silica flooding) which was emplaced both pre- and syn-ore deposition (Adshead et al., 1998). Copper-gold ratios vary systematically across the deposit and appear, based on iron-oxide and sulphide assemblages, to be related to redox conditions at the time of deposition. In the more oxidised hematite-pyrite-magnetite and magnetite-pyrite western ore zones (2M and 1S) copper-gold ratios are low (< 5000) relative to those in the more reduced, pyrrhotite rich

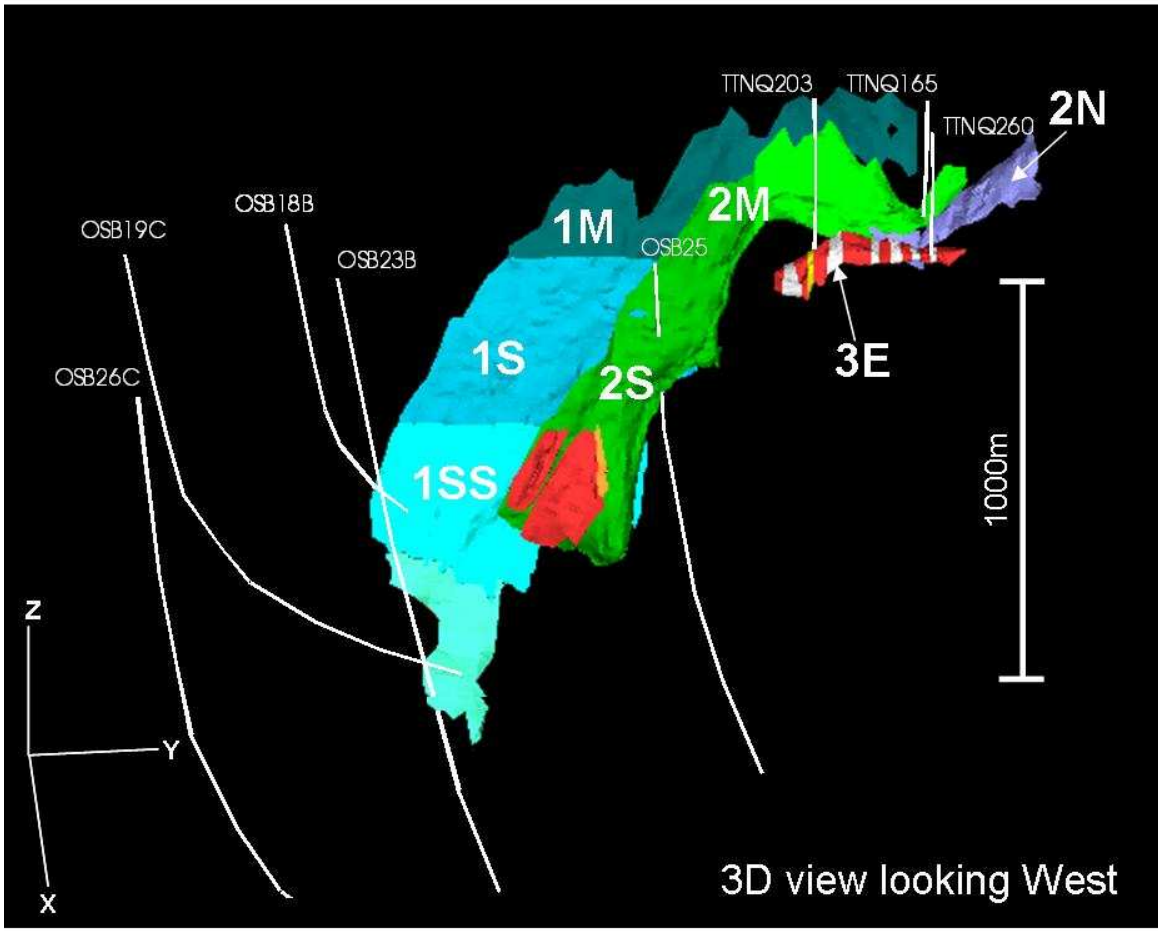

Figure 1.5: 3D distribution of ore bodies at the Osborne Mine. The largest ore body (in shades of blue) is the 1M/1S/1SS ore body, which extends further than indicated on this wireframe. Lying above it is the 2M/2S ore body (in shades of green and red). Both these ore bodies are situated in the western domain. The two smaller ore bodies are within the eastern domain; the 2N ore body (purple) and 3E ore body (red and white). Drill holes from which samples in this study were taken are shown. (Wireframe provided by Osborne Mine geologist Britt Kuhneman).

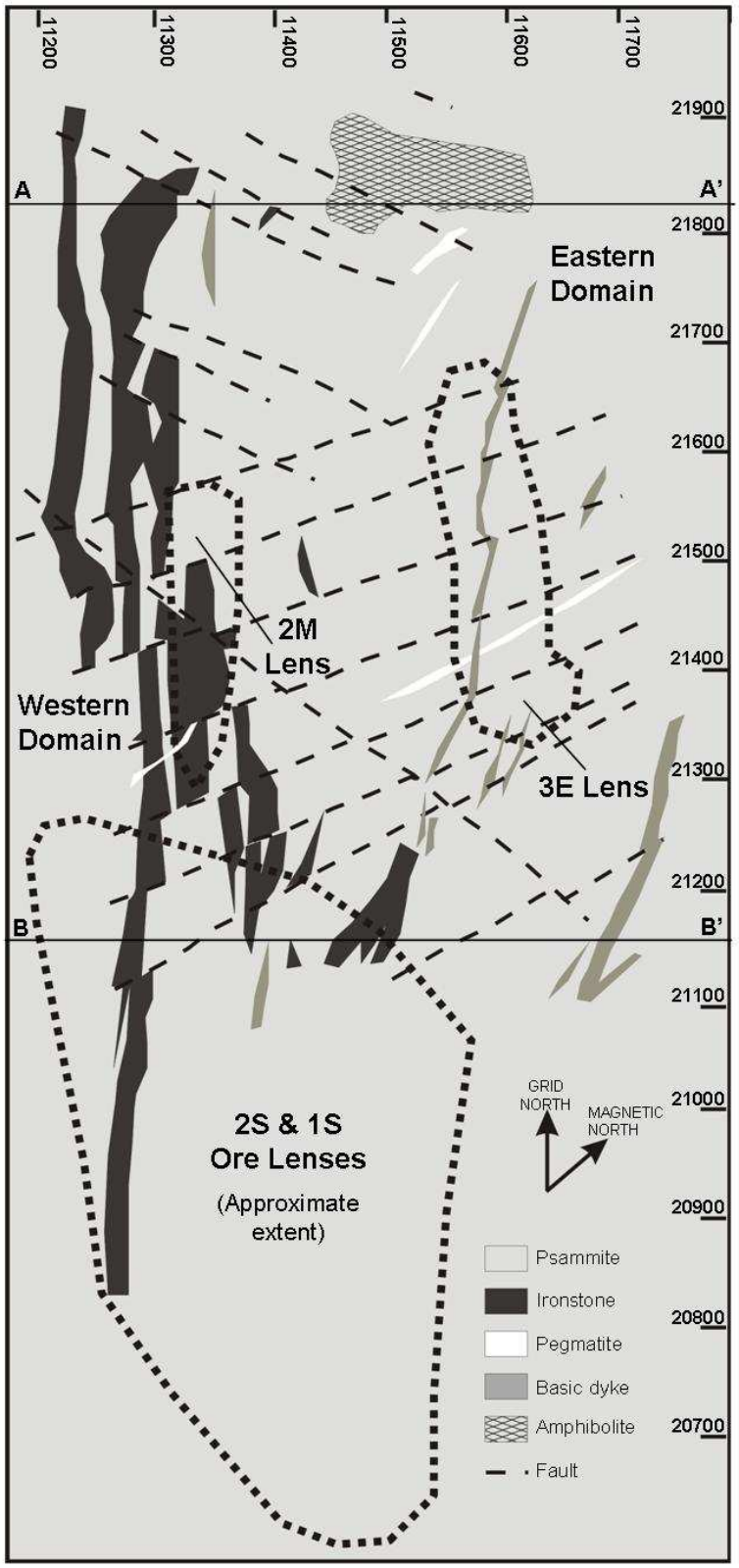

Figure 1.6: Plan view of Osborne ore body distribution.
Modified after Adshead, (1995). A-A' shows line of cross-section 21,815N and B-B' shows line of cross-section 21,150N.

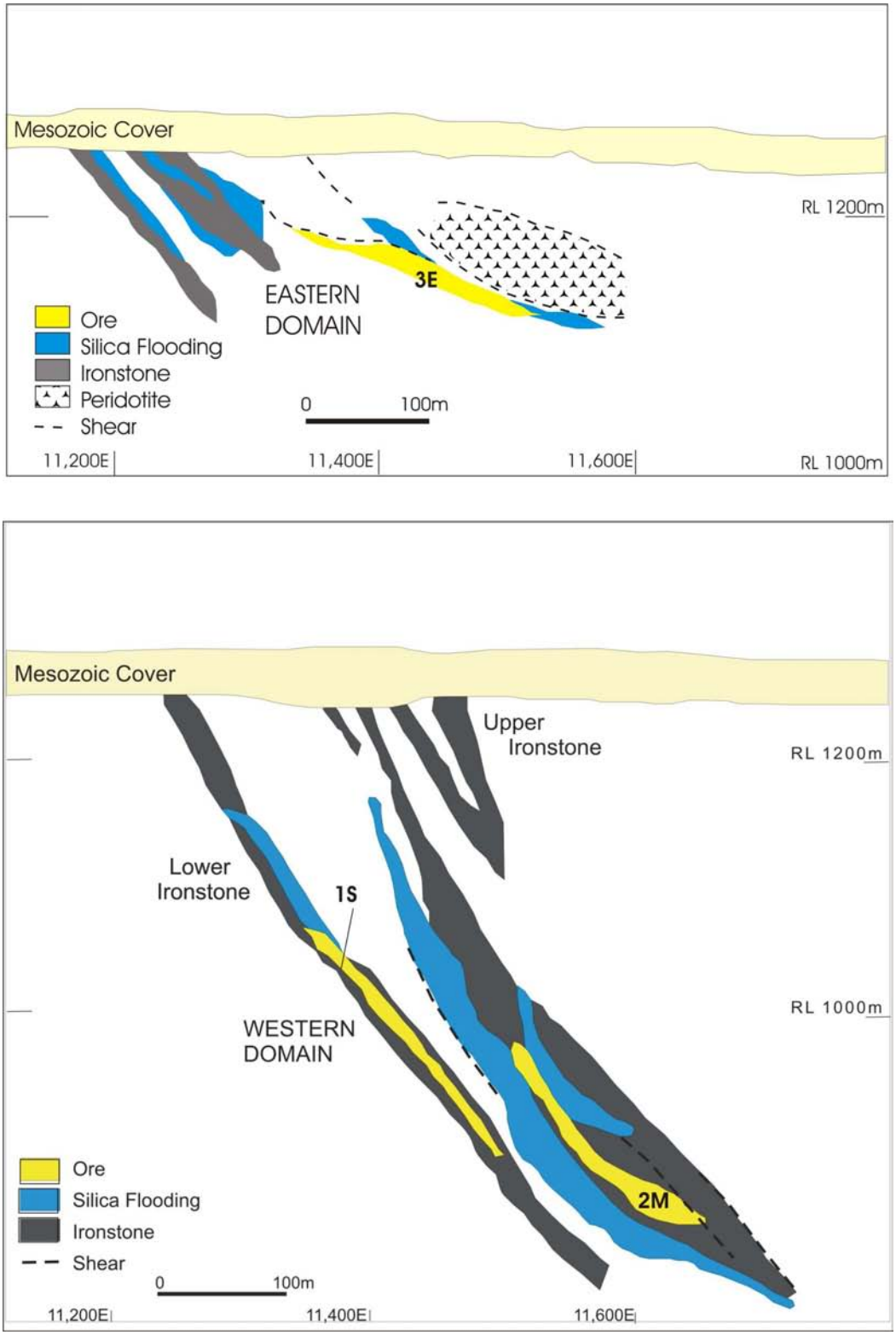

Figure 1.7: Cross-sections through ore bodies, showing host rock and ore associations in different domains. After Tullemans et al., (2001). Section lines are shown on mine plan (Fig. 1.6)

3E eastern domain (5000 - >20000) (Adshead, 1995; Adshead et al., 1998).

1.4.4.5 Geochronology

Ar-Ar dating of hydrothermal biotite and hornblende taken from a mineralised silica flooding assemblage gave ages of 1538 ± 2 Ma for Cu-Au deposition (Perkins and Wyborn, 1998). Later Re-Os dating of molybdenites gave an older age of 1595 ± 5 Ma for the mineralisation (Gauthier et al., 2001). The Re-Os dates for the ore are similar to U-Pb ages from the metamorphic pegmatites indicating that mineralization occurred soon after peak metamorphism (Gauthier et al., 2001), suggesting it may have occurred under similar conditions. Banded ironstone, feldspathic psammite and metatholeiite are common host rock relicts within the main ore bodies suggesting the copper-gold mineralisation was deposited after the peak of regional metamorphism (Adshead et al., 1998). These overprinting relationships are indicative of mineralisation during retrograde metamorphism but the age data suggest ore deposition must have occurred shortly after the metamorphic peak.

Dating of metamorphic zircons at the Cannington deposit give an ages for peak metamorphism of 1585 ± 5Ma (Giles and Nutman, 2003), while Ar-Ar ages for metamorphic hornblendes in the same rocks give ages of 1550-1540 Ma (Perkins and Wyborn, 1998). This suggests the high temperatures experienced in the south east of the Mt Isa Inlier during peak metamorphism remained above the Ar closure temperatures for significant periods of time, and the younger Ar-Ar dates at both Cannington and Osborne suggest the systems underwent resetting.

1.4.5 Fluid inclusion studies

The focus of this study is on the chemistry of the fluids associated with ore formation at the Osborne IOCG deposit. The vast majority of rocks form in the presence of fluids, e.g. sedimentary pore fluids, hydrothermal solutions, silicate melts. When a mineral grows in the presence of a fluid phase some of that fluid can be trapped in the imperfections of the growing crystal face, forming fluid inclusions (Sorby, 1858; Roedder, 1984; Bodnar, 2003). Such fluid inclusions are commonly found in a wide range of minerals and settings. There are many types of fluid inclusion; from simple monophase aqueous or gaseous inclusions through to multi-solid brine and silicate melt inclusions.

The study of fluid inclusions has long been an important component of mineral deposit studies, providing insights into the hydrothermal processes that form many major ore deposits (Roedder, 1984). Fluid inclusions provide information on temperature and pressure conditions during ore formation as well as the density and composition of the ore fluids. Thus, they provide information that can characterise the ore environment. Development of internally consistent geochemical models of the various stages in ore fluid transport and deposition relies on data from fluid inclusion studies. These models are used to help define exploration criteria (Roedder and Bodnar, 1997).

Fluid inclusions permit direct sampling of ore fluids, entrapped within minerals millions or billions of years ago (Roedder, 1984). Increasingly, studies of fluid inclusions have focused on the composition of the inclusions with both bulk analytical methods, and more recently, micro-analytical methods employed. A variety of techniques now exist to enable thorough characterisation of the chemical compositions of ore forming fluids.

Metals and other elements can be measured at parts per million levels or better and the ligands that transported ore metals can be identified.

Large volumes of high salinity fluids, which are significant in transporting metals within hydrothermal systems can form in several distinct geological environments: (1) by exsolution from a crystallising magma; (2) through evaporation of seawater, creating bittern brines; (3) by dissolution of evaporite deposits, (4) by removal of water from chloride-bearing solutions during hydration reactions in a metamorphic environment, and (5) by boiling of fluids (Hanor, 1994; Yardley et al., 2000).

Fluid sources can be identified and distinguished using tracers. Tracers are components of a system which allow the course of a process (i.e. mixing or diffusion) to be followed without themselves becoming involved in the process. In natural systems tracers are typical conservative elements or ions; the most commonly used are ratios of halogens and noble gases (Kelley et al., 1986; Banks et al., 1991; Böhlke and Irwin, 1992a; Böhlke and Irwin, 1992b; Hanor, 1994; Kesler et al., 1995; Banks et al., 2000; Kendrick et al., 2001; Ballentine et al., 2002; Kendrick et al., 2002; Burnard and Polya, 2004). The ratio Br/Cl is the most commonly used tracer in the study of brine origins; I/Cl is also of interest but is less reliable as iodine exists only in low concentrations and can be hard to measure. The involvement of I in organic processes can also mean that elevated I/Cl ratios reflect interaction of fluid with organic-rich sediments. Where I/Cl data are obtained they can refine the interpretation of brine sources (e.g. Böhkle and Irwin, 1992b). Ar isotopes can provide information on fluid sources and residence time (e.g. Kelley et al., 1986).

The sources of the metals and ligands carried by the high salinity brines in IOCG deposits have not been conclusively identified and although some researchers advocate an origin by exsolution from granitic magmas in the region (Perring et al., 2000; Pollard, 2006) a direct genetic link between magmatism and mineralisation remains unproven. Resolving the source of salinity in the ore forming fluids is an important step in establishing the mode of origin for this group of deposits. Cl is the dominant anion in most hydrothermal fluids and is an important complexing agent for the transport of ore metals in solution.

Historically, the most common bulk technique used to study fluid inclusions has been crush leach analysis (e.g Banks and Yardley, 1992) in which a sample is crushed or decrepitated, to open the fluid inclusions. The sample is then leached and the solute analysed. Analysis of the solute can be by a variety of methods including ion and gas chromatography, atomic absorption spectrometry (AAS) and atomic emission spectroscopy (AES). Bulk solute analyses can distinguish between different fluid flow events temporally and spatially, as well as enabling comparison with modern analogues (Gleeson, 2003).

Micro-analytical methods permit analysis of individual fluid inclusions. Ore formation is a dynamic process; over the duration of the hydrothermal system temperature, pressure and fluid chemistry will change. Thus the analysis of individual fluid inclusions can provide detailed information on the evolution of ore forming fluids and systems. In the last twenty years a number of techniques have been developed for microanalysis of fluid inclusions. One of the most commonly used is laser ablation inductively coupled plasma mass spectrometry (LA-ICP-MS). This is a destructive

technique in which fluid inclusions (which can be up to ~100μm deep in the sample) are ablated by a laser. The ablation releases the contents of the inclusion which are then analysed by ICP-MS. This technique is becoming widely used in the study of fluid inclusions in hydrothermal ore environments, providing compositional information and identifying controls on fluid chemistry (e.g. Audetat et al., 1998; Ulrich et al., 1999; Landtwing et al., 2002; Rusk et al., 2004).

Proton induced X-ray emission (PIXE) provides information on the distribution of elements between solid phases and ore fluid as well as giving quantative compositional data. A non-destructive technique, PIXE analysis incurs relatively large errors compared with LA-ICP-MS, although element ratios are considered more reliable as comparable errors are incurred for all elements and so are not propagated (Williams et al., 2001). To date, most PIXE studies of fluid inclusions have focused on technique development (e.g. Anderson et al., 1989; Ryan et al., 1995) but the method is becoming increasingly used in the study of ore systems (Ryan and Griffin, 1993; Perring et al., 2000; Williams et al., 2001; Kamenetsky et al., 2002).

A study of the Starra IOCG deposit in the Cloncurry district used PIXE analysis to study two generations of fluid inclusions; highlighting chemical distinctions between fluids associated with early barren ironstones and those hosted by mineralisation stage quartz and identifying three chemically different brines, all involved in the formation of the deposit (Williams et al., 2001). An advantage of PIXE over LA-ICP-MS is that it routinely measures Br concentrations. Br/Cl values in the Starra deposit were low ($<2 \times 10^{-3}$) which distinguished them from the bittern brine-like values measured in the nearby Mt Isa copper deposit (Heinrich et al., 1993).

Another analytical method which can be used for both bulk samples and for micro-analysis is combined noble gas and halogen analysis. First pioneered by Böhkle and Irwin (1992a;b), the technique is an extension of Ar-Ar methodology in which noble gases and halogens in fluid inclusions in neutron irradiated samples were analysed by laser microprobe noble-gas mass spectrometry. The irradiation process allows the halogens to be measured as nucleogenic noble gas 'proxy' isotopes, and these can be measured concurrently with naturally occurring noble gas isotopes. One strong advantage of this technique is that I/Cl ratios can be easily determined, providing additional information on fluid sources and processes. This technique has been used in the study of Phanerozoic MVT, porphyry copper and sandstone hosted Pb-Zn deposits (Böhkle and Irwin, 1992a;b; Kendrick et al., 2001; Kendrick et al., 2002; Kendrick et al., 2005), and more recently has been applied to Proterozoic systems including IOCG deposits (Kendrick et al., 2006a; Kendrick et al., 2007) and the Mt Isa copper deposit (Kendrick et al., 2006b).

Laser Raman Spectroscopy is a technique used for identification of molecular species in fluids (Burruss, 2003). The technique is semi-quantative and non-destructive. While it is particularly used in the detection of gaseous phases within fluid inclusions it has also been used to identify unusual daughter minerals, such as ferropyrosmalite (Dong and Pollard, 1997). Raman analyses have been used to calculate salinities in fluid inclusions (Mernagh and Wilde, 1989) and to investigate the effects of clathrates on volatile compositions in fluids in aqueous-carbonic inclusions (Murphy and Roberts, 1995).

1.4.6 Fluid inclusion studies in the Cloncurry district

The IOCG and affiliated deposits in the Cloncurry district host a complex assemblage of fluid inclusion populations that record the evolution of the Cu-Au bearing ore fluids. The hydrothermal brines that caused the iron oxide copper gold mineralisation are known to have been hypersaline with a significant CO_2 content. (Beardsmore, 1992; Adshead, 1995; Baker, 1996; Rotherham, 1997b; Perring et al., 2000). Mixing and unmixing of miscible and partially miscible fluids has been documented in regional fluids in sodic alteration systems in the Eastern Fold Belt of the Mt Isa Inlier (Fu et al., 2003) and within IOCG deposits in the district (Rotherham, 1997b). Evidence for both fluid unmixing and mixing have been observed within the Osborne deposit (Mustard, 2004) and are implicated as potential ore precipitation mechanisms.

These studies have identified six populations of fluid inclusions which occur in varying proportions in the Cloncurry iron-oxide copper gold systems: (i) Multisolid-bearing, containing four to nine phases at room temperature with high homogenisation temperatures (Th > 450 °C) and hypersaline salinities (30-65 wt% NaCl equiv.); (ii) Liquid rich (liquid-vapour or multisolid) inclusions with vapour >15%, containing two to four phases at room temperature and with moderate homogenization temperatures (300-400 ^{o}C) and salinities (24-37 wt% NaCl equiv.); (iii) Liquid rich (liquid-vapour or multisolid) inclusions with vapour <10% that contain two to four phases at room temperature and have low homogenization temperatures (Th < 200 ^{o}C) and moderate salinities (28-39 wt% NaCl equiv.); (iv) CO_2 rich inclusions with between one and three phases at room temperature, including rare narcolite solids. Fluid densities of 0.61-0.98 g/cm^3 have been measured; (v) CH_4 rich inclusions that contain one or two phases at room temperature; (vi) H_2O rich inclusions that contain two phases at room temperature

with vapour comprising 10-95% by volume. These inclusions have low to moderate homogenization temperatures and relatively low salinities (<4.5 wt% NaCl equivalent). Two subgroups are recognised based on homogenisation temperatures: (A) Th μ = 300°C and (B) Th μ = 191°C. A PIXE and laser ablation study of ultra high salinity inclusions (type i) associated with the barren ironstones of the Lightning Creek prospect found that they contain up to 2% Cu (Perring et al., 2000).

Previous fluid inclusion work at Osborne was undertaken by Davidson (1989) and Adshead (1995), Dong (1995) and Mustard et al., (2004). Interpreting the mineralisation as exhalative in origin, Davidson (1989) identified three inclusion types as related to epigenetic metamorphic fluid flow. These were classified as (i) prograde, primary liquid-vapour inclusions with two to four daughter phases and salinities estimated between 42 and 57 wt% NaCl equiv. and homogenisation temperatures between 416 and 483°C; (ii) prograde, high density, CO_2 inclusions associated with the primary saline inclusions and (iii) retrograde, liquid-vapour inclusions, with between two and four daughter phases and salinities between 31 and 50 wt% NaCl equiv. and homogenisation temperatures between 457 and 514°C.

A study by Adshead (1995) identified several different populations of fluid inclusion than were observed by Davidson (1989), including two generations of multiphase inclusions; a primary population with Liquid + Vapour + ≥2 Daughter Minerals (L+V+≥2D) and a pseudosecondary or secondary population of L + V ± 2S; primary and secondary populations of a carbonic liquid and monophase liquid inclusions. The primary multisolid inclusions have salinities between 65 and 82 wt% salts (calculated from phase volumetric studies) and typically decrepitated without homogenising.

Where homogenisation temperatures were recorded they range from 425 to 505^{o}C. The lower salinity inclusions have salinities between 20 and 37 wt% NaCl equiv. and homogenise between 220 and 400^{o}C (corrected for pressure). These inclusions can be seen to radiate from sulphide grains and it has been suggested that these fluids are associated with the main phase of ore deposition (Adshead, 1995). Data from the Adshead, (1995) study is presented with results from this study. (NB. At the time of Adsheads' study, in the western domain core was only available from the upper portion of the ore bodies so the deepest 1SS ore lens was not sampled).

Dong, (1995) identified similar groupings of inclusions to Adshead (1995), distinguishing two types of lower salinity pseudosecondary/secondary; one population with large (20-40%) vapour bubbles and halite and carbonate daughter minerals, the second population with small vapour bubbles (<10 vol. %) and halite and sylvite daughter minerals. Carbonic inclusions dominated by CH_4 and multi-solid inclusions with a methane-bearing vapour bubble were documented in samples from the Eastern domain (Dong, 1995).

Mustard et al., (2004), recognized high salinity, multi-solid brine inclusions and halite-bearing liquid CO_2 inclusions as end members produced by fluid unmixing. The unmixing was calculated to have occurred at high P-T conditions of >500 ^{o}C and 0.5 GPa. Preliminary PIXE results indicated low Cu concentrations in fluids associated with early quartz and minor magnetite and chalcopyrite (Mustard et al., 2004). This PIXE data was refitted and reinterpreted in Chapter 4.

Adshead, (1995) conducted a preliminary oxygen isotope study of 21 quartz and magnetite samples from ore assemblages and banded ironstones. Relative to SMOW, $\delta^{18}O_{fluid}$ is estimated to have a value of +4.5 to +8.2‰. This is based on values of between -0.9 and +10.1‰ measured in quartz and magnetite separates (Adshead, 1995). Minimum fluid temperatures estimated from equilibration temperatures for quartz-magnetite assemblages associated with mineralised silica-flooding are between 502 and 585^{o}C. The range of $\delta^{18}O_{fluid}$ values, which are considered to represent the composition of the last hydrothermal fluid to equilibrate with the magnetite-quartz assemblage, fall within the ranges measured in metamorphic fluid and eastern domain fluids also fall in the range of magmatic fluid compositions (Adshead, 1995). However, in the absence of deuterium analyses the compositions cannot be considered to be fully constrained.

Magnetite from the pyrite bearing silica-flooding of the western domain has a negative $\delta^{18}O$ of -0.6 to -0.9‰ while the magnetite from the chalcopyrite-pyrrhotite-rich mineralization of the eastern domain (3E ore lens) has higher values; +2.7 to +3.0‰ with the highest value of 4.5‰ being recorded in magnetite-rich breccia in the eastern domain. The more pyrite-rich margins of the 3E ore zone contain magnetite with a lower $\delta^{18}O$ (+1.1‰) than that within the pyrrhotite-rich part of the lode. Similar variation is seen in the quartz samples with $\delta^{18}O$ values ranging from +5.9 to +10.1‰. The quartz from the high grade 3E ore zone has $\delta^{18}O$ values that are up to 2‰ higher than in the samples from the western domain (Adshead, 1995).

Previous studies of the Osborne deposit (Davidson, 1989; Adshead, 1995) have focused on mineral chemistry and while fluid inclusion populations have been identified and studied their chemistry has not been thoroughly interrogated. In this thesis

compositional data from LA-ICP-MS and PIXE studies as well as noble gas isotopic composition and elemental halogen ratios are used to provide information on fluid origin and acquisition of salinity in the Osborne IOCG deposit. It is the intention of this study to further the understanding of genetic processes at Osborne and other IOCG deposits in the region by the examination of the ore fluid chemistry, evolution and processes**.**

2. ORE FLUID PROCESSES AND EVOLUTION AT THE OSBORNE IOCG DEPOSIT; A FLUID INCLUSION STUDY

2.1 Introduction

Petrographic and microthermometric studies of fluid inclusions can characterise inclusion populations and help determine fluid evolution and fluid processes in hydrothermal ore deposits (Roedder, 1984; Shepherd et al., 1985). Fluid inclusions can provide a record of the physiochemical conditions at the time of ore formation. A fluid inclusion assemblage may preserve multiple generations of fluids that are representative of pre-, syn- and post-ore deposition compositions. Careful characterisation of fluid inclusion assemblages constrains the relative timing of their entrapment and is essential prior to undertaking bulk-leach and/or single fluid inclusion analyses, such as those documented in Chapters 3 and 4.

This chapter reports the results of a study of quartz-hosted fluid inclusions in ore samples, associated pegmatites and late veins from the Osborne IOCG deposit, which was carried out to identify and characterise the fluids involved in ore formation. Multiple populations of high salinity brines and carbonic fluids are hosted by several generations of quartz.

2.2 Sample Selection and Description

The samples in this study are taken from zones of silica-flooding which host the ore and from pegmatite sheets situated within the mineralised zone (Table 2.1). The ore assemblages comprise Cu-Fe-O-S phases, including Magnetite + Pyrite + Chalcopyrite ± Pyyrhotite ± Hematite.

Sample Number	Sample Type	Hole ID	From	To	Ore Lens	Analysis
Osb 15	NQ Core	Osb 26c	1480.70	1480.83	1S	MT, LA, LR, P, NG
Osb 20	NQ Core	Osb 19c	1061.44	1061.59	1S	MT, LR, NG
Osb 22	NQ Core	Osb 19c	1070.81	1071.00	1S	MT, NG
Osb 27	NQ Core	Osb 18b	919.02	919.22	1S	MT, NG
Osb 36	NQ Core	TTNQ 165	239.60	240.03	2M	MT, LA, P, NG
Osb 37	NQ Core	TTNQ 260	220.00	220.19	3E	MT, LA, LR, P, NG
Osb 40	NQ Core	TTNQ 203	222.72	222.94	2M	MT, LR, NG
Osb 43	NQ Core	TTNQ 203	249.90	250.05	2M	MT, NG
Osb 47	NQ Core	TTNQ 372	271.75	271.90	3E	MT, NG
Osb 59	NQ Core	Osb 23b	1206.60	1206.80	1S	MT, NG
Osb 315	HQ Core	TTHQ 041	220.40	283.40	1S	MT, LA, P, NG
Osb 852	HQ Core	Osb 25	825.00	825.10	1S	MT, LA, LR, P, NG

Table 2.1 Samples analysed in this study.
The drill hole from which they were taken (see Fig 1.5) and the methods used for analysis (see also Chapters 3 and 4). MT = microthermometry; LA = Laser Ablation; LR = Laser Raman; P = PIXE; NG = Noble Gas and Halogen Analysis.

A majority of samples were taken from the largest 1S ore lens, with samples collected from shallow depths (220 metres) and the deeper extensions (825 – 1480 metres). Samples were also selected from the smaller 2M and 3E ore lenses which do not extend to great depths. Sample selection was intended to represent ore from all three ore lenses and from different levels within the mine.

The silica-flooding samples are dominated by coarse-grained quartz (between 1 to 5 mm in diameter and anhedral to subhedral in shape) with magnetite, pyrite, chalcopyrite and pyrrhotite present in variable amounts (Fig 2.1a;b;c;d; Fig 2.2b), along with minor phases such as biotite, tourmaline, muscovite, molybdenite, ferropyrosmalite and apatite. In some samples pyrrhotite is present as rims on pyrite/chalcopyrite grains (Fig 2.1b; Fig 2.2b). Sulphides in sample Osb47 show evidence of strain and partly define a distinct foliation (Fig 2.2d). Pegmatite samples are dominated by medium to coarse grained quartz and feldspar (Fig 2.2e) with minor biotite and tourmaline. Sample Osb22A contains silica flooding quartz, cross-cut by a later quartz vein. Magnetite is absent from the vein selvages which consequently appear bleached.

Sample				Fluid Inclusion Assemblage Proportions (%)				
ID	**Description**	**Ore Lens**	**Paragenetic Stage***	**MS**	**LVD**	**LV**	**CO2**	**CB**
Osb40	Coarse quartz-feldspar pegmatite with perthitic textures, minor tourmaline and rare specular hematite.	2M	Peg Qtz	45	5	15	30	5
Osb852	Quartz-feldspar pegmatite with rare perthitic textures.	1SS	Peg Qtz	20	0	5	70	5
Osb15	Magnetite bearing coarse-grained silica flooding with minor chalcopyrite.	1SS	Q1 + Q2	70	10	5	14	1
Osb36B	Silica flooding with magnetite rich zones and coarse chalcopyrite with occasional fine grained pyrrhotite coats	2M	Q1 + Q2	60	10	18	10	2
Osb37B	Magnetite-chalcopyrite-pyrrhotite bearing silica flooding	3E	Q1 + Q2	35	20	20	24	1
Osb43	Silica flooding with magnetite rich zones and coarse chalcopyrite and minor pyrrhotite	2M	Q1 + Q2	45	15	25	15	0
Osb315	Silica flooding with minor magnetite and coarse chalcopyrite.	1M	Q1 + Q2	45	25	10	15	5
Osb20	Quartz vein containing pyrite and chalcopyrite cross-cut by quartz-magnetite-pyrite-chalcopyrite veins in psammite with accessory hematite and pyrite.	1SS	Q2 + Q3	10	50	35	5	0
Osb22A	Magnetite rich silica flooding with chalcopyrite hosted within magnetite rich zones with quartz-feldspar vein with coarse chalcopyrite and hematite dusting on feldspar grains hosted by mineralised silica-flooding.	1SS	Q1 + Q2 + Q3	20 (q) 0 (v)	35 (q) 35 (v)	35 (q) 65 (v)	10 (q) 0 (v)	0

Table 2.2: Sample and fluid inclusion assemblage descriptions
** see section 2.4.2*

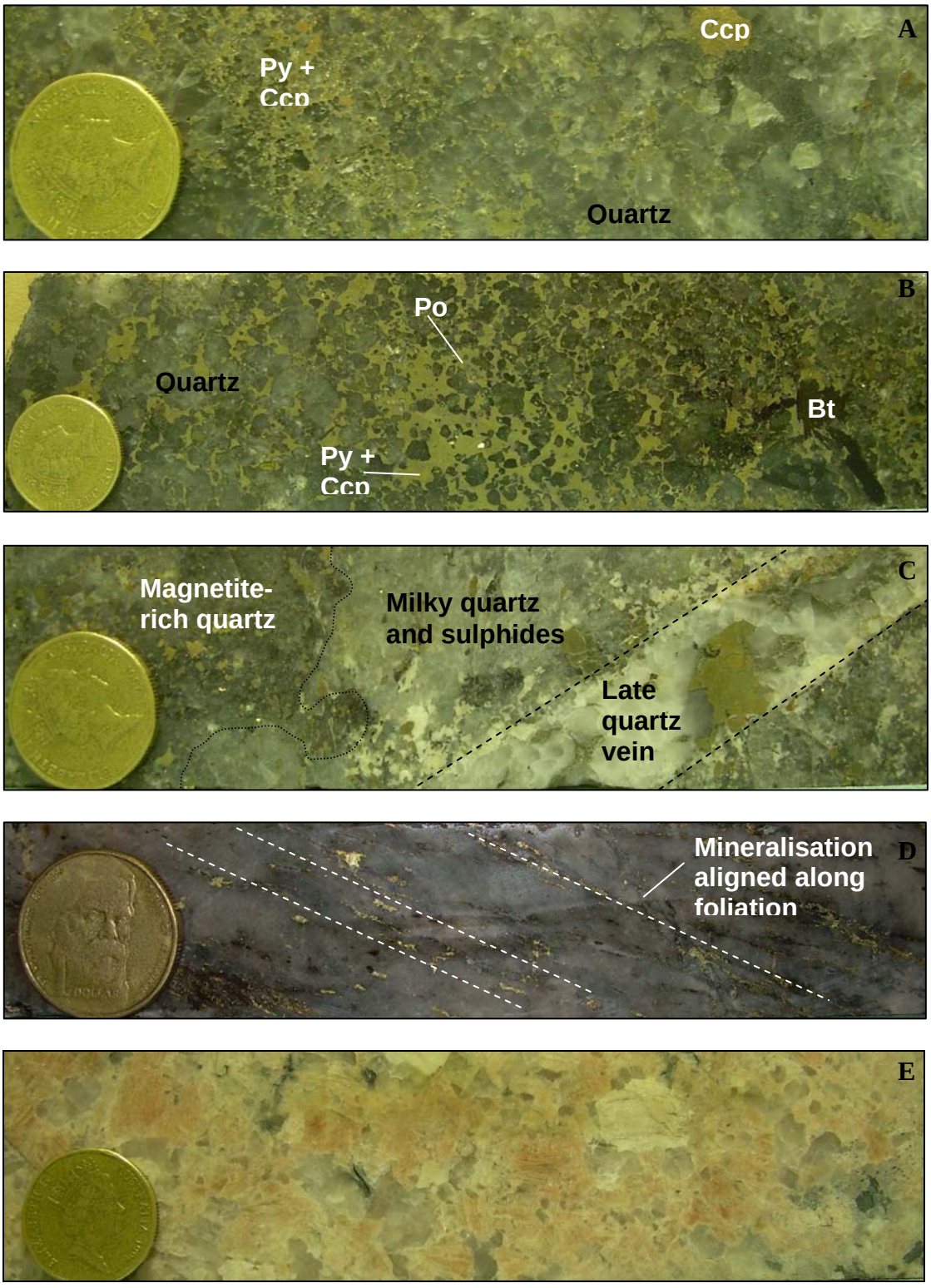

Figure 2.1: Polished core samples. (A) Sample Osb59: pyrite and chalcopyrite hosted in quartz, minor magnetite; (B) Sample Osb37B: pyrite and pyrrhotite hosted by biotite-bearing quartz; (C) Sample Osb22B: magnetite-quartz-pyrite bearing quartz cross-cut by mineralised quartz-feldspar vein. There is a bleaching effect around the vein in which magnetite-bearing quartz has been replaced by sulphide-bearing quartz; (D) Sample Osb47: Coarse-grained quartz with aligned pyrite and chalcopyrite from 3E ore lens that appears to have experienced strain syn-post mineralisation; (E) Sample Osb40: Coarse-grained quartz-albite-tourmaline pegmatite from the western domain. Coin is AUD $1 – 25mm diameter.

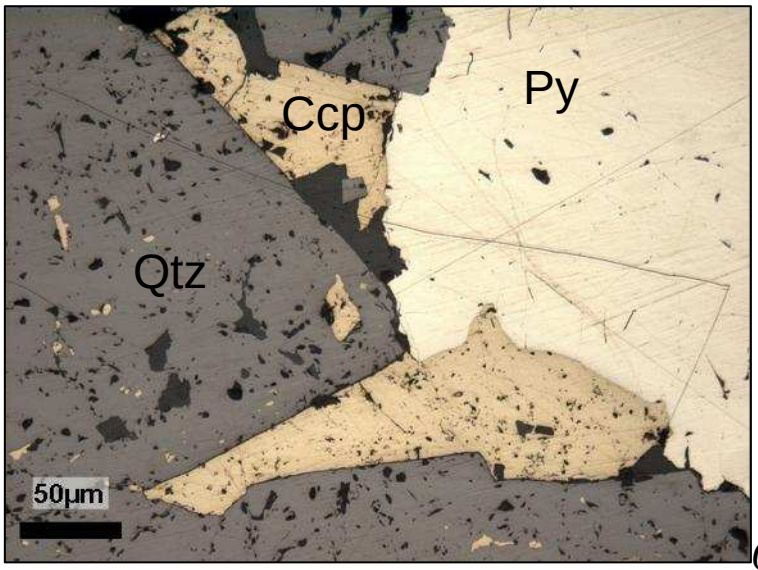

(A)

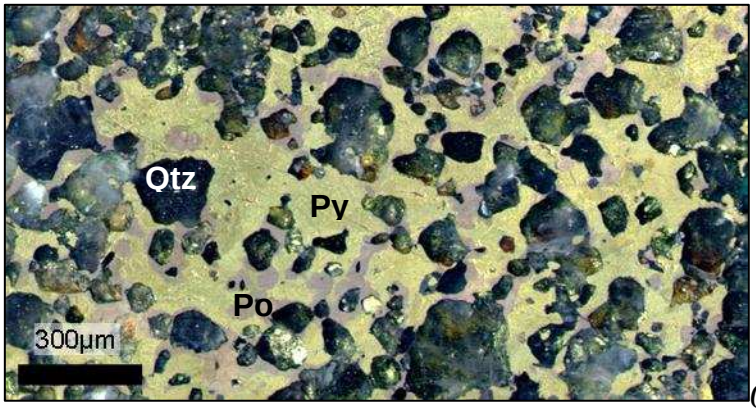

(B)

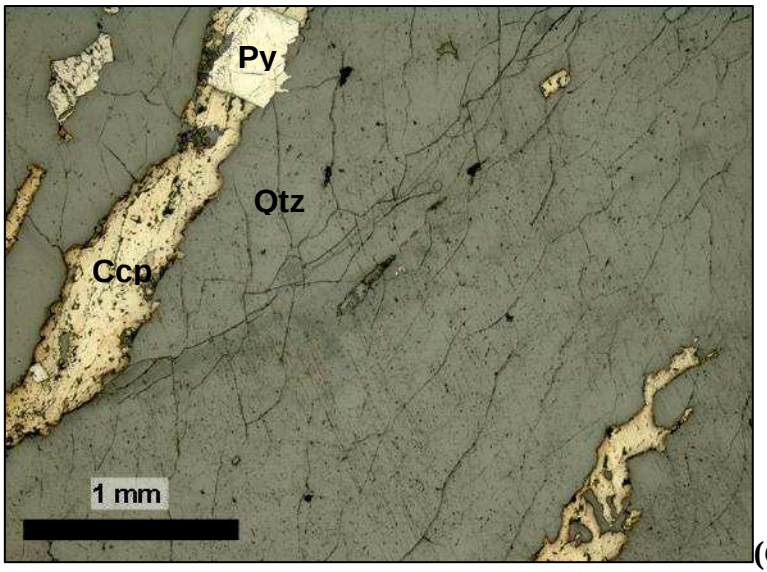

(C)

Figure 2.2: Sulphide associations in Osborne samples
(A) Reflected light photomicrograph: Osb36B chalcopyrite and pyrite in quartz. Chalcopyrite appears to have an infill texture.
(B) Polished fluid inclusion wafer: Osb37, sulphides are intergrown with quartz. Pyrrhotite and pyrite are intergrown.
(C) Reflected light photomicrograph: Osb47, orientated pyrite and chalcopyrite grains within quartz.

The samples are taken from mineral assemblages with parageneses that bracket the main phase of ore formation (Table 2.2). Within the silica flooding, the early quartz (Q1) predates mineralisation while a second generation (Q2) formed syn-ore and hosts the majority of sulphide grains (Fig 2.1; Fig 2.5; Table 1.2). Later quartz veins (Q3), that cross-cut the main phase of quartz mineralisation, are late syn- to post-ore depositional features and also contain sulphide mineralisation (Fig 2.2c).

2.3 Analytical Methodology

Fluid inclusion studies were conducted on samples from three ore zones, pegmatites and cross-cutting veins that represent several stages of the paragenesis, bracketing the period of ore formation. Following a detailed petrographic study of fluid inclusion-bearing quartz samples from the Osborne Mine, 9 samples that are representative of 3 ore lenses and from both shallow and deep mine levels were selected for microthermometric analysis (Appendix A). Temporal variations in fluid characteristics were investigated by examination of inclusions in different mineral stages with different parageneses (i.e. primary and secondary; Roedder, 1984).

2.3.1 Microthermometry

Microthermometry was undertaken on a Linkam MDS600 heating-freezing stage at James Cook University. The stage was calibrated regularly between temperatures of -56.6^{o}C and 374.1^{o}C using synthetic CO_2 and pure H_2O standards. At temperatures in the range 0 to -100^{o}C precision is estimated to be <0.1^{o}C while at temperatures between 0 and 600^{o}C precision is <1^{o}C. Laser Raman spectroscopic data were collected at the Geoscience Australia using a Dilor® SuperLabram spectrometer. Laser Raman spectroscopy provides a non-destructive procedure for identification of various gases,

complex ions containing covalent bonds in aqueous solutions (e.g. HCO_3^-) and some daughter minerals (specifically those containing covalent bonds, e.g. sulphates, carbonates, silicates; Cl-salts are not identifiable) within individual fluid inclusions.

2.3.2 Laser Raman Spectroscopy

Laser Raman spectra of fluid inclusions were recorded on a Dilor® SuperLabram spectrometer equipped with a holographic notch filter, 600 and 1800 g/mm gratings, and a liquid N_2 cooled, 2000 × 450 pixel CCD detector. The inclusions were illuminated with 514.5 nm laser excitation from a Melles Griot 543 argon ion laser, using 5 mW power at the samples, and a single 30 second accumulation. A 100× Olympus microscope objective was used to focus the laser beam and collect the scattered light. The focused laser spot on the samples was approximately 1 μm in diameter. Wavenumbers are accurate to ± 1 cm^{-1} as determined by plasma and neon emission lines.

For the analysis of CO_2, O_2, N_2, H_2S and CH_4 in the vapour phase, spectra were recorded from 1000 to 3800 cm^{-1} using a single 20 second integration time per spectrum. The detection limits are dependent upon the instrumental sensitivity, the partial pressure of each gas, and the optical quality of each fluid inclusion. Raman detection limits (Wopenka and Pasteris, 1987) are estimated to be around 0.1 mole percent for CO_2, O_2 and N_2, and 0.03 mole percent for H_2S and CH_4 and errors in the calculated gas ratios are generally less than 1 mole percent (Mernagh, pers. comm. 2005).

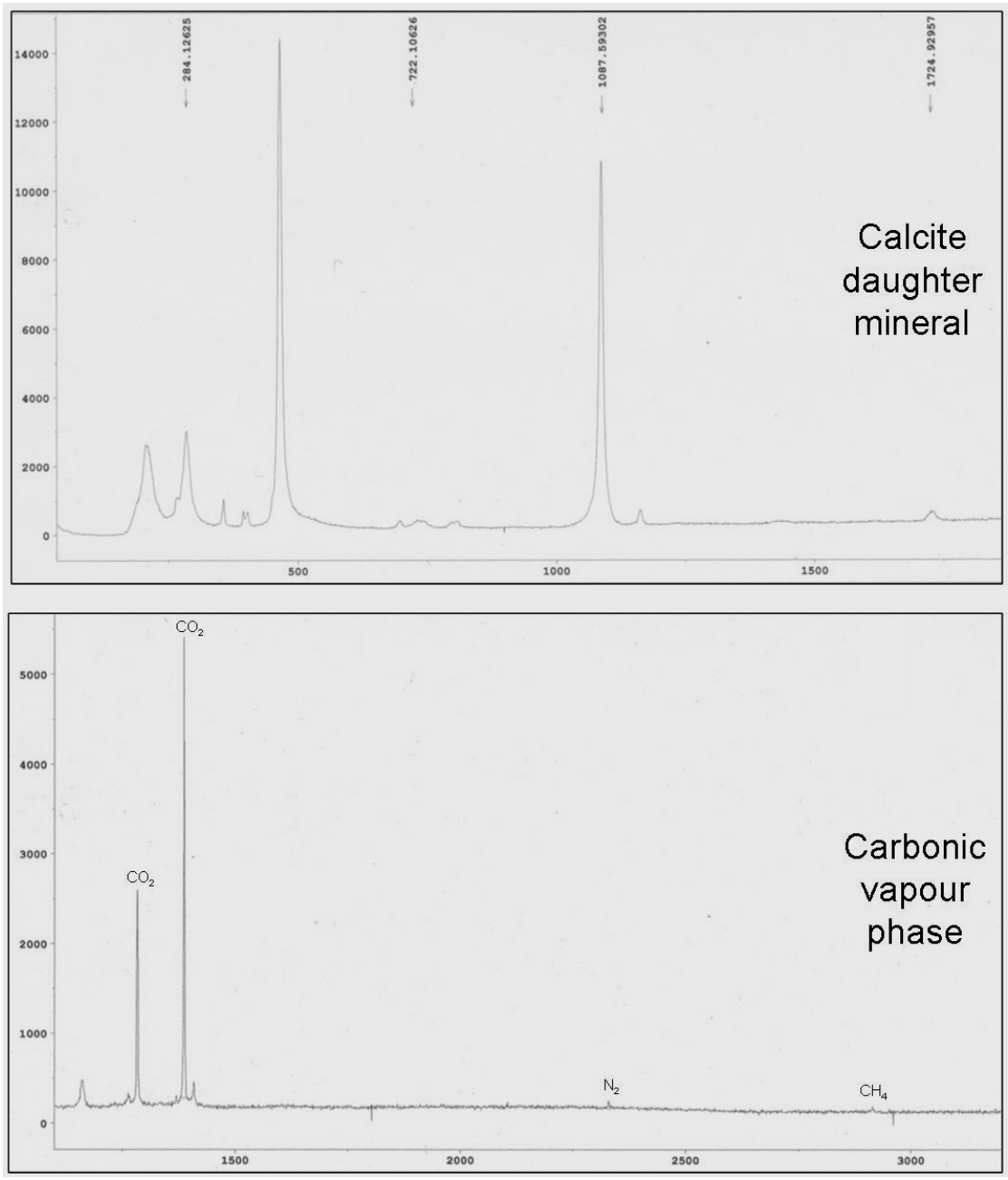

Figure 2.3 Laser Raman spectra from a CB inclusion in sample Osb40.
(A) Spectrum from calcite daughter mineral
(B) Spectrum from carbonic vapour phase shows CO_2 with minor N_2 and CH_4.

2.3.3 Cathodoluminescence

Cathodoluminescence analysis of sulphide bearing quartz samples was conducted using a Jeol JSM-54102V SEM at room temperature. Polished thin sections were made for selected samples.

2.3.4 Phase Volume Calculations

During microthermometry many of the high salinity MS and CB inclusions studied decrepitated without homogenising (Appendix A). Therefore in order to estimate the salinities of these inclusions phase volume calculations have been performed for a small selection of inclusions from pegmatite and ore-hosting samples (Appendix B).

These calculations are based on the methods of Kwak et al., (1986). These calculations require accurate measurements of the different phases and a good understanding of the compositions of the daughter minerals and the liquid phase. The volumes of the fluid inclusions have been calculated assuming ellipsoidal geometry, and to ensure accuracy inclusions with regular inclusion shapes have been preferentially selected. Vapour volumes are calculated using spherical geometries and halite and sylvite are modelled as spheres. Ferropyrosmalite is modelled as a rectangular prism or cube depending on appearance. The dissolved content of the fluids is also calculated based upon solubility data for the main salts: NaCl, KCl, CaCl2 and FeCl2.

2.3.5 Microthermometry Background

Microthermometry is a widely used and generally non-destructive (although many inclusions in this study decrepitate at high temperatures) analytical technique (Roedder, 1984; Shepherd et al., 1985). The method involves observing, recognising and

recording phase changes within inclusions during heating or freezing. By heating and cooling fluid inclusions, measurements can be made that provide information on the composition of the fluids, their salinities, densities and the temperature and pressure of the fluids at the time of trapping. As most natural systems contain more components than can be modelled and many complex salt systems have never been investigated experimentally, the compositional estimates given by this method can only be considered to be semiquantative (Shepherd et al., 1985).

2.3.5.1 Interpretation Considerations

Several assumptions are made in microthermometric studies of fluid inclusions: (1) that at the moment of trapping, the inclusion represents an homogeneous system although cooling, unmixing and saturation effects mean that at room temperature many inclusions are multiphase; (2) that daughter salts within the inclusions precipitated after trapping and are not captive phases; (3) that the inclusions have behaved as closed systems with no loss or addition of material. Inclusions that have ruptured and resealed will not preserve a fluid representative of trapping conditions and may give misleading data. Such inclusions can often be identified by a larger than usual vapour bubble or elevated homogenisation temperatures, compared with the rest of the population (Roedder, 1984). A more subtle but still significant change in chemical conditions can result from the diffusion of H_2 into and out of fluid inclusions (Mavrogenes and Bodnar, 1994). Also, components such as SiO_2 may precipitate on inclusion walls and not redissolve on heating for kinetic reasons (Roedder, 1984).

2.3.5.2 Heating and Homogenisation Temperatures

Two phase inclusions, containing liquid and a vapour bubble, will homogenise to a

single phase upon heating. There are three possible modes of homogenisation (Shepherd et al., 1985); homogenisation into the liquid state (L+V→L); homogenisation into the vapour state (L+V→V) and critical homogenisation by fading of the liquid-vapour meniscus (L+V→supercritical fluid). The homogenisation temperature represents the minimum temperature of the fluid at the time it was trapped within the inclusion unless the fluid was trapped in the two phase field (e.g. boiling or immiscible assemblages) in which case homogenisation temperatures record the true trapping temperatures (Shepherd et al., 1985).

2.3.5.2 Freezing Measurements

Fluid inclusions are commonly difficult to freeze; requiring supercooling to nucleate ice. Consequently phase changes within a fluid inclusion are studied as it is heated. In aqueous inclusions the first melting or eutectic temperature provides information about the dominant salts present e.g. the NaCl-H_2O system has eutectic temperature of -21.2 ^oC while NaCl-$CaCl_2$-H_2O systems start melting at -52^oC (Borisenko, 1977; Crawford, 1981; Oakes et al., 1990). The most common salts in natural systems are NaCl, KCl and $CaCl_2$, although $MgCl_2$, $FeCl_2$ and others may also be present. In the absence of CO_2, ice melting temperatures give accurate estimates of salinity with the depression of the freezing point of water correlating with its salt content (Potter et al., 1978; Shepherd et al., 1985). This effect varies depending on which salts are present, so, conventionally, salinities are recorded as equivalent wt% NaCl. In the presence of Ca, Mg or K these measurements may have up to 5% error margin (Shepherd et al., 1985). In relatively saline fluids (<26 wt% NaCl) hydrohalite may also form, and will melt at different temperatures to the ice present. In a simple NaCl-H_2O system hydrohalite is the stable phase after first melting in inclusions containing between 23.3 and 26.3 wt%

NaCl. In NaCl-$CaCl_2$-H_2O systems the relative melting temperatures of antarctite and hydrohalite can be used to constrain the relative proportions of NaCl and $CaCl_2$ and better define the fluid composition (Borisenko, 1977; Shepherd et al., 1985) and in systems containing ice and hydrohalite, the temperature at which the last phase melts can be used to calculate salinity.

Non-aqueous inclusions (e.g. CO_2, CH_4, N_2, H_2S) can behave in a similar manner to aqueous inclusions. In carbonic inclusions the eutectic is an indicator of the fluid composition with pure CO_2 inclusions melting at 56.6 ^oC. This temperature lowered by the presence of other gaseous phases such as N_2 and CH_4. This freezing point depression can be used to estimate the composition of the fluid in terms of mole percent gases (Hollister and Burruss, 1976; Touret, 1982).

At room temperature, many carbonic inclusions contain both CO_2 liquid and vapour while others are monophase. The temperature at which the two phases homogenise is related to their bulk density. Homogenisation can be to the liquid or vapour states. Fluids with densities close to the critical value (0.468 g cm^{-3}) homogenise by fading of the meniscus. The maximum temperature of homogenisation for all carbonic fluids, excepting those containing H_2S, will be less than the homogenisation temperature of pure CO_2 (31.1^oC; Shepherd et al., 1985).

2.3.5.3 Daughter Minerals

High salinity (> ~22 wt% NaCl equiv.) fluids trapped at high temperatures commonly become saturated with respect to salts on cooling and precipitate crystals termed daughter minerals. Daughter minerals can provide information about both the

components in, and salinity of the fluid phase. The presence of crystals of sylvite, halite, calcite or more complex salts identifies the dominant salts present in the fluid. In many cases daughter minerals of many salts can be identified based on optical properties such as crystal form, colour, refraction, isotropy and birefringence (Shepherd et al., 1985). Opaque minerals are harder to conclusively identify through optical methods, particularly in deeper inclusions, but may be recognised through other analytical methods such as laser Raman or PIXE (see Chapter 4).

When multiphase inclusions are heated the daughter minerals begin to dissolve (Shepherd et al., 1985). The rate of dissolution is linked to their solubility in the liquid phase and the other phases present in the system. Sylvite (KCl) daughter minerals will dissolve at a lower temperature to similar sized halite (NaCl) crystals, indicating higher solubility. For a simple saturated NaCl-H_2O system the temperature at which dissolution is completed is directly proportional to the wt% NaCl in solution (Potter et al, 1978; Shepherd et al., 1985). In systems containing more than one salt it is necessary to refer to data for mixed salt systems in order to constrain the fluid composition accurately, e.g. Oakes et al., (1990) and Schiffries, (1990). Although natural fluids may contain numerous components it is not possible to characterise their composition in terms of more than two or three salts using microthermometry.

2.4 Results

2.4.1 Classification

Fluid inclusions types were initially classified based on phases present at room temperature (Shepherd et al., 1985). Five types of inclusion were identified (Fig. 2.4; Table 2.3). All inclusion types were present in all the silica flooding samples, although

proportions varied (Table 2.2). This variation does not appear to be related to the mineralogy of the samples but may reflect the differences in the proportions of each quartz generation (Q1 / Q2) present in the samples.

2.4.1.1 CO_2-bearing brine inclusions (CB)

CO_2-bearing brines (CB) (Fig 2.4a) are the least abundant type of inclusion observed, forming less than 2% (based on visual estimates) of the total assemblage. They range in size from 15 to 40μm and contain between four and six phases at room temperature (L + L_{CO2} + V_{CO2} + nS). Liquid CO_2-bearing bubbles account for 40-60% of the inclusion by volume and at room temperature may contain an oscillating small CO_2 vapour bubble. The inclusions contain between 1 and 3 daughter minerals. Large cubic halite crystals are identified by their optical relief whereas smaller rounded isotropic phases, with lower relief than halite are identified as sylvite. A darker-coloured, rectangular or rounded phase was identified as calcite by Laser Raman spectroscopy (Figure 2.3A).

2.4.1.2 Multi-solid brine inclusions (MS)

High salinity, multisolid aqueous brines (MS), equate to the type I primary brine inclusions (Table 2.3) of Adshead, (1995) (Fig 2.4b). These inclusions make up between 10 and 70% of the total fluid inclusion assemblage in individual samples (Table 2.2).

MS inclusions are 5 to 50μm in size (mean 10 to 20μm) and contain between four and eight phases at room temperature (L + V + nS). Vapour bubbles occupy 5 to 10 vol.% of the inclusion. Common daughter minerals, identified by habit and relief, include halite, sylvite and calcite. Halite daughter minerals can be large, in some cases

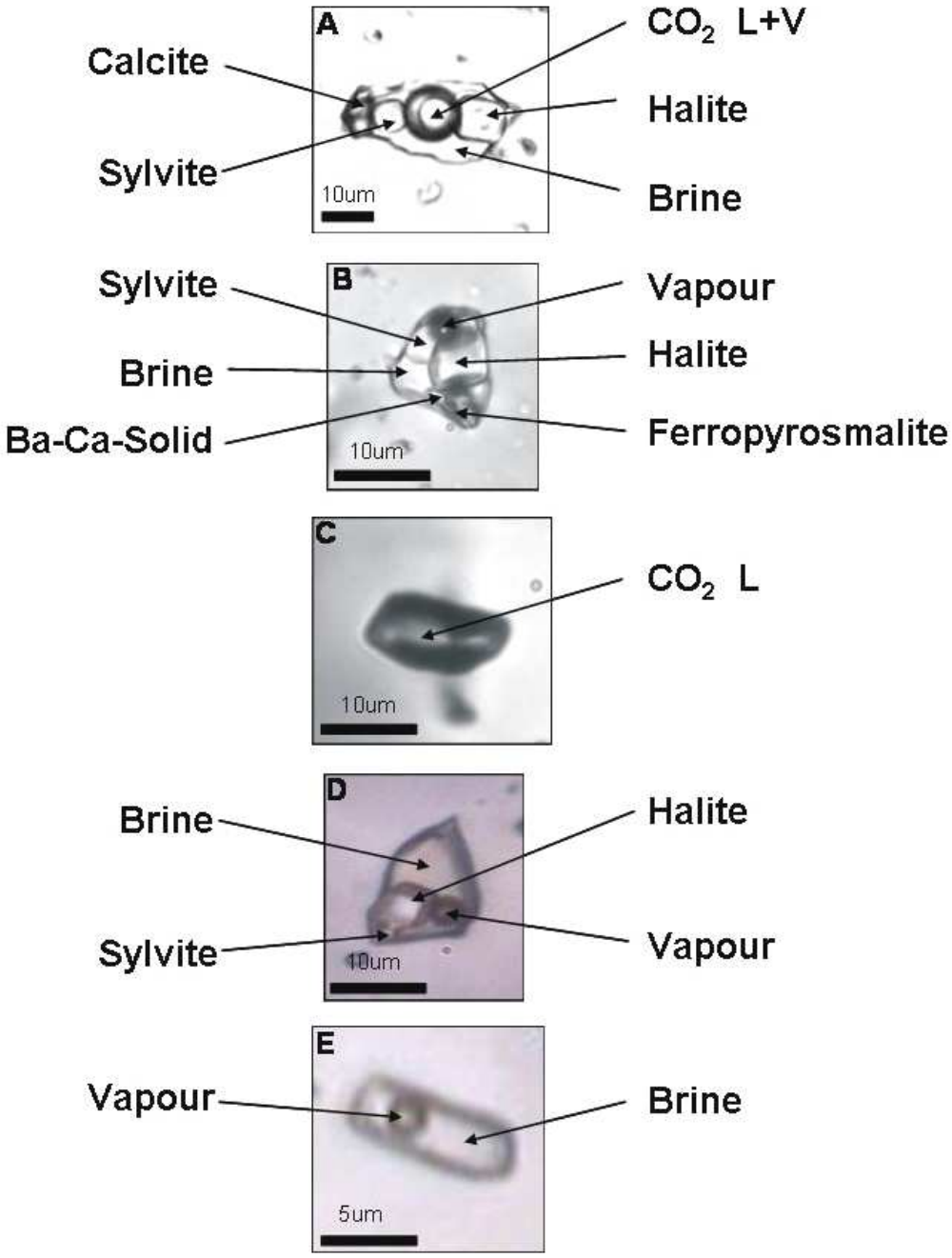

Figure 2.4: Fluid inclusion types observed at Osborne Mine.
(A) Mixed multisolid brine-CO_2 inclusion (CB) with halite, sylvite and calcite daughter minerals from sample Osb40; (B) MS brine inclusion with halite, sylvite, ferropyrosmalite daughter minerals from sample Osb36B ; (C) CO_2 inclusion from sample Osb37B; (D) LVD brine inclusion with cubic halite daughter from sample Osb22A; (E) LV brine inclusion from sample Osb37B.

accounting for up to 50% of the inclusion volume. A pale green, prismatic daughter mineral with high relief has been identified in previous studies as ferropyrosmalite (Dong and Pollard, 1997). A semi-opaque mineral with strong red colouration found exclusively in fluid inclusions in samples taken from the 1S ore zone is identified as hematite while in other inclusions a rounded opaque daughter mineral is tentatively identified as magnetite, due to slight movement upon proximity of a magnet.

2.4.1.3 Carbonic inclusions (CO_2)

The third population of inclusions consist of CO_2-rich carbonic inclusions (CO_2) (Fig 2.4c). Ranging in size from <5 to 40 μm (mean 10 to 15μm) the inclusions are monophase at room temperature with vapour bubbles nucleating upon cooling. CO_2 inclusions are equivalent to the type III inclusions (Table 2.3) of Adshead, (1995).

2.4.1.4 Moderate salinity inclusions (LVD)

LVD liquid-rich inclusions range in size from 10 to 40 μm and contain between two and four phases at room temperature (Fig 2.4d). They correspond to the type IIa pseudosecondary/secondary brine inclusions of Adshead, (1995) (Table 2.3). The majority are L+V+1-2D inclusions, with halite being the most common daughter mineral, although not always present, and sylvite also observed in some inclusions.

High $CaCl_2$ content is indicated by the formation of brown ice during freezing (Shepherd et al., 1985). Vapour bubbles occupy 5 to 15% of the inclusion. Trails of LVD inclusions cross-cut clusters of MS inclusions, suggesting that they can be considered to be a distinct temporal group, separate from the MS population (Fig. 2.8B;C;E).

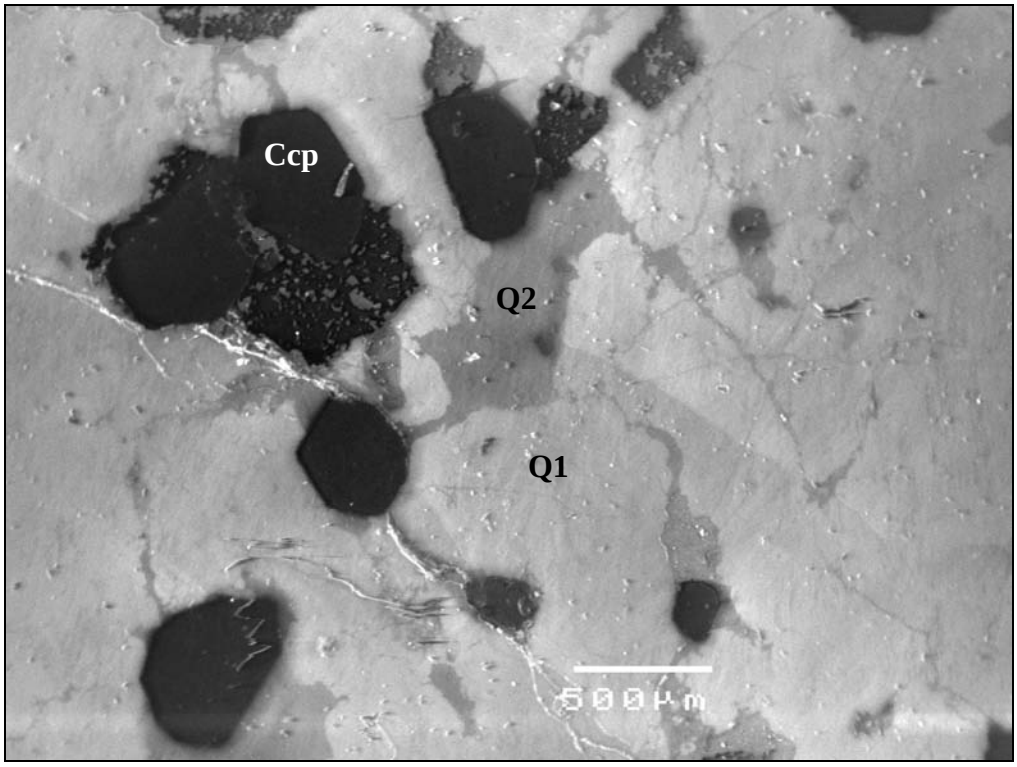

Figure 2.5: CL image of sample Osb22A
Sulphides are intergrown with a later generation of dark grey luminescing quartz.

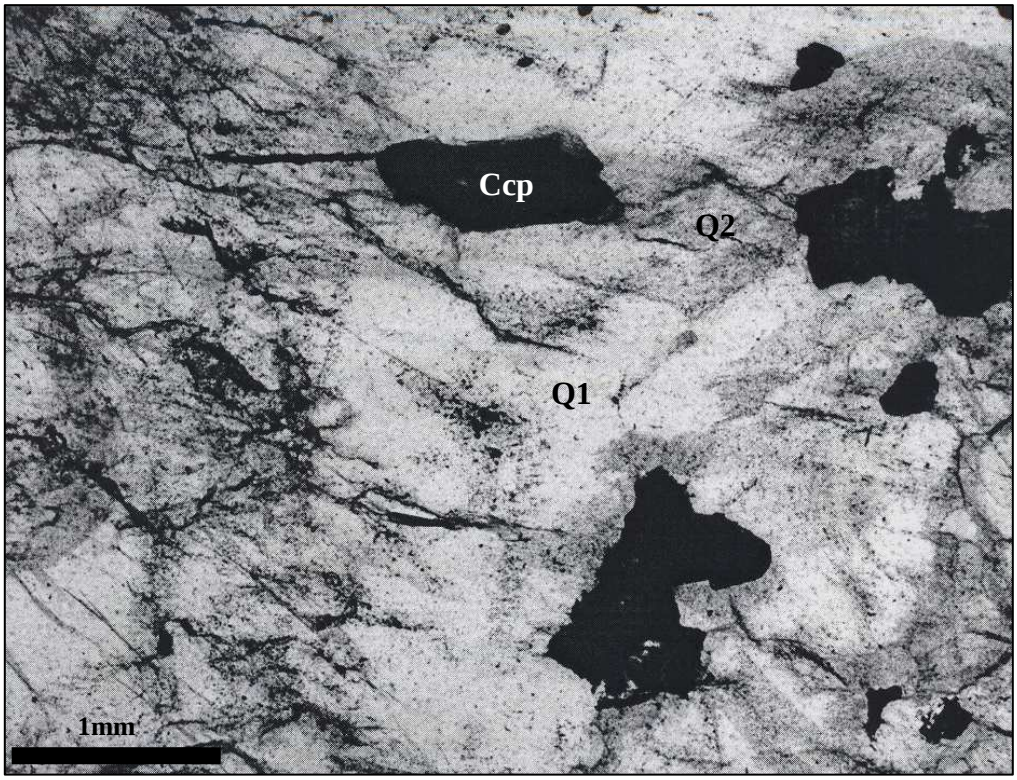

Figure 2.6: Sample Osb315 under plane polarized light.
Two generations of quartz can be observed with fluid inclusion poor quartz cross-cut by fluid inclusion rich quartz that appears to be associated with mineralisation, surrounding sulphide grains.

Davidson (1989)		Adshead (1995)		Dong (1995)		This Study
						CB $L_{aq} + L_{CO2} \pm V_{CO2} \geq 3S$ mixed brine and CO_2 Primary in Q1 Th >390 ^oC
Prograde Brine L + V + 2-4S brine Primary 42 – 57 wt% NaCl equiv. 416 – 483 ^oC	≈	**Type I** L + V + ≥ 2S brine Primary 65 – 82 wt% NaCl equiv. 425 – 505 ^oC	≈	**Type 1** L + V + nS (n = 2-6) Pre- and syn- mineralisation 33 – 60 wt% NaCl equiv. 260 – 505 ^oC	≈	**MS** L + V + ≥ 6S brine Primary in Q1 47 – 64 wt% NaCl equiv. 340 - >600 ^oC
Retrograde Brine L + V + 2-4S brine 31 – 50 wt% NaCl equiv. 457 – 514 ^oC	≠	**Type IIa** L + V ± 2S Pseudosecondary/secondary 20 - 37 wt% NaCl equiv. 220 – 400^oC	≈	**Type 2** L + V + nS (n = 1-2) Syn-mineralisation 6 -21 wt% NaCl + 15-25 wt% $CaCl_2$ (27 – 37 wt% salts total) 308 – 375 ^oC **Type 3** L ± V ± nS (n = 1-2) Post-mineralisation 16 – 32 wt% NaCl equiv. 98 - 220^oC	≈	**LVD** L + V ± 2S brine Primary in Q2/Q3 Pseudosecondary/secondary in Q1 17-38 wt% NaCl equiv. 100-292 ^oC
Prograde CO_2 L + V CO_2 Primary High density	≈	**Type III** CO_2 Primary		**Type 4** $CO_2 \pm CH_4 \pm H_2O$ / $CH_4 \pm H_2O$ Pre-, syn- and post-mineralisation	≈	**CO_2** L + V Primary/pseudosecondary in Q1 (rare secondary) 0.66-0.99 g/cc
		Type IIb CO_2 Secondary	≈			
		Type IV/V Monophase liquid	≈		≈	**LV** L + V brine (some monophase, not measured) Secondary in Q1, Q2 and Q3 1-12 wt% NaCl equiv. 98-250^oC

Table 2.3: Correlation of different fluid inclusion populations identified in studies of Osborne

2.4.1.5 Low salinity inclusions (LV)

LV inclusions observed are between <2 and 20μm in size and are mainly two phase liquid-vapour, in some cases monophase, at room temperature with a small (<10% vol.) vapour bubble (Fig 2.4e).

The fluid inclusion types identified at Osborne are comparable with populations identified in previous studies at Osborne (Table 2.3) and at deposits across the region (see Chapter 1, section 1.4.6).

2.4.2 Fluid Inclusion Paragenesis

Samples examined using cathodoluminescence showed two generations of quartz within the ore hosting silica-flooding. The earlier quartz (Q1), representing the main stage of silica flooding, is infilled and variably replaced by a second generation of quartz (Q2). The majority of sulphide grains are associated with this paragenetically later quartz (Fig. 2.5; 2.6). Late quartz veins (Q3) cut both generations of silica flooding (Fig 2.1C).

The fluid paragenesis was determined by identifying primary, pseudo-secondary and secondary fluid inclusions within the different generations of inclusions. Primary inclusions are those that form as the mineral forms, they can be isolated or form in trails along crystal faces. Pseudosecondary inclusions form in trails that within crystals and are recognised as not being truely secondary as the trails do not cross grain boundaries, the inclusions forming in fractures that formed before the grain as a whole had finished growing. Secondary inclusions develop after the mineral has formed and are generally observed in trails that cross-cut grain boundaries and other features. They often form within cracks that have resealed and are frequently small in size (Roedder, 1984; see Fig. 2.7).

2.4.2.1 Inclusion assemblages in pegmatites

The fluid inclusion assemblage in the pegmatites is very similar to that observed within the ore-associated silica flooding, with CB, MS and CO_2-types appearing to be primary inclusions within the primary magmatic quartz and while CO_2, LVD and LV inclusions are observed in secondary trails (Fig. 2.8). As the pegmatite samples are thought to form at the peak of metamorphism (Mark et al., 1998; Rubenach, 2005a) they can be considered to predate the mineralisation event, including silica flooding. Therefore it is possible that the quartz in the pegmatites could have been replaced during this event, which would mean that the inclusions entrapped in the pegmatites are the primary ore fluids associated with copper-gold mineralisation. In this case, while the inclusions appear primary, they would not be representative of fluids exsolved from the pegmatites.

2.4.2.2 Fluid inclusion assemblages in early quartz (Q1)

Primary CB, MS and CO_2 inclusions occur in Q1 quartz. The MS and CO_2 inclusions are commonly found in the same clusters and have been observed together in single within-grain trails (Fig. 2.8a; 2.9d Mustard et al., 2004). MS inclusions are also observed in isolation, in small gropus and on trails parallel to crystal face within grains (Fig. 2.8). CO_2 inclusions also occur as pseudosecondary, and rare secondary trails. LVD inclusions are present in secondary trails that radiate from and around sulphide grains and cross-cut the earlier Q1 quartz generation. The Q1 quartz generation predates the main phase of sulphide mineralisation so the fluids entrapped in primary inclusions can be considered to be pre-ore fluids.

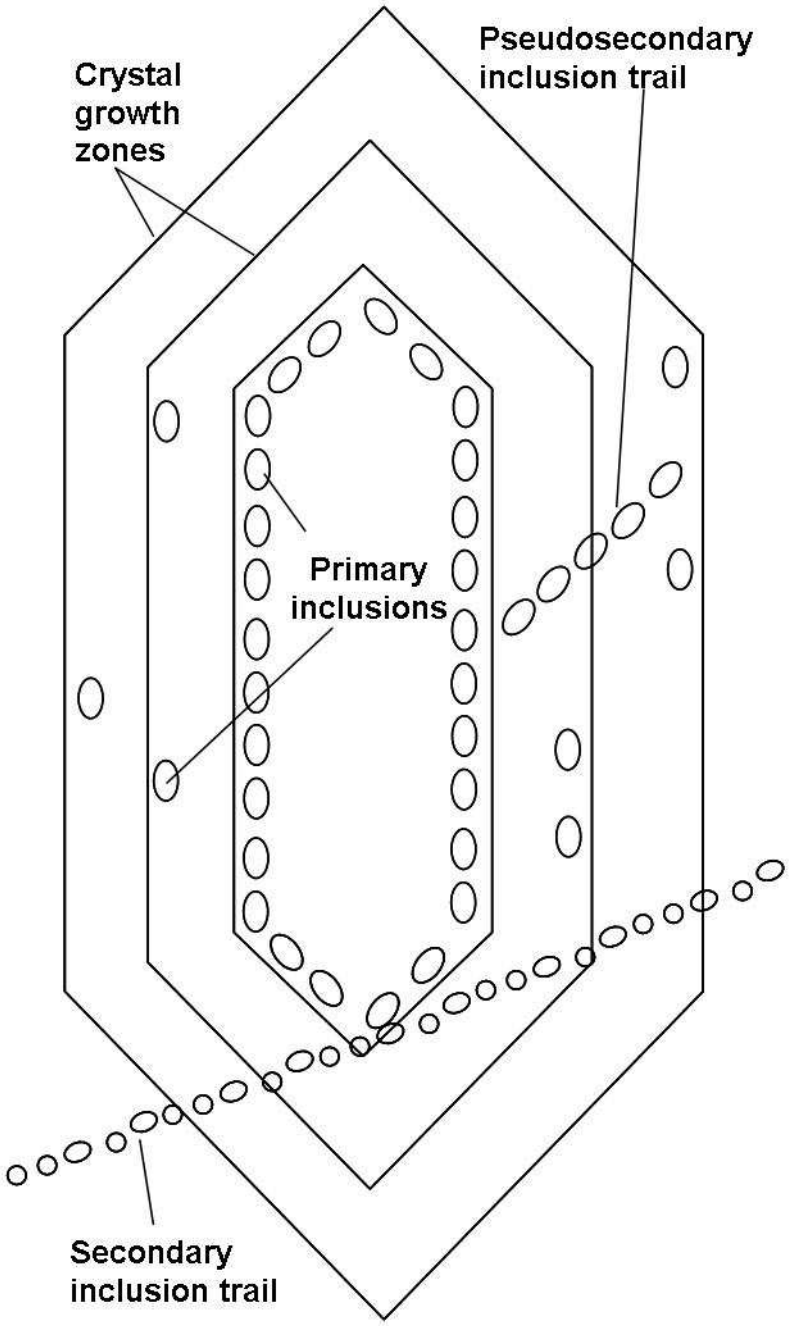

Figure 2.7: Schematic diagram showing primary, pseudosecondary and secondary inclusions in a single crystal.

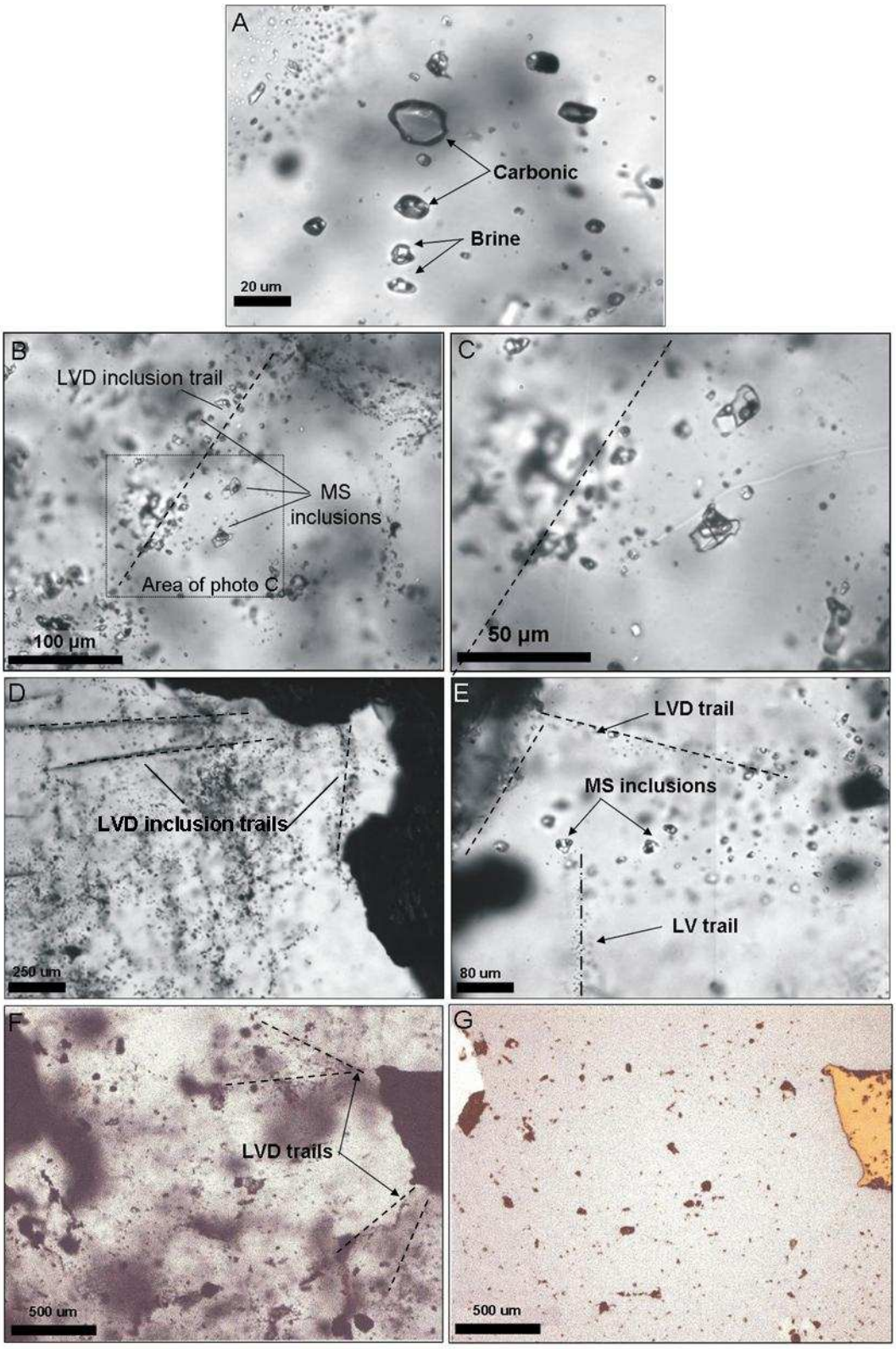

Figure 2.8: Fluid inclusion assemblages in Osborne silica flooding samples.
(A) Osb37B, unmixing trail contains both carbonic and brine inclusions in Q1 from Mustard et al., (2004); (B) Osb36B LVD inclusion trails cross-cut groups of MS inclusion: This relationship indicates that the LVD inclusions are temporally distinct from the MS inclusions; (C) Magnification of image B; (D) Osb15 secondary LVD trails run to/from a sulphide grain cutting through Q1; (E) Osb36B MS inclusion cluster cross-cut by secondary LVD and LV trails in Q1; (F) Osb36B, secondary LVD trails radiate from sulphides (G) Osb36B, picture F under reflected light, sulphide grain = chalcopyrite

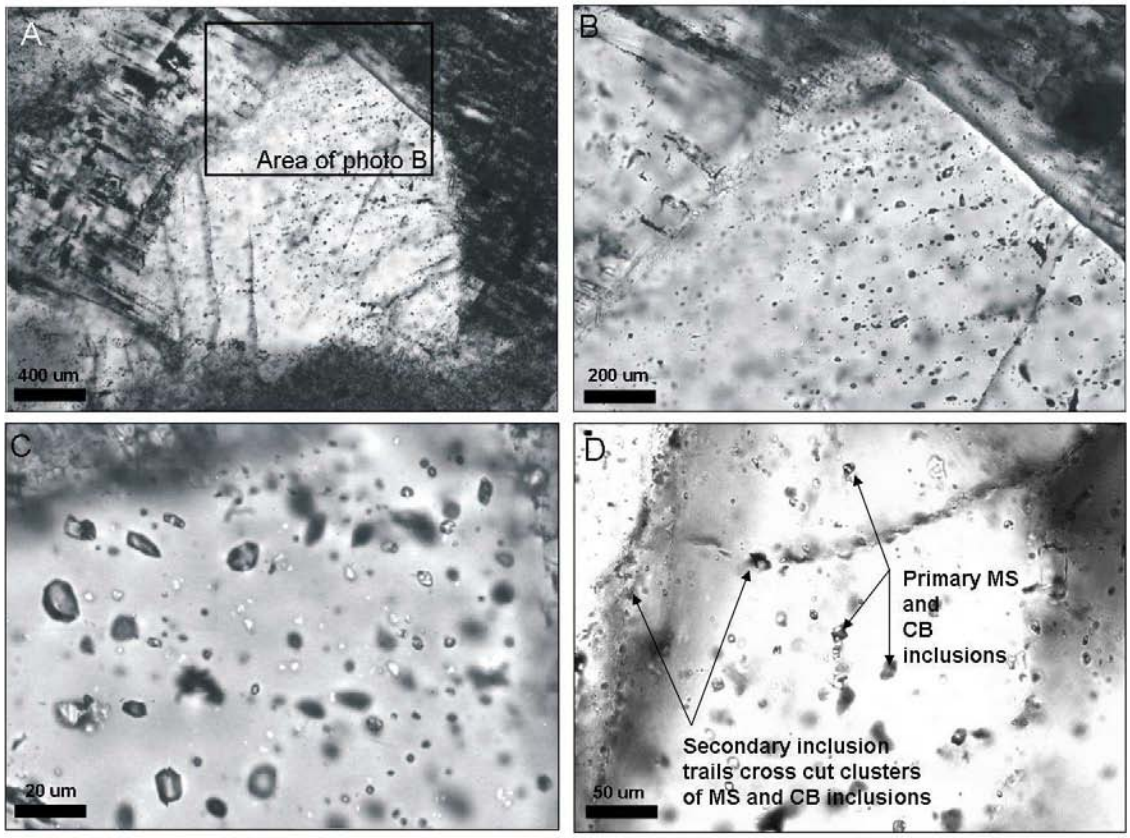

Figure 2.9: Fluid inclusion relationships in pegmatite samples
(A) Osb852, grain 1, pseudosecondary MS and CO_2 trails inclusions in quartz grain of pegmatite; (B) Magnified detail of Osb852, fluid inclusion trails do not cut grain boundaries and so are considered pseudosecondary; (C) Osb852, grain 2, fluid inclusion assemblage is dominated by primary CO_2 inclusions with some CB and MS inclusions; (D) Osb40, MS and CB inclusions in pegmatitic quartz appear to be primary and are cross-cut by trails of secondary LVD and LV inclusions.

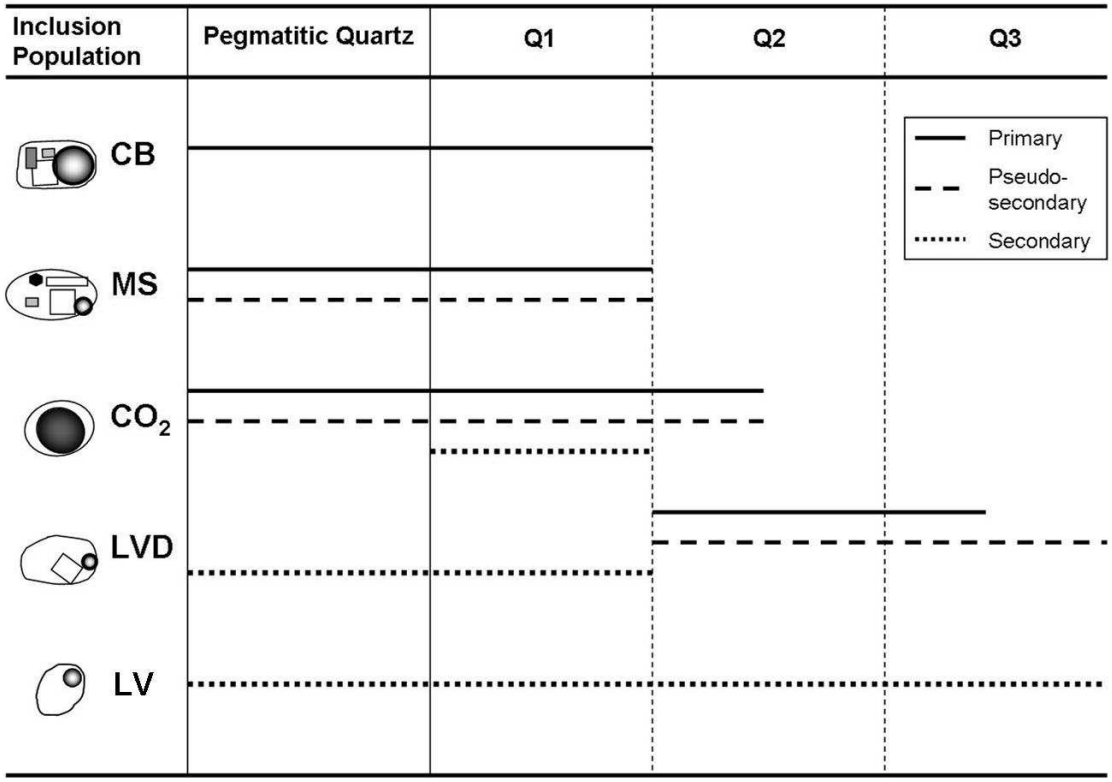

Figure 2.10: Fluid inclusion paragenesis.
Multiple generations of fluid inclusions are found as primary, pseudo-secondary and secondary populations within the successive generations of quartz in the Osborne ore assemblage and associated pegmatites (see also Fig 2.11).

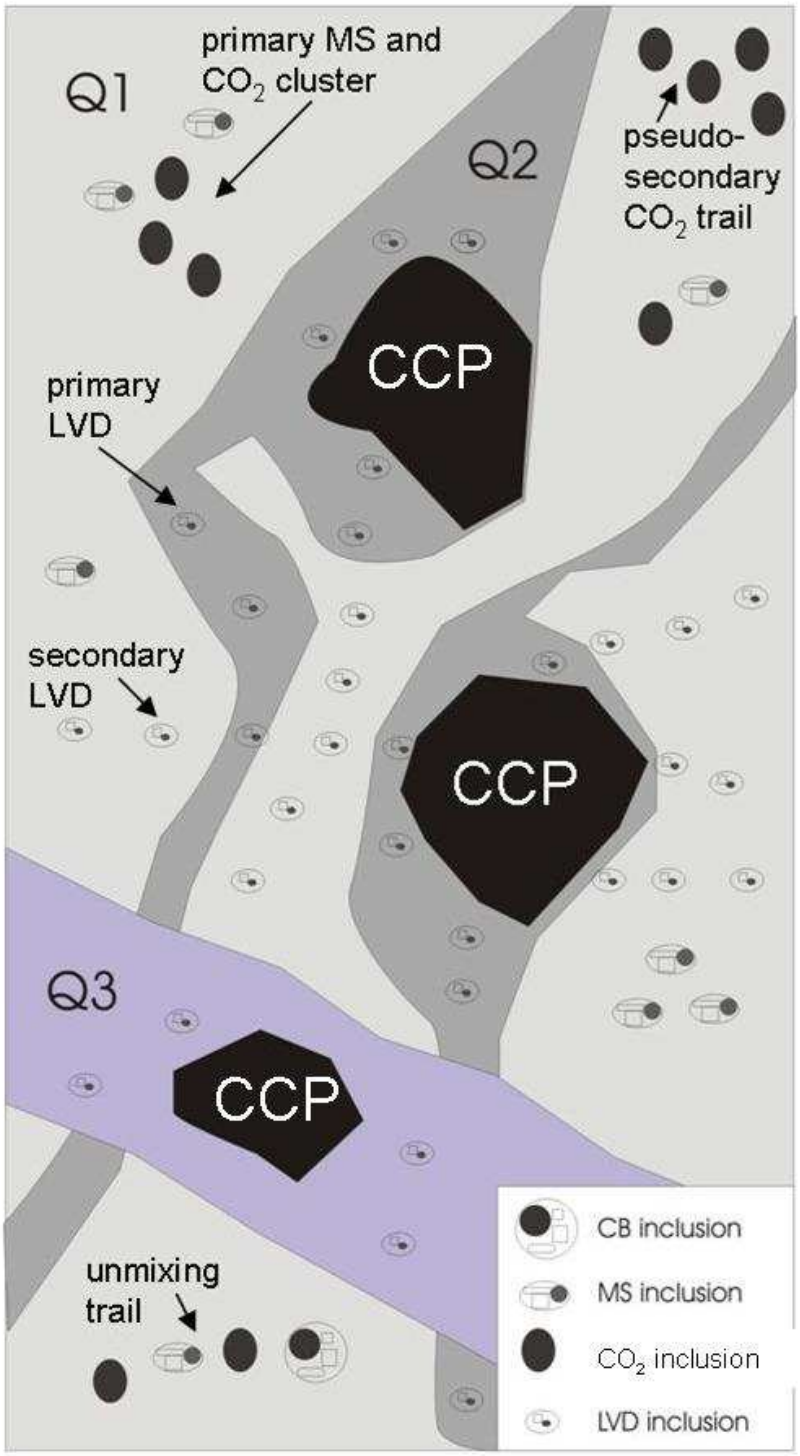

Figure 2.11: Schematic representation of fluid inclusion populations, relationships and occurrences in multiple generations of quartz in Osborne ore assemblages.
Three generations of quartz, Q1, Q2 and Q3, host 4 main populations of fluid inclusion associated with ore genesis. Key fluid inclusion relationships are highlighted including unmixing of the early CB fluid to form MS and CO_2 fluids. LVD inclusion trails radiate from sulphide grains. LVD inclusions are primary in Q2 and Q3, secondary in Q1.

2.4.2.3 Inclusion assemblages in later paragenetic stages

MS and CO_2 inclusions are absent or very rare in the second generation of quartz (Q2) and the cross-cutting veins. Primary LVD inclusions occur within Q2 quartz and are also observed in Q3 vein quartz. The LVD inclusions are most clearly associated with the sulphide mineralisation and so the fluids entrapped within them can be considered representative of the syn- and post-ore fluids. The typically small LV inclusions are found in trails that cross-cut all other features and are therefore considered to be a late secondary population which post-date all stages of ore deposition.

2.4.3 Microthermometry and Laser Raman data

2.4.3.1 Aqueous inclusions

Eutectic melting temperatures below -50 ^{o}C were recorded in MS inclusions indicating the presence of divalent salts, most probably $CaCl_2$ (Borisenko, 1977; Schiffries, 1990). The observed daughter minerals also indicate the presence of high concentrations of NaCl, KCl, $FeCl_2$ and SiO_2. Small volumes of volatiles were indicated by the formation and melting of clathrate phases between +0.9 and +13.8 ^{o}C (Appendix A). The range of temperatures suggests the clathrate present is dominantly CO_2 (as $CO_2.5^3/_4H_2O$; Shepherd et al., 1985). The presence of antarcticite must also be considered, but the distinctive brown colouration is not observed.

While many MS inclusions decrepitated prior to homogenization, those that homogenised followed a general sequence. The MS inclusions totally homogenised at temperatures from ~200 ^{o}C to greater than 600 ^{o}C (exceeding the heating limit of the stage). In the majority of inclusions the first phases to homogenise were the vapour and sylvite; sylvite dissolution occurred between 45 to 250 ^{o}C with most values in the 150 to

250 ^{o}C range, whereas the vapour bubble disappeared between 90 and 505 ^{o}C with the majority of values clustering between 100 and 200 ^{o}C (Fig. 2.12A). Final homogenization of inclusions was by dissolution of halite and, where present, of ferropyrosmalite. Halite dissolved between 200 and 530 ^{o}C with most values falling between 300 and 450 ^{o}C (Figure 2.13). Decrepitation prior to homogenisation predominantly occurred after halite dissolution and prior to ferropyrosmalite dissolution. The majority of ferropyrosmalite daughter minerals do not dissolve and many inclusions containing a ferropyrosmalite daughter mineral decrepitated without homogenising. Where ferropyrosmalite dissolution occurred it was recorded between 230 and 530 ^{o}C with a mode in the 400 to 500 ^{o}C interval (Fig. 2.13). In inclusions containing $CaCl_2$ a transformation of ferropyrosmalite to clinopyroxene has been reported upon heating (Koděra et al., 2003). Dong and Pollard, (1997), reported the dissolution of ferropyrosmalite in fluid inclusions from Cannington between 430 and 500 ^{o}C followed by the formation of a new insoluble phase. This reaction is not observed in Osborne samples, which may be due to the limited dissolution of the phase or to Ca concentrations not being high enough to promote the formation of hedenbergite.

A peak in both total homogenization and decrepitation temperatures for the MS inclusions is seen between 400 and 500 ^{o}C (Fig. 2.14). However, many of these inclusions neither decrepitated nor homogenised below 600 ^{o}C suggesting a bimodal distribution. Many of these higher temperature inclusions are identical in appearance to those that homogenise between 400 to 500 ^{o}C. In the absence of Fe-bearing daughter minerals (e.g. ferropyrosmalite, magnetite, hematite), the MS inclusions homogenise by disappearance of halite with estimated salinities of <64 wt% NaCl. Homogenisation

temperatures are minimum temperatures of trapping, with the difference between measured and true values a function of pressure (Roedder and Bodnar, 1980). However the variation in homogenisation temperatures is over 200^{o}C and is unlikely to solely represent differences in trapping pressures, and may be due to fluid cooling prior to mineralisation. The estimated salinity for MS inclusions calculated by phase volumetric methods ranges between 65.8 to 73 wt% total salts (Fig. 2.14; Adshead, 1995).

The LVD inclusions homogenise between 98 and 292 ^{o}C. During the heating cycle the first phase changes observed were the dissolution of a sylvite daughter mineral, where present, and homogenization of the vapour phase. Sylvite dissolved between 45 and 196 ^{o}C with most values falling between 80 and 140 ^{o}C, while the vapour phase disappeared between 89 and 210 ^{o}C with a peak in data in the 120 to 160 ^{o}C interval. The final phase change, which for most inclusions was homogenisation rather than decrepitation, was the dissolution of halite which occurred between 98 and 292 ^{o}C, with the majority of values clustering between 140 and 200 ^{o}C (Fig. 2.12; 2.13). A small proportion of inclusions within this group are liquid-vapour only and their microthermometric results have been grouped with the LVD inclusions due to their spatial association with LVD trails, similar high salinities and high Ca content indicated by brown ice. Salinities, calculated from halite dissolution and ice-melting temperatures using the equations of Bowers and Helgeson (1983), Bakker (2003) and Potter et al., (1977), fall between 17 and 38 wt% with a peak between 20 to 26 wt% and a second peak at 32 to 34 wt% (Fig. 2.14; 2.15). The classification of inclusions from both these sub-populations as a single population is supported by there occurrence in the same inclusion trails.

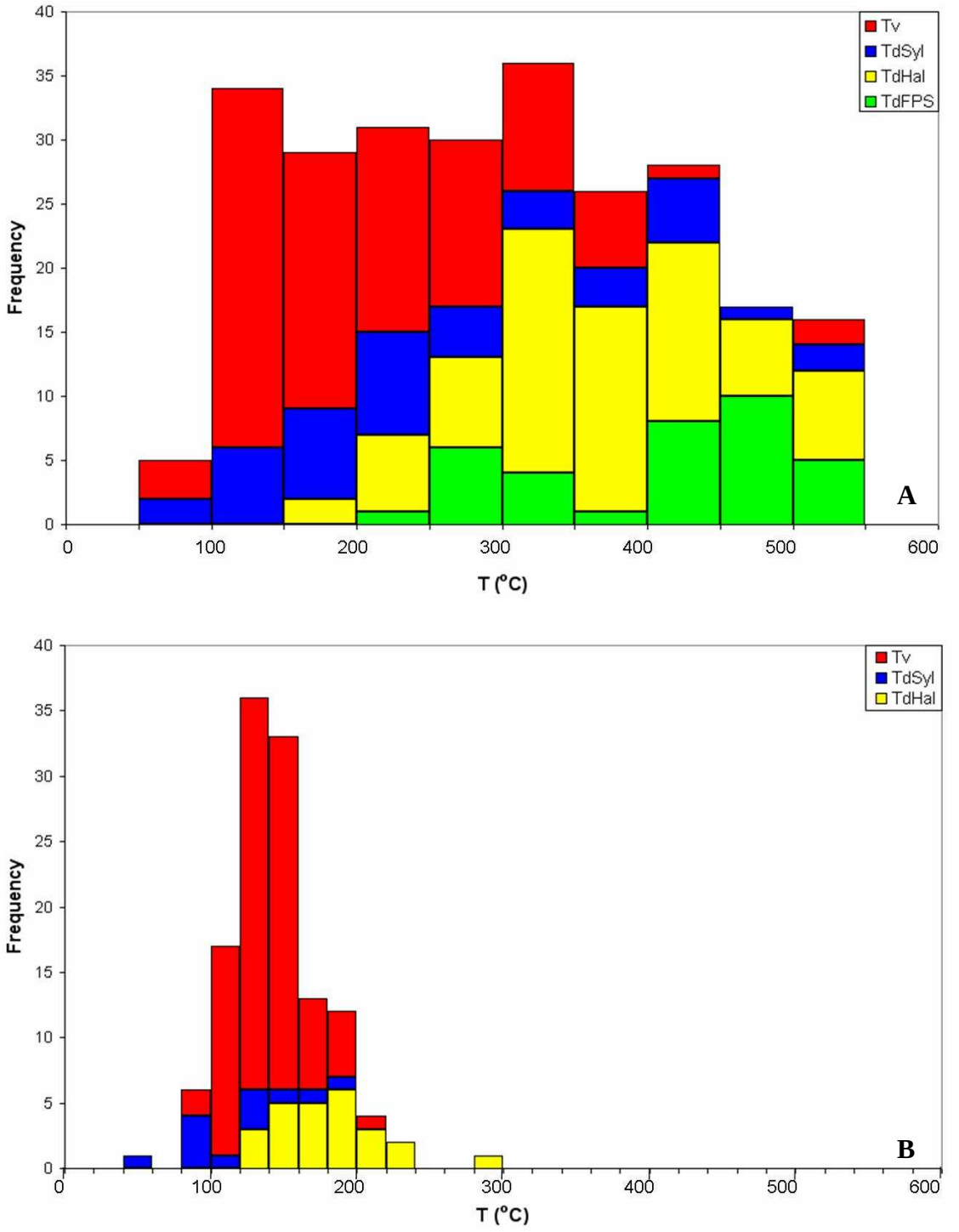

Figure 2.12: Histograms of vapour and daughter mineral dissolution temperatures.
(A) MS inclusions, $Th_{vapour}<Th_{syl}<Th_{hal}<Th_{fps}$, final homogenization occurs by dissolution of halite or ferropyrosmalite. Inclusions with magnetite and hematite daughter minerals decrepitated without homogenising.
(B) LVD inclusions, $Th_{vapour} \approx Th_{syl} <Th_{hal}$, homogenization is completed by halite dissolution (see Appendix A)
.
Tv = Th vapour; Td_{syl} = Temperature of sylvite dissolution; Td_{Hal} = Temperature of halite dissolution; Td_{FPS} = Temperature of ferropyrosmalite dissolution

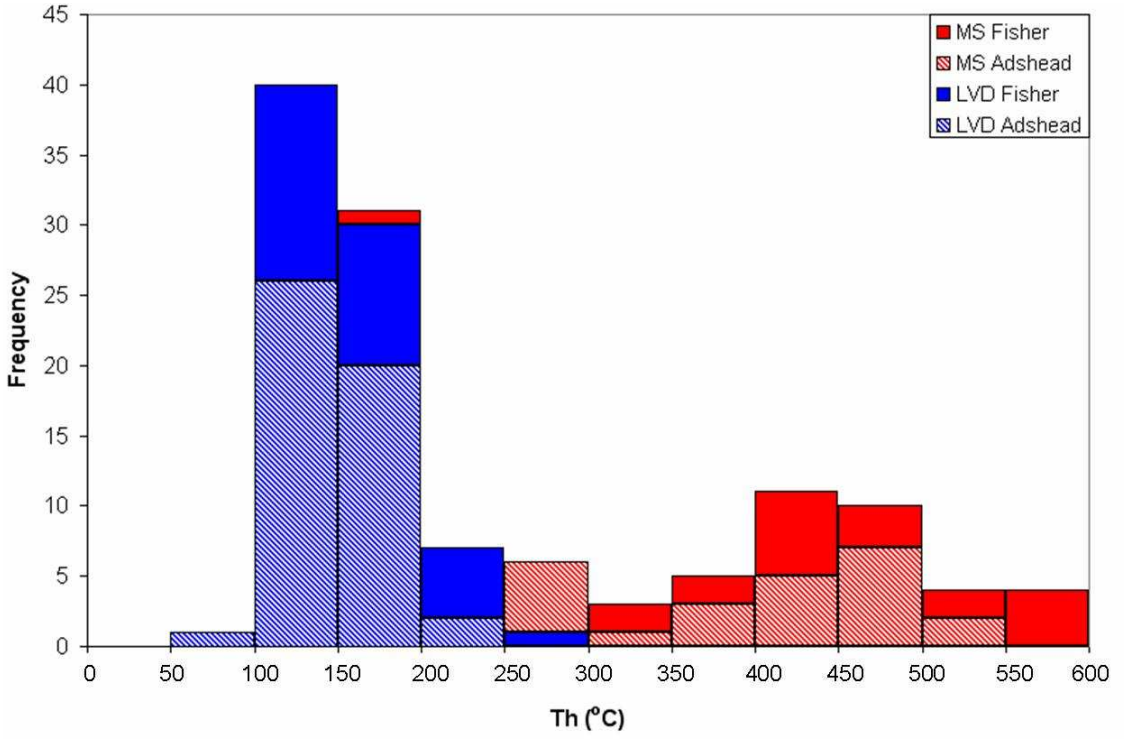

Figure 2.13: Histogram of homogenisation temperatures.
Overall Th of MS and LVD measured in this study compared with data from Adshead (1995).

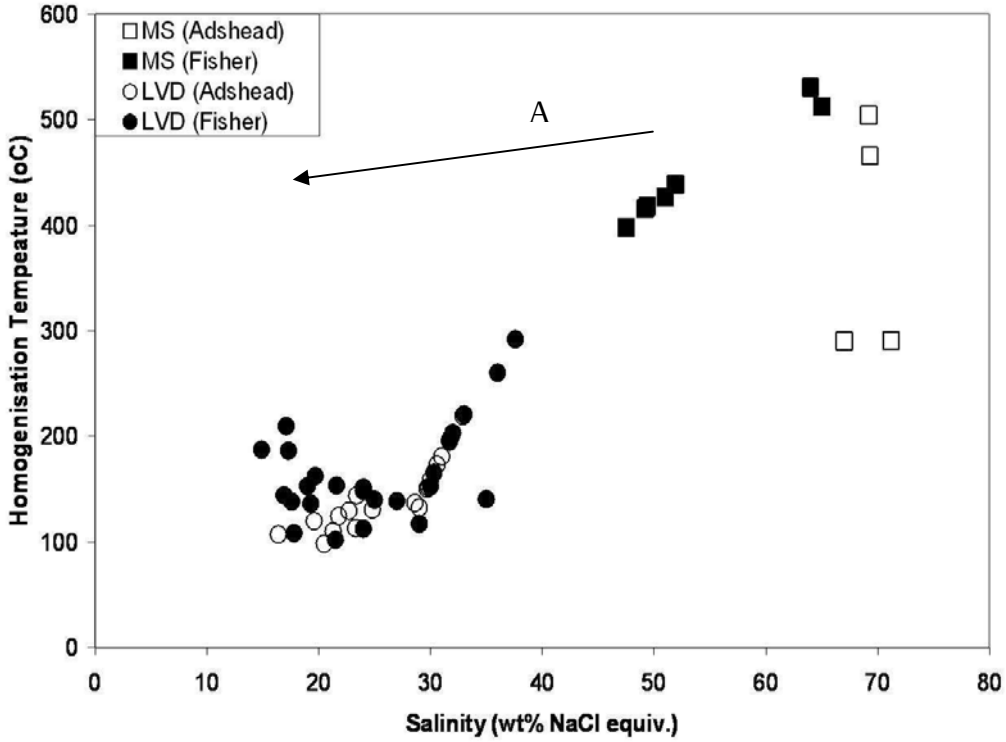

Figure 2.14: Homogenisation temperature vs salinity.
Data from this study (Fisher) are plotted along with data from Adshead (1995). A decrease in salinity can be observed as fluids evolve with time (path A). A decrease in temperature may have also occurred. The absence of data showing fluids with salinities between 40 and 50 wt% salts could be interpreted as evidence that these are two distinct fluids and do not represent an evolution. However, two different calculations are used to determine salinities in the LVD and MS-type inclusions. The apparent gap may be an artefact of this process. It should also be noted that many of the MS inclusions decrepitate without homogenising so a full data set can not be presented. Some of the trend identified within both MS and LVD inclusions may only be a decrease in homogenization temperature and not a true cooling.

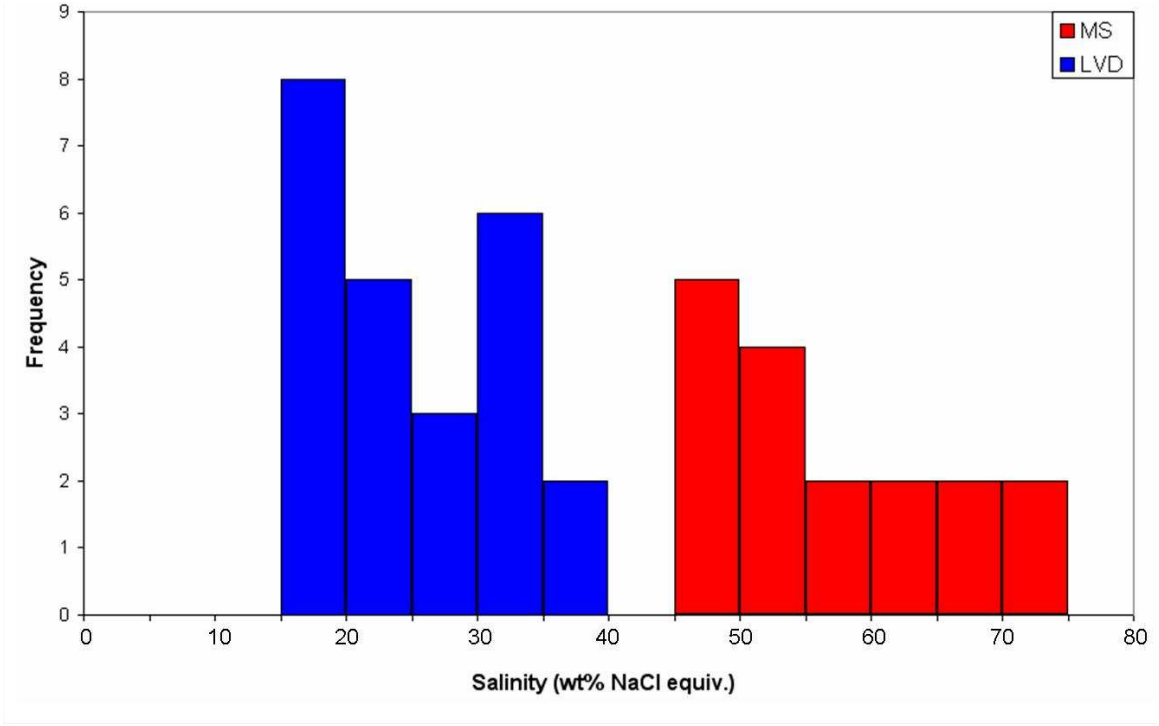

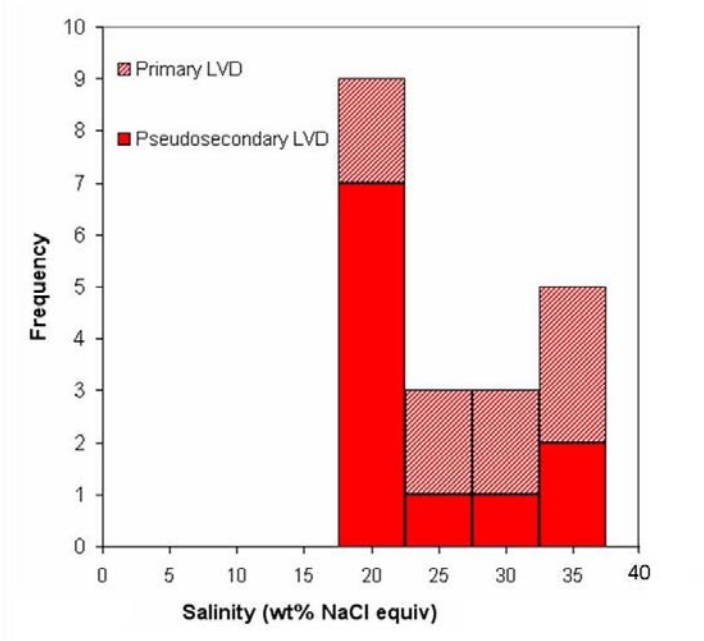

Figure 2.15: Histograms of fluid inclusion salinities
LVD inclusions have salinities between 17-38 wt% NaCl equiv., while MS inclusions have salinities between 47-72 wt% NaCl equiv. Data plotted is from microthermometric data only.
Second histogram shows distinction between LVD salinities measured in pseudosecondary inclusions (in Q2) and primary inclusions (in Q3). The two populations show similar distribution suggesting the fluid observed in late quartz veins (Q3) may be the same as in pseudosecondary inclusions that radiate from sulphides hosted in the later phase of silica flooding (Q2).

2.4.3.2 Carbonic phases

The solid CO_2 phase in CO_2 and CB inclusions melts between -63 and -56.6 ^oC with most values clustering around -57.5 to -56.6 ^oC (Fig. 2.16). Homogenisation of the carbonic phase to liquid occurs over a wide temperature range from -12.7 to +28.5 ^oC, with the greatest range observed exhibited by pegmatite hosted inclusions. The majority of ore lens-hosted inclusions homogenise between +5 to +20 ^oC, with a peak between +10 and +15 ^oC (Fig. 2.17). Inclusions from the 1S ore lens have the lowest homogenisation temperatures while highest temperatures were measured in the 3E ore lens. The 1S ore lens samples show the greatest range of values. CB inclusions have a higher average homogenization temperature than CO_2 inclusions although final melting temperatures exhibit the same range as for CO_2 inclusions in the same samples (Fig 2.18).

Complete homogenization of a CB inclusion (to the liquid state) was observed in only one case and occurred at 392 ^oC, and the majority of inclusions decrepitated without homogenising or did not completely homogenise by 600^oC which is the limit of the microthermometric stage. Shepherd et al., (1985) demonstrated that where CO_2-bearing brines containing more than 50 wt% CO_2 homogenise to the liquid state, they do so at very high internal pressures and consequently decrepitation is likely to occur before complete homogenisation.

A preliminary Laser Raman study was conducted on CB and CO_2 inclusions in the pegmatite sample Osb40 to determine whether the differences in behaviour observed between CB and CO_2 inclusions (see above) could be attributed to compositional variation. The compositions of vapour phases in MS brine inclusions were examined in

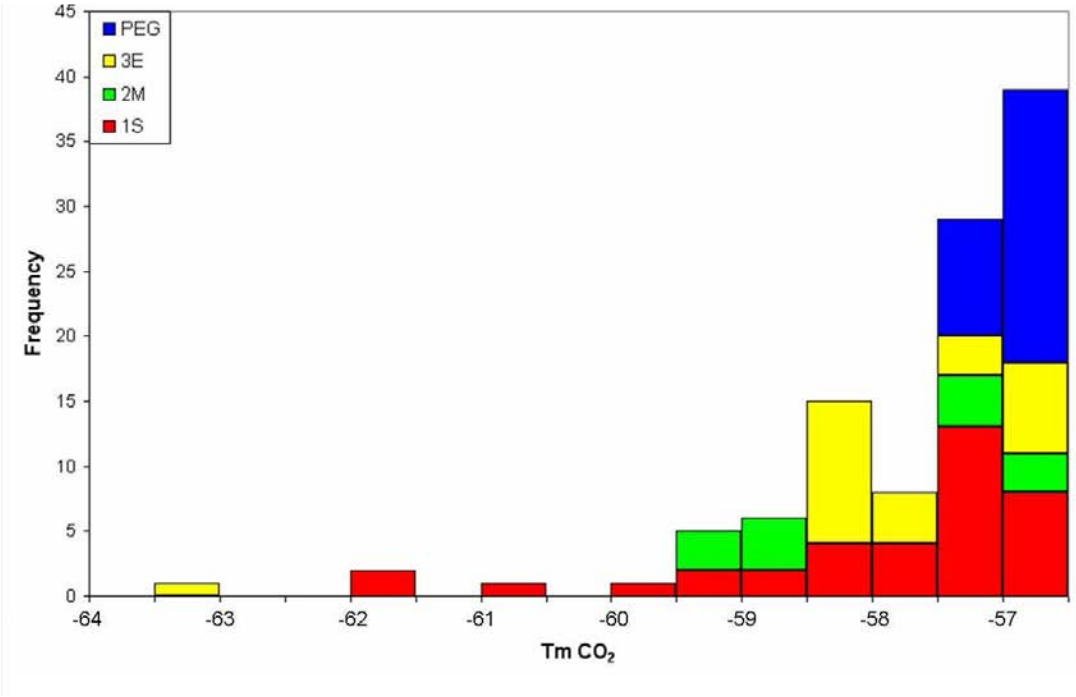

Figure 2.16: Final melting temperatures for CO_2 inclusions.
Inclusions are hosted by samples from 3 ore lenses and pegmatites.

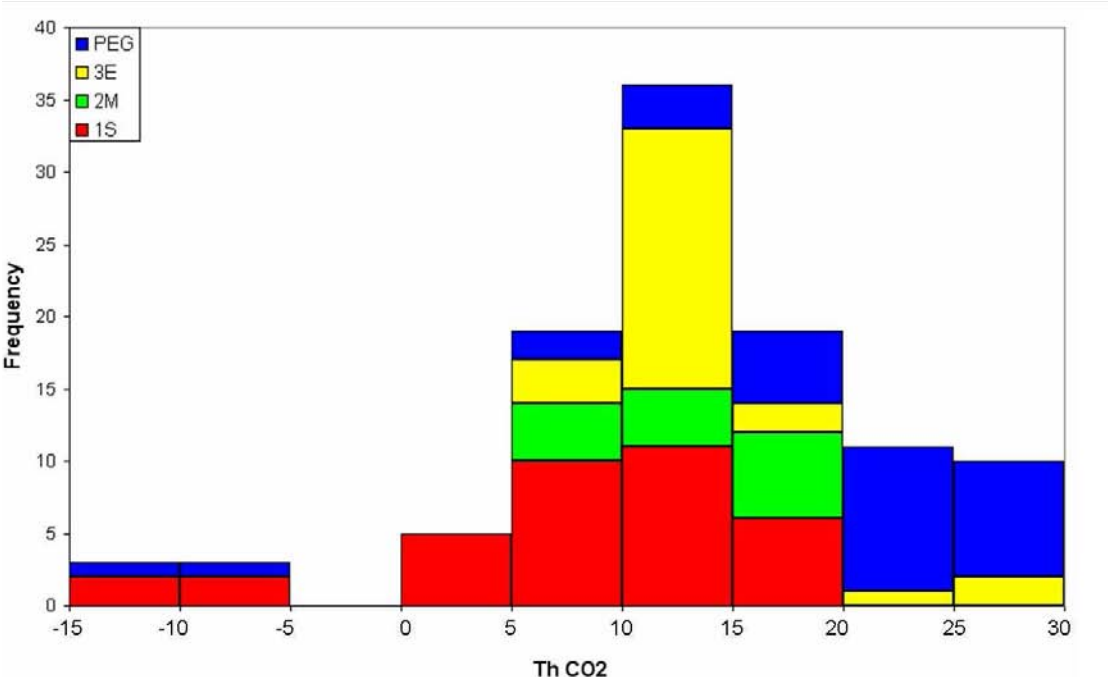

Figure 2.17: Homogenisation temperatures of CO_2 inclusions.
Homogenisation was to the liquid phase in all cases. The majority inclusions from pegmatite samples homogenise at higher temperatures than those from ore samples. The lowest homogenization temperatures were measured in a 1S sample.

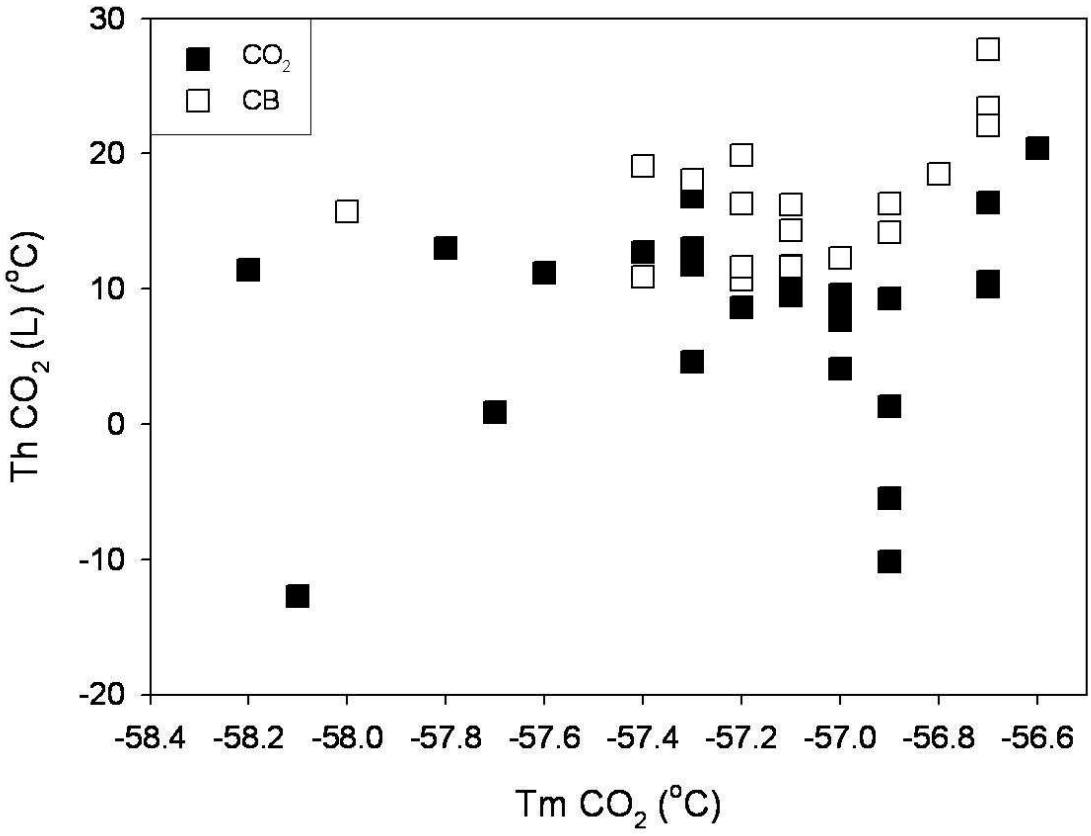

Figure 2.18: Comparison of microthermometric behaviour of CB and CO_2 inclusions.
When Th and Tm values for the carbonic phase in CO_2 and CB inclusions from sample Osb40 are plotted a distinction is observed between the two inclusion types. This suggests differences in pressure or composition. Pressure calculations for the CB inclusions show higher pressures than for the majority of CO_2 inclusions (Fig. 2.19) and laser Raman data (Fig. 2.18) show no consistent composition differences suggesting this behaviour can be attributed to interactions between the carbonic and saline phases in the mixed CB inclusions.

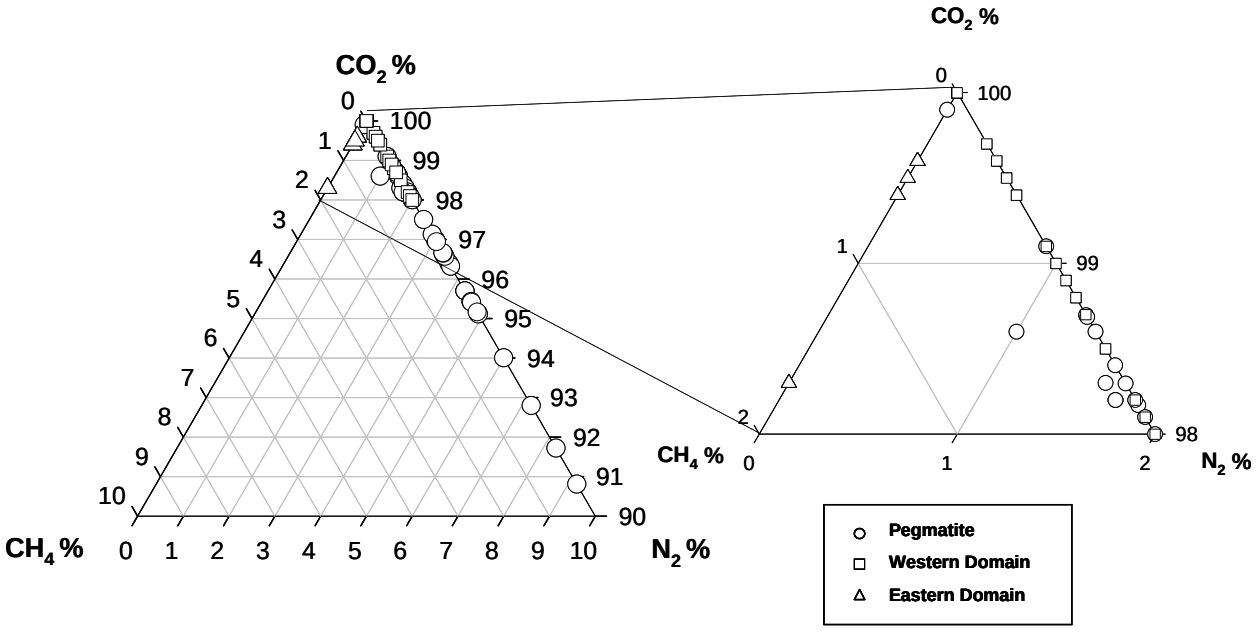

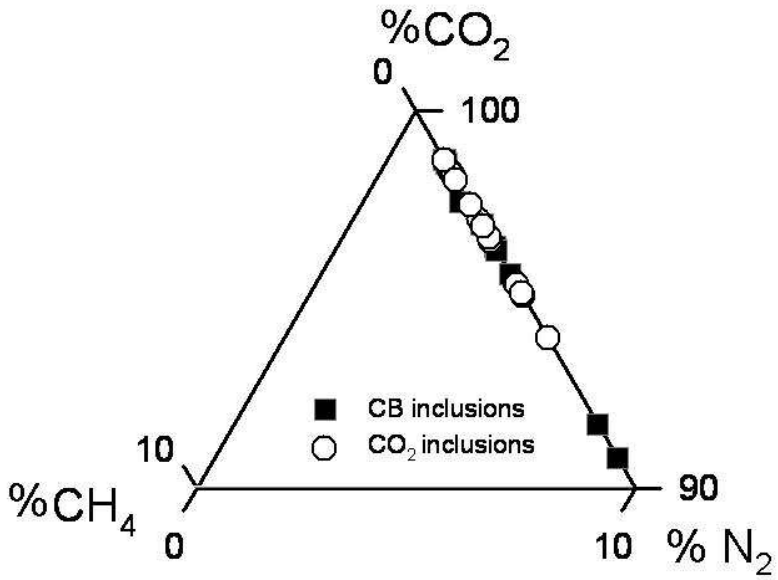

Figure 2.19: Laser Raman determined compositions of carbonic inclusions within ore and pegmatite samples.
Data for CB and CO_2 inclusions from sample Osb40, plotted on the lower diagram, show that the compositions of the two inclusion types are similar and thus compositional differences can not account for the variation in thermometric behaviour noted in Fig. 2.17. A full laser Raman data set is presented in Appendix C

.
a limited number of inclusions. Additional Laser Raman data from CO_2 inclusions in samples Osb15, Osb20, Osb37B and Osb852 were collected by Roger Mustard (unpublished data).

The deviation from the pure CO_2 melting temperature (-56.6 ^oC) indicates that the carbonic fluid system is not pure CO_2 (Duan et al., 1992; Duan et al., 1996). This is confirmed by Laser Raman data which show up to 9 mol% minor gases in the carbonic fluid (Fig. 2.19). CO_2 inclusions from the pegmatites and the more oxidised Western domain ore lenses contain minor amounts of nitrogen (N_2), with the ore lens samples containing <2 mol% N_2 and the pegmatite-hosted inclusions containing <9 mol% N_2. A few CO_2 inclusions within the pegmatites also contain minor methane (<0.4 mol%).

Greater amounts of CH_4 are measured in CO_2 inclusions from the reduced Eastern domain 3E ore lens, with concentrations of <1.7 mol%. N_2 was not found in the Eastern domain samples. A previous Laser Raman study of Osborne samples identified carbonic inclusions dominated by CH_4 and MS-type inclusions with CH_4 vapour (Dong, 1995). The occurrence of these inclusions was restricted to Eastern domain samples.

2.5 Discussion

Information on the physical conditions under which the successive generations of fluid inclusions were trapped and compositional data were obtained through microthermometric and Laser Raman analysis (Table 2.4).

Type	Phases	Primary/ Secondary	Chemical data	Th (°C)
CB	$L_{aq} + L_{CO2} \pm V_{CO2} \pm H \pm Syl \pm C$	Primary	Inclusions decrepitate before homogenizing, <60% salts estimated volumetrically (Adshead, 1995)	>390
MS	L + V + H ± Syl ± FPS ± C ± Hem ± Mag ± Ukn	Primary	47-64 wt% NaCl equiv.	>340
CO_2	L + V	Primary / pseudo-secondary, rare secondary	Densities of 0.66 – 0.99 Contain minor CH_4 and/or N_2	-
LVD	L + V ± H ± Syl	Secondary in early paragenetic stages, primary in late paragenetic stages	17-34 wt% NaCl equiv.	100-292
LV	L + V	Secondary in all samples	1-12 wt% NaCl equiv.	90-250

Table 2.4: Summary of microthermometric data for all fluid inclusion types.
Daughter minerals include H = halite; Syl = sylvite; FPS = ferropyrosmalite; C = calcite; Hem = hematite; Mag = magnetite; Ukn = unknown

2.5.1 Pegmatite anatexis and fluids

The pegmatites at Osborne have been interpreted as a product of anatexis of albitised gneisses synchronous with peak metamorphic conditions at ~1595Ma (Mark et al., 1998; Kennedy, 2000; Rubenach, in press). The fluid inclusion assemblages in the pegmatites are similar in appearance to those in the ore hosting silica flooding. Petrographically the CB, MS and CO_2 inclusions appear to represent primary fluid phases in the melt, although it is possible that the silica flooding may have recrystallised the quartz in the pegmatites meaning that these primary inclusions did not exsolve from the pegmatite melt (see section 2.4.2.1). However, in studies of unmineralised pegmatites elsewhere in the Eastern Fold Belt, a similar assemblage of saline and CO_2-bearing brine inclusions has been observed (Bertelli, 2007) although overall salinities are lower than observed at Osborne.

There is a distinction in the compositions of the carbonic phase, in CB and CO_2, observed between pegmatite hosted inclusions and ore sample hosted inclusions, with

the pegmatite-hosted carbonic inclusions containing greater amounts of N_2 compared with the ore-hosted inclusions. As this nitrogen is inferred to be derived from melting of micas (see below) during pegmatite anatexis this can be considered evidence for the preservation of primary pegmatite quartz and fluid inclusions. No studies have been undertaken of the nitrogen content of the micas at Osborne, however, studies of micas in similar environments have documented such processes (e.g. Andersen et al., 1993; Sadofsky and Bebout, 2000). As the pegmatite samples are taken from horizons within the mineralisation if the quartz had been recrystallised during silica flooding you would expect to find similar quantities of N_2 in inclusions in the silica flooding inclusions. Immiscibility and exsolution of fluids from the melt has been found to be a phenomenon that occurs during cooling or decompression, or as a result of the crystallization of volatile free solids (Burnham, 1979).

A decrease in pressure and temperature after the peak of metamorphism could have caused the exsolution of a fluid phase in the anatectic melt. Rapid decompression is also invoked as a cause of the extensive quartz precipitation that formed the ore-hosting silica flooding at Osborne (Adshead, 1995). Adshead (1995) postulated that this sudden decrease in pressure may be the result of movement on faults.

Differences are observed in the composition of the carbonic phase in the CB and CO_2 inclusions in the ore lens hosted samples and the pegmatite samples. The sulphide associated and vein quartz samples host a carbonic fluid that is CO_2 rich with minor CH_4. In the pegmatitic quartz, however, the minor phase is N_2. As the inclusions appear to be primary they would most probably record the derivation of local volatile species from the rocks that were melting. It has been documented that NH_4^+ groups can

substitute for K^+ in the structure of some silicate minerals, including K-feldspar, biotite and white mica (Dubessy et al., 1989; Andersen et al., 1993; Moine et al., 1994; Sadofsky and Bebout, 2000; Cesare et al., 2007). Up to 900ppm NH_4^+ or NH_3 has been measured in biotites (Cesare et al., 2003) and the melting of NH_4^+-bearing biotites during anatexis would release either N_2 or NH_3 into the fluid (Moine et al., 1994). In the presence of natural fluids the concentration of nitrogen in the fluids is controlled by the following reaction:

$$N_2 + 3H_2O + 2H^+ = 2NH_4^+ + 3/2O_2 \qquad \text{(Moine et al., 1994)}$$

Or $$N_2 + 2H^+ + 3H_2 = 2NH_4^+$$

This relationship implies the N_2 concentration will be controlled by oxidation state. The rock assemblage at Osborne is not thought to have reached conditions that would melt biotite (French, 1997; Rubenach et al., 2001), so the nitrogen in the fluids is most likely sourced from melting of muscovite.

The similarities between the fluid inclusion assemblages observed in ore and pegmatite samples suggest that the pegmatites may have been a source of hydrothermal fluids to the deposit, with the reduction of the NH_4 prior to entrapment in the silica flooding. Fluid-rock reactions with the banded ironstones offer one potential method of reduction. Alternately the diffusion of H_2 out of the inclusions, as documented by Mavrogenes and Bodnar, (1994), may have resulted in N_2 becoming the stable gas. The presence of magnetite and hematite in the banded ironstones that host the upper portion of the 1S ore lens would have buffered the f_{O_2} of a fluid if it had reached equilibrium with the

rocks. Therefore CO_2:CH_4 ratios, which are also controlled by f_{O_2}, in the carbonic fluids analysed by laser Raman should reflect interaction with this buffer:

$$8Fe_3O_4 + CO_2 + H_2O \leftrightarrow 12Fe_2O_3 + CH_4$$

Although it should be noted that the CO_2:CH_4 buffer will be stabilised at lower fO_2 values than magnetite-hematite so that CO_2 will also be stable in the presence of magnetite within a narrow range of fO_2 conditions. Adshead et al., (1998) noted that specular hematite is not a consistent component of the banded ironstones, instead having an irregular distribution. The occurrence of hematite could be the result of variable reaction of the ironstones with CO_2-bearing fluids. The variable CH_4 content of the carbonic fluid, measured by laser Raman in this and previous studies (Section 2.4.3; Dong, 1995) reflects the sporadic distribution of hematite. The presence of CO_2 should stabilise hematite, while CH_4 promotes the stability of magnetite. The dominance of magnetite in the presence of a mainly CO_2-rich fluid is interpreted as evidence of disequilibrium at Osborne.

Alternately the predominance of CO_2 may be the result of post-entrapment processes, namely the loss of H_2 by diffusion (e.g. Mavrogenes and Bodnar, 1994). Hall and Bodnar (1990) studied the effect of varying f_{H_2} on CO_2:CH_4 ratios in fluid inclusions and suggested that CH_4 measured in inclusions trapped in granulite facies are the product of H_2 infusion into the inclusions during metamorphism. H_2 diffusion out of inclusions has also been documented, with Mavrogenes and Bodnar (1994) demonstrating that such diffusion will result in Cu-sulphide daughter minerals not dissolving upon microthermometric heating. Such an effect may explain why, in this study, many

inclusion containing ferropyrosmalite or opaque minerals (presumed to be magnetite) decrepitated prior to homogenisation. No significant differences are noted between the thermometric behaviour and apparent compositions of the primary, pseudosecondary and secondary carbonic fluids suggesting multiple pulses of fluid throughout precipitation of the silica flooding.

2.5.2 Trapping Conditions

2.5.2.1 Data quality

The vapour homogenisation and halite dissolution and final homogenisation temperatures measured by microthermometry (Appendix A) for CB, MS and LVD-type fluid inclusions are used to calculate isochores and estimate the pressure and temperature conditions at which the fluid inclusions were trapped. Isochores are calculated using the BULK and ISOC programs (Bakker, 2003), which compile the equations of state for a number of different salt systems over a range of pressure and temperature conditions.

Due to difficulties in quantifying the proportions of the different salts present in the system by microthermometry the isochores have been calculated for the H_2O-CO_2-NaCl system. This assumption will increase the errors associated with the plotted solvus and isochores as will the presence of small amounts of CH_4 and N_2 in the carbonic phase indicated by Laser Raman (section 2.4.3). The Osborne deposit is thought to have formed at near peak-metamorphic conditions; thermodynamic data for high pressure and temperature systems is extremely limited which will restrict the extent to which this data can be used to interpret fluid conditions at Osborne.

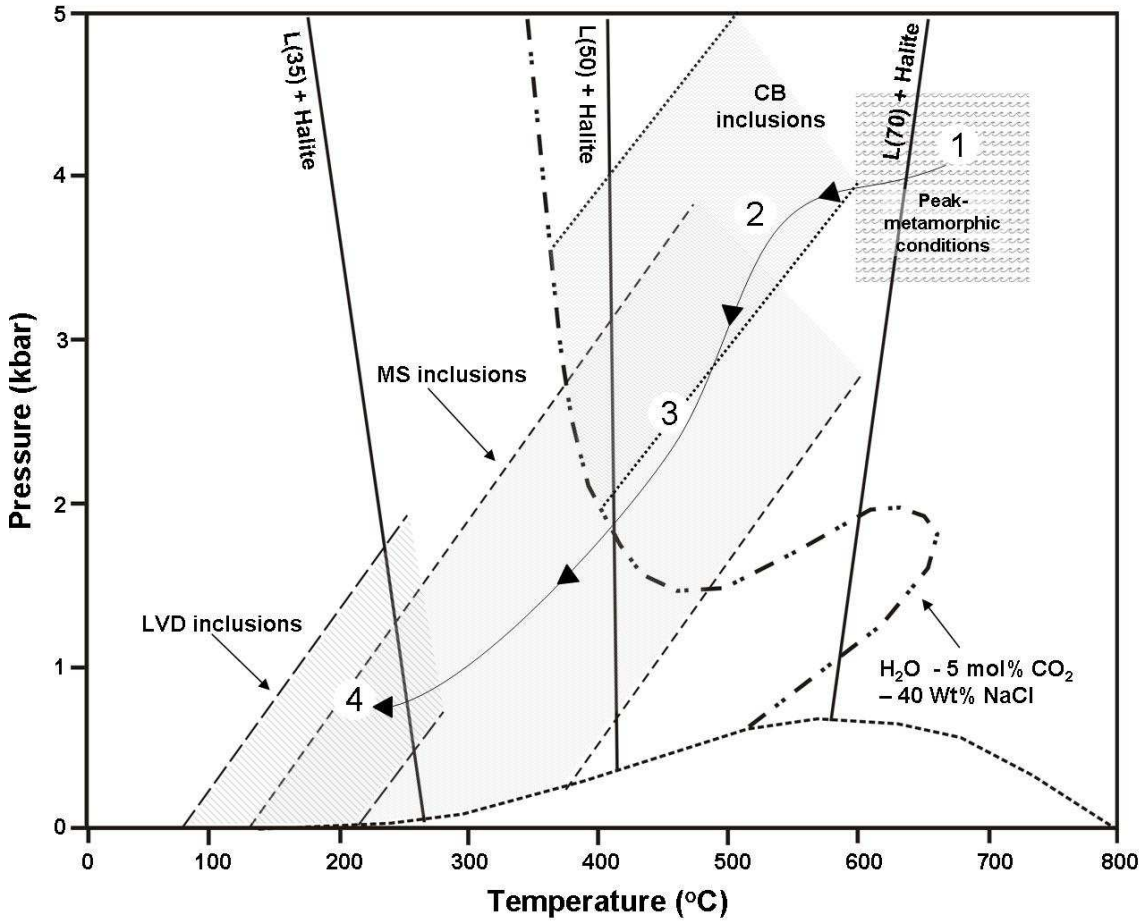

Figure 2.20: Evolution of PT conditions during Osborne ore formation.
A pressure-temperature diagram showing estimated isochores for the main brine fluid inclusion types at Osborne. The evolution of conditions are documented by mineral assemblages (French, 1997; Rubenach, 2005a), oxygen isotope studies (Adshead, 1995) and fluid inclusion thermometry and barometry (this study). Isochores estimated using the BULK and ISOC programs (Bakker, 2003) and equations of Bowers and Helgeson, (1983) and Bakker et al. (1999). CO_2 isochores not are plotted as confidence in them is lower than the other inclusion types as they may not be true end-members. Liquidus for 35, 50 and 70wt% NaCl calculated from equation given by Bodnar, (1994). Solvus for the H_2O- 5 mol% CO_2 - 40wt% NaCl from experimental study by Schmidt et al., (1995). While this composition is similar to that measured in CB inclusions the salinity is lower than found at Osborne. This may explain why the PT data for the MS and CO_2 inclusions seems to sit mainly in the one-phase field even though they are the products of phase separation. There is not data available for compositions equivalent to those found at Osborne but extrapolation of previous work suggests that higher salinities would drive the solvus to the right of the diagram (Takenouchi and Kennedy, 1964; Gehrig, 1980; Schmidt et al., 1995). Evolution from CB to MS inclusions involved mainly isothermal decompression while the shift to LVD conditions shows decreases in both pressure and temperature. The interpreted fluid PTt path at Osborne is marked with (1) the earliest and (4) the latest.

2.5.2.2 Isochore calculation

The evolution of the pressure and temperature conditions during fluid entrapment and ore formation is summarised in Fig. 2.20. Minimum trapping temperatures of the highest salinity fluids, trapped in primary MS inclusions, fall in a range from 340 to >600 ^{o}C. This is comparable with the 500 to 590 ^{o}C range calculated for fluid temperature by Adshead (1995) using oxygen isotope data for quartz-magnetite pairs from mineralized silica-flooding. Small amounts of CO_2 and CH_4 are present within the MS brine inclusions are indicated by the formation of clathrates upon freezing and by laser Raman measurement of phases in the vapour bubbles (Appendix C; Dong, 1995). The presence of these carbonic phases, along with the observation of salt crystals within CO_2 inclusions, entrapped on a single trail, suggest that these primary fluid phases were variably immiscible at the time of trapping and, thus, trapping pressures cannot be estimated without identification of end member fluids (Roedder, 1984).

The evolution of conditions are documented by mineral assemblages (French, 1997; Rubenach, 2005a), oxygen isotope studies (Adshead, 1995) and fluid inclusion thermometry and barometry (this study). Isochores were estimated using the BULK and ISOC programs (Bakker, 2003) and equations of Bowers and Helgeson, (1983) and Bakker et al. (1999). Isochores for MS-type inclusions calculated from vapour homogenisation and halite dissolution temperatures give a pressure range of 2 to 4 kbar at temperatures of 340 to 590 ^{o}C. As some MS-type inclusions homogenised by dissolution of a ferropyrosmalite daughter mineral and some did not homogenise by 600^{o}C the pressure range calculated may not reflect the full range.

It is also possible to obtain pressure estimates from the LVD inclusions using data for the disappearance of daughter minerals. These inclusions appear as secondary trails in early paragenetic stages and as primary and secondary inclusions in later paragenetic stages and thus can be considered to be later than the CO_2 inclusions which are rarely observed in later paragenetic stages. For the majority of inclusions complete homogenization occurs by dissolution of halite, after vapour disappearance. Where this is the case the minimum pressure of trapping can be calculated following the solid-liquid curve (Roedder, 1984). Using ISOC program (Bakker, 2003) and the equations of Bowers and Helgeson (1983) and Bakker (2003), minimum trapping pressures of between 0.6 and 1.5 kbar are calculated for LVD inclusions. The presence of $CaCl_2$ in the fluid, which is not accounted for in the equation, may make the estimate artificially high (Stewart and Potter, 1979). However, inclusions that homogenise in this manner may have been entrapped at high pressures and the inclusions could have been trapped at higher PT conditions than those calculated from homogenization (Roedder, 1984).

Allowing for the uncertainties inherent in these pressure calculations an apparent decompression can be inferred from the microthermometric behaviour of primary inclusions in early paragenetic stages to those in later paragenetic stages. This correlates with a decrease in homogenisation temperatures. Evolution from CB to MS inclusions involved mainly isothermal decompression while the shift to LVD conditions shows decreases in both pressure and temperature. A rapid decrease in pressure or temperature may have triggered the extensive deposition of the quartz in silica flooding cement. Studies of the behaviour of silica in hydrothermal systems have shown that the main control on silica solubility is temperature, with pressure less

significant (Fournier and Potter, 1982). The exception to this is during fracturing where pressure drops from lithostatic to hydrostatic, this type of decompression will result in a very rapid decrease in solubility, although the effect of such a decompression is lessened by increasing salinity (Rimstidt, 1997). In a study of rocks in the Selwyn range, north of Osborne, Sayab (2006) proposed that the early high pressure metamorphism (>5.5 kbar) was followed by a rapid, and near isothermal decompression (<3-3.5kbar), before further deformation and metamorphism. However, this decompression would have occurred over a longer time scale than required to give the rapid decrease in pressure required for extensive quartz deposition and ore deposition at Osborne seems to have occurred within ~5 Ma of peak metamorphism (Gauthier et al., 2001; see Chapter 1). A more likely scenario is that the ore deposition processes were locally controlled by PT shifts associated with movement on local faults or shear zones causing a pressure drop and promoting fluid flow and mixing. The Osborne deposit is sited between biotite shear zones along which dextral movement is documented, which would have caused dilation (Adshead, 1995; McLellan, 2000).

2.5.3 Fluid Evolution

The primary inclusions hosted by silica-flooding quartz document a close association between high salinity aqueous brines and CO_2-rich fluids. The rare CB inclusions that preserve a mixed brine-CO_2 fluid and trails containing co-existing MS and CO_2 inclusions could be interpreted as the result of either unmixing or mixing processes. The observation of salt crystals within CO_2 inclusions and of CO_2 clathrates in MS brines would support unmixing of the two fluid phases, brine and CO_2, becoming progressively more immiscible over the hydrothermal history of the deposit. Increasing immiscibility can be attributed to decreases in pressure and temperature (Fig. 2.20;

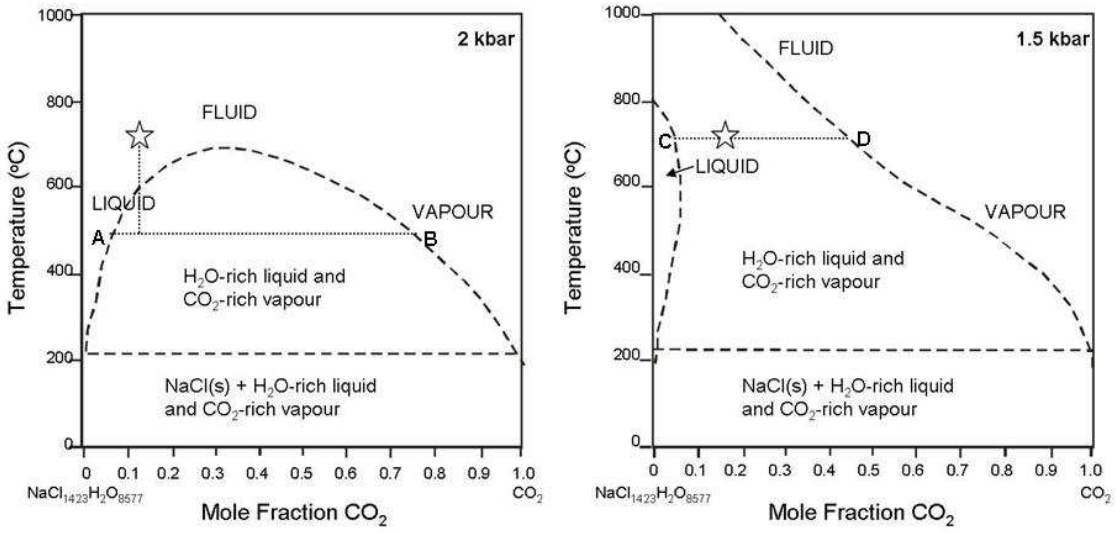

Figure 2.21: T-XCO_2 diagrams for high salinity (35 wt% NaCl) brine-CO_2 fluids (from Bowers and Hegelson, 1983). CB fluid inclusions contain a CO_2 bearing brine with XCO_2 of up to 0.15 (calculated by phase volumetric methods; Appendix B). The stars on each diagram denote this composition and show that a decrease in temperature would also drive the phase separation producing a brine with composition A and a vapour with composition B. A decrease in pressure would trigger phase separation forming MS and CO_2 populations with compositions C and D respectively.

Bowers and Helgeson, 1983). Isochores calculated using the ISOC program (Bakker, 2003) for the MS-type inclusions suggest that these were entrapped over a lower pressure than the CB-type inclusions (Fig. 2.20).

Fluid inclusions in later paragenetic stages (Q2/Q3) have a decreased XCO_2, supported by the lack of CO_2 inclusions and clathrate formation observed within the primary LVD inclusions. The loss of CO_2 from the ore fluid would increase the pH of the fluid, changing saturation thresholds and precipitating ore metals or gangue minerals. It would also change the redox state of the fluid, altering fO_2. The fugacity of sulphur, fS_2, is controlled by a number of factors, including temperature, pressure, pH and fO_2 (Barnes and Kullerud, 1961). Therefore, phase separation could change fS_2 driving the fluid conditions towards a state in which Fe-Cu-sulphides were precipitated.

Silica flooding-hosted MS fluid inclusions can be considered to have high iron contents, indicated by the presence of ferropyrosmalite ($[Fe,Mn]_8Si_6O_{15}[OH,Cl]_{10}$) as a daughter mineral. The ironstones at Osborne, and at the nearby Starra deposit, are considered to have formed at an early stage (Williams, 1994; Williams, 1995; Rotherham, 1997a; Marshall et al., 2006), and are possibly syn-sedimentary (Davidson et al., 1989). The high iron content, inferred from the presence of ferropyrosmalite, magnetite and hematite as daughter minerals, of the MS inclusions can therefore be considered to be related to Fe- and Cu-Fe-sulphide deposition. The high salinity fluid found in MS inclusions has been suggested to be linked to the widespread albitisation in the region; Williams, (1994) postulated a link between sodic metasomatism in the Cloncurry district and Fe mobilization. However, it has been suggested that the albitisation examined in that study is much younger than the Osborne system (Oliver et al., 2004;

Mark et al., 2006). Several generations of albitisation at Osborne have been dated to ~1680, ~1630 and 1595 Ma (Perkins and Wyborn, 1998; Rubenach et al., 2001; Rubenach et al., in press), all predating the majority of regional albitisation in the Cloncurry District and prior to or coincident with peak metamorphic conditions so this high salinity fluid can be interpreted as representing an early episode of hydrothermal fluid flow at Osborne and may be linked to the older, localised albitisation.

Cathodoluminescence textures and fluid inclusion paragenesis indicate the deposition of sulphides and a second generation of quartz was associated with the fluid preserved in the LVD secondary inclusions. The LVD inclusion trails emanate from or run into chalcopyrite grains and so may represent post deposition 'spent' or 'spending' ore fluids. The absence of sulphide daughter minerals in the fluid inclusions would support these fluids being 'spent'. A drop in salinity from up to 64wt% NaCl equiv. at the time of early silica flooding to as low as 17 wt% NaCl equiv. at the time of sulphide deposition in veins is recorded in the ore stage fluids, this is interpreted as a result of fluid dilution (path A on Fig. 2.14). An electron microprobe study found elevated concentrations of Cl in alteration minerals at Osborne with biotite, hornblende and ferropyrosmalite containing up to 2 wt% Cl (Zhou and Adshead, 1996; see additional discussion in Chapter 4). It was postulated that the observed decrease in salinity of the ore fluids could be attributed to the uptake of Cl during silicate alteration. However, the decrease in salinity coincides with a drop in apparent homogenisation temperatures from >400 ^{o}C to 120 to 370 ^{o}C, which can also be considered evidence of dilution by mixing with a lower salinity, cooler fluid. Th and salinity data for the two fluid inclusion populations (Fig. 2.14) shows an apparent gap with no fluids showing salinities in the 38-47 wt% NaCl equivalent range. However, this may be a function of

the differing calculations used to calculate salinities for the LVD- and MS-type inclusions. Additionally, many of these inclusions decrepitate without homogenising which limits the data set presented.

LVD inclusions are the most abundant population in sulphide-bearing quartz veins which cross-cut the main silica-flooding hosted ore. The similarity of the vein hosted LVD inclusions to main-stage ore hosted LVD inclusions suggests these veins may have been emplaced shortly after the main sulphide ore was deposited. The deposition of the second generation of quartz and sulphides within the silica flooding can be interpreted as evidence for a shift in physiochemical conditions during an episode of quartz deposition.

2.6 Conclusions

Five fluid inclusion types are observed within the Osborne Mine samples and show a number of similarities with populations documented both regionally and at other IOCG deposits in the Cloncurry district. The unmixing of a CO_2-bearing high salinity brine (trapped in CB-type inclusions) early in the depositional history is interpreted to have resulted from a decrease in pressure, probably due to dilation caused by movement on a shear zone. This decrease in pressure is inferred to have caused the ore fluids to become supersaturated with respect to silica triggering the precipitation of the extensive silica-flooding that is a notable feature of the Osborne assemblage. Cu-Au ore sulphides are hosted by a second generation of quartz that variably infills and replaces the earlier silica-flooding. This later quartz hosts primary fluid inclusions that preserve a moderate salinity brine, and which record lower pressure and temperature conditions than are calculated from inclusions in earlier paragenetic stages. This later fluid,

preserved within LVD inclusions has previously been interpreted as representing an entirely separate fluid that deposited the Cu-Au, after the peak of metamorphism and up to 50Ma after the silica-flooding formed (Adshead, 1998; Perkins and Wyborn, 1998). However, Re-Os dates for mineralisation coincident with peak metamorphism (Gauthier et al., 2001; see Chapter 1) suggest the rapid decrease in temperature could be attributed to fluid mixing causing dilution and cooling and ore deposition. The decrease in pressure that precipitated the silica flooding has been attributed to movement on faults (Adshead, 1995). Active faults could have acted as fluid conduits allowing an influx of cooler, more dilute fluids and creating the rapid fluid mixing and ore deposition close to the time of peak metamorphism which is suggested by the decrease in homogenisation temperatures measured in ore-stage LVD inclusions and by Re-Os dates on ore-associated molybdenite.

3. NOBLE GAS AND HALOGEN EVIDENCE FOR A CRUSTAL FLUID ORIGIN IN THE OSBORNE IOCG DEPOSIT OF THE EASTERN MOUNT ISA INLIER, AUSTRALIA.

3.1 Introduction

Neutron irradiation of samples and the subsequent analysis of halogen-derived nucleogenic noble gas isotopes (extended Ar-Ar methodology) enables simultaneous measurement of the halogens together with naturally occurring noble gas isotopes of Ar, Kr and Xe (Kelley et al., 1986; Turner and Bannon, 1992; Kendrick et al., 2001; Kendrick et al., 2002; Kendrick et al., 2006a;b).

In this chapter noble gases and halogens are utilised as conservative fluid tracers to test the importance of fundamentally different sources of hydrothermal fluid in the Osborne iron oxide-Cu-Au deposit and examine differences with other deposits in the Eastern Fold Belt (see Kendrick et al., 2006a, 2007). One suggested source of ore-forming fluids are near-surface sedimentary formation waters that acquire an ultra-high salinity by the dissolution of halite during convective circulation to the mid-crust (Barton and Johnson, 1996; see Chapter 1). Such fluids can be distinguished by low Br/Cl and I/Cl values similar to halite (Böhkle and Irwin, 1992a), and $^{40}Ar/^{36}Ar$ values of 300-2000 similar to sedimentary formation water (Turner and Bannon, 1992; Kendrick et al., 2002).

Alternatively, ultrasaline brines could have exsolved during the crystallisation of granitic magmas). Such an origin is unlikely at Osborne where mineralisation predates regional A-type granitoids (Gauthier et al., 2001). This is in contrast to the interpreted

presence of deeply-derived magmatic fluids reported in the Ernest Henry IOCG deposit which are distinguished by Br/Cl of ~1-2×10^{-3}, I/Cl of ~11×10^{-6} and high $^{40}Ar/^{36}Ar$ values of up to ~29,000 (Kendrick et al., 2007).

Finally, the ore fluids could have a 'local' metamorphic origin (Williams, 1994; De Jong et al., 1998; Hitzman et al., 2000; Morrison, 2005). The composition of 'local' metamorphic fluids produced during partial melting of the Soldiers Cap Group is investigated here by analysis of pegmatitic fluid inclusions, interpreted as having been trapped during peak-metamorphic anatexis. The unusual near peak-metamorphic timing of mineralisation at Osborne and the direct comparison of IOCG and pegmatite fluid inclusions enables an improved understanding of the possible role of metamorphic volatiles in Cloncurry IOCG genesis.

3.2 Noble Gas and Halogen Methodology

3.2.1 Introduction

Information on the origin of fluids and the source of their salinity can be obtained through the measurement of K, the noble gases (Ar, Kr, Xe) and nucleogenic noble gas isotopes measured as proxies for halogens ($^{38}Ar_{Cl}$, $^{80}Kr_{Br}$, $^{128}Xe_{I}$). Extended Ar-Ar methodology allows simultaneous analysis of the naturally occurring noble gas isotopes and determination of K, Cl, Br and I from nucleogenic noble gas isotopes produced during sample irradiation. Ca can also be measured using $^{37}Ar_{Ca}$ as a proxy, however this isotope has a short half-life and so meaningful data can only be obtained if the samples are rapidly analysed after irradiation which was not the case in this study.

This technique is advantageous over other methods used for halogen determination in that it measures iodine, which is usually present in low abundances. Noble gas mass spectrometers have high sensitivity to noble gas isotopes meaning that as irradiation converts a few ppm of the parent isotope to noble gas isotopes it is relatively easy to measure iodine (as $^{128}Xe_I$) by this method. However, the technique is a bulk analysis and the data collected may represent more than one population of inclusions. Careful characterisation of the decrepitation temperature ranges of inclusion populations can make the technique semi-selective during step heating (discussed further in section 3.2.9)

This method also allows simultaneous determination of both nucleogenic and naturally occurring isotopes from the same sample. While the focus of this study is on halogen systematics, the naturally occurring noble gas isotopes provide complementary information on fluid sources and reactions and they are determined simultaneously in small samples. The small sample size allows examination by microthermometry of the fluid inclusions within the quartz chips from the same samples used for the noble gas analysis.

3.2.2 Analytical Equipment

3.2.2.1 Mass Spectrometer

Measurements on samples were made on the MAP 215-50 mass spectrometer at University of Melbourne. This has a Nier-type electron bombardment source with an EHT of 4kV. It has a 90^o magnetic sector with a 50cm radius flight tube ($1500cm^3$ volume) and a magnetic dispersion length of 78.57 cm.

3.2.2.2 Detectors

The MAP 215-50 has two detectors; a Faraday cup and a Johnson electron multiplier operating in analogue mode. The electron multiplier has a variable width collector slit. In its narrowest setting it gives a maximum resolution of 1200* but to optimise sensitivity is operated at 650. The Faraday cup operates at a lower resolution of 250. The more abundant Ar isotopes are measured on the Faraday cup while the more scarce Kr and Xe isotopes are measured on the electron multiplier at a relative gain of ~400.

3.2.2.3 Extraction Line

The line consists of stainless steel piping (38mm diameter) with internal welds where possible connected by mini conflat flanges. The layout of the extraction line manifold is shown in Fig 3.1.

3.2.2.4 Pumps

An ultra high vacuum (UHV) of 10^{-9} torr is maintained throughout the sample extraction line by a Varian 20 l/s StarCell® VacIon® ion pump. The mass spectrometer is pumped by a second ion pump and is isolated from the extraction line except during sample admission. A turbo molecular pump backed by a rotary pump, which can pump any part of the line, is responsible for evacuating high pressures from atmosphere to UHV after loading of samples and maintains a secondary vacuum around the furnace. Two SAES GP50 getters with a Zr-alloy (st707) remove active gases from the sample gas.

* Resolution = (Magnetic dispersion length, μm) / (detector slit, μm + source slit, μm)

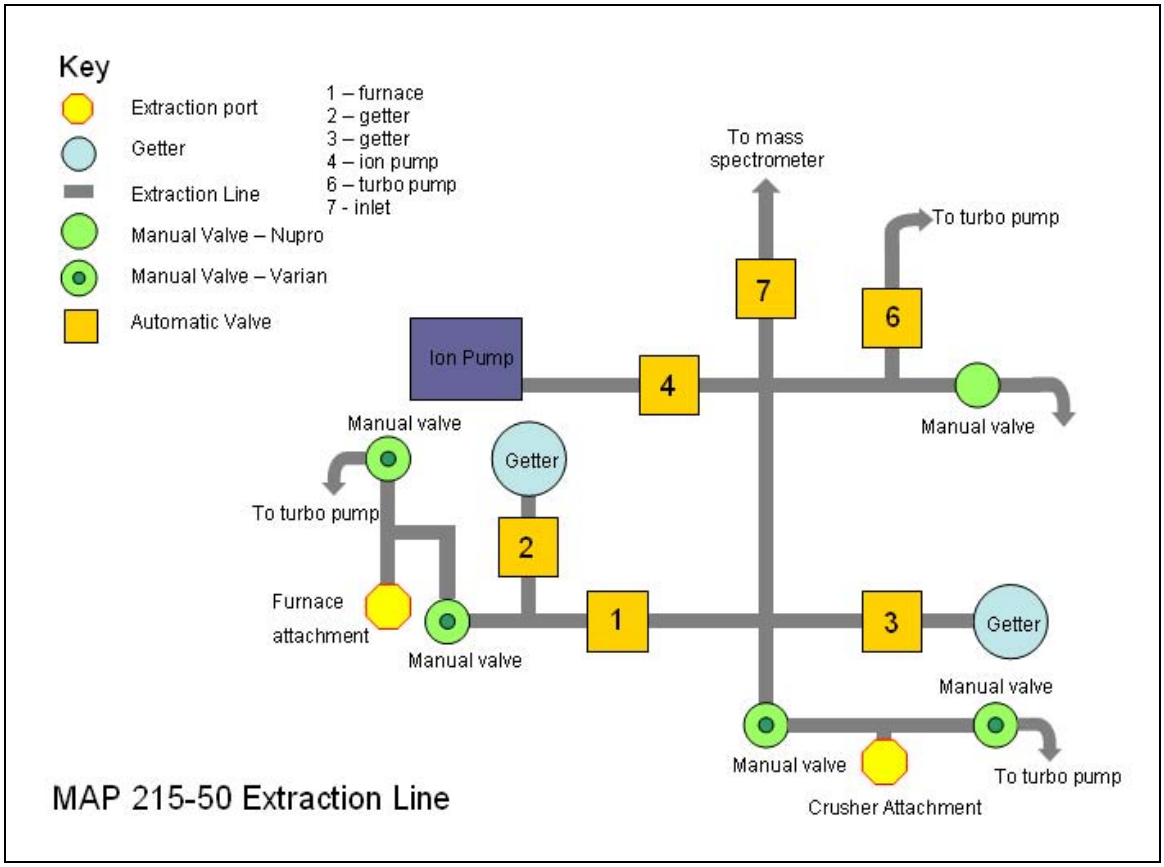

Figure 3.1 MAP-215-50 Extraction Line Schematic Diagram

3.2.2.5 Extraction Ports

The extraction line is connected to a tantalum-resistance furnace capable of heating samples to 1600^{o}C and five modified Nupro® valves for in-vacuo crushing. Up to 100mg of sample can be loaded into each crusher while larger samples can be analysed in the furnace. Sample size in the furnace is typically between 50-100mg, restricted to these sizes to minimise blanks.

3.2.3 Sample Preparation and Loading

Prior to analysis samples were characterised through microscopy and microthermometry as described previously in chapter 2. Samples consisted of 70-120mg of fragmented fluid inclusion wafers that were handpicked under a binocular microscope to produce quartz separates. These were cleaned in an ultrasonic bath using distilled water and acetone. The wafer chips in the samples are of a comparable size to those studied for microthermometry. This is important as the decrepitation behaviour of inclusions can be influenced by the size and dimensions of the wafer chip, and the similarity will make the semi-selective step heating (discussed below) more accurate.

Once cleaned, the samples were weighed and loaded into Al-foil packets, labelled and placed into silica tubes for irradiation. The tubes maintain the relative position of samples to one another allowing the flux recorded by monitors between the samples to be extrapolated throughout the package. Samples in this study were irradiated in position 5C of the McMaster University Reactor, Canada for 50 MW hours. The irradiation was designated UM#8.

Irradiated samples are monitored and handled when activity is below 100cps. Samples are unloaded from the irradiation canister and the Al-foil packets opened. Noble gases are extracted in one of two ways; by in-vacuo crushing, in modified Nupro® valves, or by step-heating in a furnace. For step heating samples are repacked into Sn-foil capsules and placed in a vacuum sample chamber coupled to a tantalum-resistance furnace. Samples for crushing are placed in stainless steel buckets which fit into modified Nupro® valves.

After sample holders have been attached to the extraction line manifold the line is baked out. During a bake out the extraction line and sample holders are heated at <130^{o}C to remove adsorbed atmosphere and achieve UHV. Care is taken not to exceed 130^{o}C and so avoid premature decrepitation of fluid inclusions.

3.2.4 Irradiation Monitors

Nucleogenic isotopes are used to determine K, Cl, Br, I and Ca. Monitors are used to determine irradiation parameters (J, α and β) that describe neutron flux during irradiation. Additional standards are used to monitor interference reactions.

Neutrons are classified according to their energy. Thermal neutrons have low energy behaving like a gas, with a high probability of colliding with a nuclide and being captured. Fast neutrons are high energy neutrons and are less likely to be captured. The neutron capture cross-section, measured in barns ($10^{-24}cm^{2}$), determines the probability of a neutron being captured and then triggering a nucleogenic reaction. This is highest for thermal neutrons.

Neutrons with energies between slow and fast in the epithermal region are termed resonant neutrons. The isotopes have large cross-sections for resonant neutrons of specific energies which, like thermal neutrons, can be significant in triggering nucleogenic reactions. Every nuclide reaction has a different number of resonances (peaks in capture cross-sections), so the flux of resonant neutrons can not be easily predicted from the flux of thermal neutrons. Resonant neutrons are important in the generation of $^{128}Xe_I$ and $^{80}Kr_{Br}$ from I and Br (Böhkle and Irwin, 1992a).

3.2.4.1 Determination of irradiation parameters

The abundance of Cl, Br, I, K, U, and Ca represented by a given abundance of nucleogenic noble gas isotopes (eg. $^{38}Ar_{Cl}$, $^{80}Kr_{Br}$) is controlled by the neutron flux that the samples were exposed to:

$$N = P \times (\varphi_t \times \sigma_t) \times \gamma$$

Where N = abundance of nucleogenic noble gas isotope; P = abundance of parent element × isotopic ratio; φ_t = thermal neutron flux; σ_t = neutron cross-section (probability of a reaction occurring); γ = yield of nucleogenic daughter isotope from decay of the parent. The thermal neutron flux is determined from the J value and irradiation parameters α and β.

3.2.4.2 Thermal Neutron Flux Monitors

Monitors are used to measure parameters based on thermal neutron flux. The three parameters measured are:

(1) the J-value; $\mathbf{J} = \frac{\left(e^{\lambda t} - 1\right)}{{}^{40}Ar*/{}^{39}Ar}$

(2) alpha; $\left(\frac{K}{Ca}\right) = \boldsymbol{\alpha}\left(\frac{{}^{39}Ar}{{}^{37}Ar}\right)$

(3) beta; $\left(\frac{K}{Cl}\right) = \boldsymbol{\beta}\left(\frac{{}^{39}Ar}{{}^{38}Ar}\right)$

The J-value and α and β irradiation parameters measure the efficiency with which ^{39}Ar, ^{38}Ar and ^{37}Ar are produced during the irradiation of K, Cl and Ca. J and β are used to calculate the fluence of fast and thermal neutrons. The irradiation parameters for this study are given in table 3.1.

- **Hb3Gr** (hornblende standard) has a precisely known age of 1.072 ± 0.011 Ga and a K:Ca:Cl composition of 1.247 ± 0.008 wt% K, 7.45 ± 0.05 wt%, 2379 ± 16 ppm Cl (Roddick, 1983; Turner, 1971). This allows the J-value and α and β irradiation parameters to be calculated (Kelley et al., 1986).
- **GA1550** is also used to calculate the J-value. This is a biotite separated from a subvolcanic monzonite from Mt Dromedary, NSW and has a known age of 98.8 Ma (Renne et al., 1998). The Cl composition of this standard is less precisely known so other parameters are not calculated.

3.2.4.3 Halogen Monitors

- **Shallowater** (meteorite; pyroxene separates) has consistent ^{129}Xe/^{127}I ratio (1.095 ± 0.029 x 10^{-4}) (Turner, 1965) so it can be used as a monitor for I in correction for resonant neutrons. Assumptions are made regarding the relative based on cross-sections of ^{80}Kr and ^{128}Xe, that also enable $^{80}Kr_{Br}$ to be corrected.

- **Quartz 2320** (from St Austell) is an internal standard. It has a well known composition based on multiple analyses (Bottrell and Yardley, 1988; Yardley et al., 1992; Irwin and Roedder, 1995). Banks et al., (1992), determined bulk Br/Cl value as 0.62 x 10^{-3}.

	Average values for can	**% error**	**Neutron Flux**		**% error**
J	0.0187	1.0	**Thermal**	9.66×10^{18}	6.5
α	0.550	2.4	**Fast**	3.55×10^{18}	1.0
β	4.849	6.5			
Quartz 2320 average Br/Cl = 0.68			**Shallowater resonance corrections:**		
			Br correction factor = 1.25		10% err
			I correction factor = 1.60		20% err

Table 3.1: Irradiation parameters for samples

3.2.4.4 Interference Correction Monitors

A number of corrections need to be made for interference by atmospheric or minor nucleogenic noble gas isotopes.

- **Ca-Salt and K-glass:** Irradiation of Ca produces Ar isotopes that interfere with the measurement of K, as ^{39}Ar, and the atmospheric isotope ^{36}Ar. Similarly, irradiation of K interferes with the measurement of Cl, as ^{38}Ar, and the naturally occurring isotope ^{40}Ar. These interference reactions are corrected for based on the abundance of K and Ca, measured as $^{39}Ar_K$ and $^{37}Ar_{Ca}$, and the Ar isotope production ratios (^{38}Ar/^{39}Ar, ^{40}Ar/^{39}Ar from K, and ^{39}Ar/^{37}Ar, ^{36}Ar/^{37}Ar from Ca) measured by irradiating Ca salts and K-glass.

3.2.5 Sample Analysis

40-90 mg of irradiated sample were analyzed by stepwise heating between 200-1560ºC. The first extraction step is 200ºC and the size of subsequent steps, typically 50ºC or

100°C, is determined by the volume of gas released in the previous step. Stepped heating was carried out cyclically with samples heated from an idle temperature of 100°C to the specific step temperature over a period of 3 minutes. The duration of each heating step was 20 minutes and between 200-700°C steps increased in increments of 50-100°C. Above 700°C the steps were larger; between 200-300°C. Four samples were additionally analyzed by sequential in-vacuo crushing (in 4-6 steps).

Noble gases extracted during stepped heating were expanded through an UHV extraction line and purified using a cold Zr-Al getter for 20 minutes during stepped heating and hot (250°C) and cold getters for a further 15 minutes during gas transfer, removing active gases such as H_2O, H_2, CH_4, CO_2 and SO_2. Gases extracted from in-vacuo crush samples were gettered for 15 minutes on hot and cold getters before admission to the MAP-215 noble gas mass spectrometer. Ar, Kr and Xe isotopes were simultaneously analyzed in 9 cycles of measurement over a period of 50 minutes.

3.2.6 Air Calibration and Blanks

Air calibrations provide a check on the integrity of equipment, relative sensitivity of the two detectors and mass discrimination. An air bottle filled with air at a low pressure acts as a reservoir for air aliquots. The airshot is expanded from the aliquot to the mass spectrometer.

Blanks are measured after reloading and periodically (every two samples) between sample analysis. Blanks must be below 10% of the expected sample size and preferably closer to 1%. If the blank is too high analysis is postponed until further bakeouts or time reduce the blank.

In this study isotopes with a measurable machine blank, expressed as a percentage of gas released from samples in the 200-700^{o}C had average values of 1-10% for ^{40}Ar, with atmospheric ^{40}Ar/^{36}Ar values; <5% for ^{84}Kr; <1.5% for ^{80}Kr and <0.1% for ^{128}Xe.

3.2.7 Mass Spectrometer Operation

Analysis is controlled by the LabSpec program, written by Bruce Idleman in the labview environment. It runs on a PC platform and has a windows interface. Measurement starts with peak centering; scanning over the peaks for the most abundant isotopes and locating the peak centre; for air calibrations the most abundant isotopes are ^{40}Ar, ^{84}Kr and ^{132}Xe and for sample measurements they are ^{40}Ar, ^{80}Kr and ^{128}Xe. A series of measurements are then made going down mass. The relative peak spacing in Halls Probe V has been entered into LabSpec. The Mass Spectrometer jumps between peak centres measuring beam intensity. Firstly, ^{136}Xe, ^{134}Xe, ^{132}Xe, ^{131}Xe, ^{130}Xe, ^{129}Xe, ^{128}Xe then ^{86}Kr, ^{84}Kr, ^{82}Kr and ^{80}Kr are measured on the electron multiplier. Secondly, ^{40}Ar, ^{39}Ar, ^{38}Ar, ^{37}Ar and ^{36}Ar are measured on the Faraday cup. Background (zero) measurements are made above and below each isotopic region (Xe, Kr, Ar) at apparent masses of 137.0 and 127.0 (Xe), 86.7 and 78.5 (Kr) and 40.5 and 35.5 (Ar). These define a base line and are subtracted from peak measurements. Measurement of all Xe, Kr and Ar isotopes completes the first cycle. The process is then repeated over a total of 9 cycles, taking around 60 minutes.

3.2.8 Data Reduction

The Labspec program records the time of sample inlet (t=0) and the time every isotopic measurement is made. At the end of an analysis, data are reduced by plotting time(s) against peak intensity for every isotope and extrapolating back to inlet time. Three

regressions are performed for each data set (linear, quadratic and exponential) and the best fit is selected. Any anomalous points, sometimes attributed to poor peak centering, which do not lie close to the regression can be removed. This allows the operator to exert some control over the quality of the data obtained. Performing these regressions generates the raw data.

3.2.8.1 Processing Raw Data

Initial corrections must be made for interference reactions and thermal and resonant neutron flux during irradiation and for decay of radiogenic nuclides since irradiation. The sequence in which corrections is made is important and is as follows:

- A mass discrimination correction is applied with the correction factor determined from air standard calibrations. The correction factors for the Osborne samples was 0.062 for ^{40}Ar, 0.51×10^{-4} for ^{39}Ar, 0.30×10^{-2} for ^{38}Ar, 0.33×10^{-4} for ^{37}Ar and 0.12×10^{-3} for ^{36}Ar.
- Correction for radioactive decay of $^{37}Ar_{Ca}$

  To calculate Ca abundance an initial correction for radioactive decay must be made on ^{37}Ar which has a short half-life of 35.1 days.
- Correction for nuclide interference reactions (detailed in table 3.2)

Element	Measured	Other Isotopes	Interference
Cl	$^{38}Ar_{Cl}$	$^{36}Ar_{Cl}$,	$^{36}Ar_{atm}$
Ca	$^{37}Ar_{Ca}$	$^{39}Ar_{Ca}$, $^{36}Ar_{Ca}$	$^{39}Ar_{K,}$ $^{36}Ar_{atm}$
K	$^{39}Ar_{K}$	$^{40}Ar_{K,}$ $^{38}Ar_{K}$	$^{40}Ar_{atm}$, $^{38}Ar_{Cl}$

Table 3.2. Nuclide Interference Reactions

An additional correction is made for fissionogenic Kr and Xe isotopes produced by fission of Uranium. The isotopes produced by this process necessitate an

interference correction for the atmospheric isotope ^{84}Kr and the nucleogenic isotopes $^{128}Xe_I$ and ^{131}Xe. The correction is made based on the abundance of ^{134}Xe which is produced solely by the fission of U.

- Correction for atmospheric isotopes

  As the noble gas composition of the atmosphere is fixed and known this is relatively simple. Where possible, corrections are made using the most abundant isotope. Naturally occurring ^{38}Ar is subtracted from $^{38}Ar_{Cl}$ based on concentrations of ^{36}Ar. Kr and Xe are corrected using ^{84}Kr and ^{129}Xe concentrations respectively.

3.2.8.2 Analytical Precision

Analytical precision, determined by the reproducibility of air calibrations, is at the 1 % level. Total uncertainty in Br/Cl and I/Cl values is estimated at 10% for Br/Cl and 15% for I/Cl and is determined by the relative flux of thermal to resonant neutrons (Kendrick et al., 2006a). All ratios given in this chapter are molar.

3.2.9 Sample Selection

Quartz wafers were prepared for ore related samples from each of the ore lenses and a quartz and a feldspar wafer were prepared for pegmatite veins collected from the 1S and 2M ore lenses (Table 3.3). The majority of samples selected had been characterised by microthermometry (see Chapter 2) but additional samples were selected to ensure complete representation of the different ore lenses. Silica-flooding composed predominantly of early quartz has a dominant population of secondary fluid inclusions that are similar to rare primary and more common secondary fluid inclusions in secondary quartz. The multiple generations of secondary fluid inclusion indicate

repeated pulses of mineralising fluids. The high salinity primary inclusions are interpreted as pre-mineralisation ore fluids and the secondary, lower salinity, inclusions as post-mineralisation fluids; as a result the entire fluid inclusion assemblage in both early and late quartz is representative of different stages in the evolving IOCG system.

Although combined noble gas and halogen analysis is a bulk analytical technique it can be made semi-selective through study of the decrepitation behaviour of the fluid inclusion assemblage in the samples. During fluid inclusion microthermometry decrepitation temperatures of the different populations of fluid inclusion were determined. This allows the noble gas and halogen composition released at different temperatures during stepped heating to be related to the decrepitation of specific fluid inclusion populations observed during microthermometry.

Previous studies of volatile release during stepwise heating of quartz have shown that volatiles released between 200 to 700^{o}C can be correlated with fluid inclusion decrepitation (Kendrick et al., 2006a). In the Osborne samples, heating during microthermometry has shown that carbon dioxide fluid inclusions are amongst the first to decrepitate with a peak at ~400^{o}C and only the smallest CO_2 inclusions persist to higher temperature. The least saline aqueous fluid inclusions (LV) tend to decrepitate at lower temperatures than the most saline fluid inclusions (MS). MS and LVD inclusions mainly decrepitate between 200 and 700^{o}C with LVD inclusions having a mode between 300 and 500^{o}C and some MS inclusions remaining undecrepitated at 600^{o}C (the temperature limit of the stage). Therefore sample decrepitation and volatile release between 500 and 700°C is considered to be dominated by the highest salinity MS fluid inclusions. This pattern is similar to that previously reported at Osborne and at other

Sample					Fluid Inclusion Assemblage Proportions (%)*					Analysis
ID	Description	Mineral	Ore Lens	Paragenetic Stage	MS	LVD	LV	CO2	CB	H- step heat C - crush
Osb15	Magnetite bearing coarse-grained silica flooding with minor chalcopyrite.	Qtz	1SS	P	70	10	5	14	1	H, C
Osb20	Quartz vein containing pyrite and chalcopyrite cross-cut by quartz-magnetite-pyrite-chalcopyrite veins in psammites with accessory hematite and pyrite.	vein qtz	1SS	P	10	50	35	5	0	H, C
Osb22Am	Magnetite rich silica flooding with chalcopyrite hosted within magnetite rich zones.	Qtz	1SS	P	20	35	35	10	0	H, C
Osb22Av	Quartz-feldspar vein with coarse chalcopyrite and hematite dusting on feldspar grains hosted by mineralised silica-flooding.	vein qtz	1SS	O	0	35	65	0	0	H
Osb27	Chalcopyrite bearing quartz vein, hosted by hematised feldspathic psammite and ironstone..	Qtz	1SS	ep/p	25	10	10	50	5	H, C
Osb59	Silica flooding with thin bands of magnetite. Chalcopyrite has infill texture.	Qtz	1SS	P	20	40	30	10	0	H
Osb315	Silica flooding with minor magnetite and coarse chalcopyrite.	Qtz	1M	P	45	25	10	15	5	H, C
Osb852	Quartz-feldspar pegmatite with rare perthitic textures.	feldspar + qtz	1SS	peak-met	20	0	5	70	5	H
Osb36B	Silica flooding with magnetite rich zones and coarse chalcopyrite with fine grained pyrrhotite coats	Qtz	2M	P	60	10	18	10	2	H
Osb40	Coarse quartz-feldspar pegmatite with perthitic textures, minor tourmaline and rare specular hematite.	Qtz	2M	peak-met	45	5	15	30	5	H
Osb43	Silica flooding with magnetite rich zones and coarse chalcopyrite and minor pyrrhotite	Qtz	2M	P	45	15	25	15	0	H
Osb37B	Magnetite-chalcopyrite-pyrrhotite bearing silica flooding	Qtz	3E	P	35	20	20	24	1	H
Osb47	Fine grained silica flooding, with undulose extinction. Chalcopyrite follows a foliation.	Qtz	3E	P	35	40	20	5	0	H

Table 3.3: Sample and fluid inclusion assemblage descriptions (ep = early pre-ore; p = pre-ore; o = ore stage; peak-met = peak of metamorphism)
**Fluid inclusions proportions based upon visual estimates (~20% errors can be assumed)*

deposits in the region including Eloise (Kendrick et al., 2006a) and Ernest Henry (Kendrick et al., 2007).

3.3 Results

Full data tables are presented in Appendix D.

3.3.1 The halogens

Fluid inclusions in the Osborne samples exhibit considerable variation in their molar halogen ratios with Br/Cl varying between 0.31×10^{-3} and ~$2\text{-}2.5\times10^{-3}$ in most samples, but with a maximum of 3.8×10^{-3} in sample Osb22a. I/Cl varies between 2×10^{-6} and 27×10^{-6} (Fig 3.2). These data are based on stepped heating analyses, but in contrast to some previous studies (Kendrick et al., 2001; 2007), sample duplicates analysed by both stepped heating and in-vacuo crushing yielded similar mean Br/Cl values (samples Osb20; 27; 47 and 315; Table 3.4).

Sample	**Crush**		**Furnace**	
	Br/Cl (× 10^{-3})	**I/Cl (× 10^{-6})**	**Br/Cl (× 10^{-3})**	**I/Cl (× 10^{-6})**
Osb20	1.24	6.08	1.20	4.38
Osb27	2.24	10.39	1.93	8.90
Osb47	0.82	12.37	0.81	4.52
Osb315	0.58	5.19	0.40	4.30

Table 3.4: Comparison of in-vacuo crush and step-heating data

I/Cl values show more variation. The variation is not systematic, although in all cases the value measured by stepped heating is lower than that measured by crushing. For three of the four samples the mean furnace I/Cl values are between 65-85% of the measured crush value, however, for sample Osb47 the furnace value is only 36% of that of the crushed aliquot. Emphasis in the interpretation is based upon step heating data which is available for all samples.

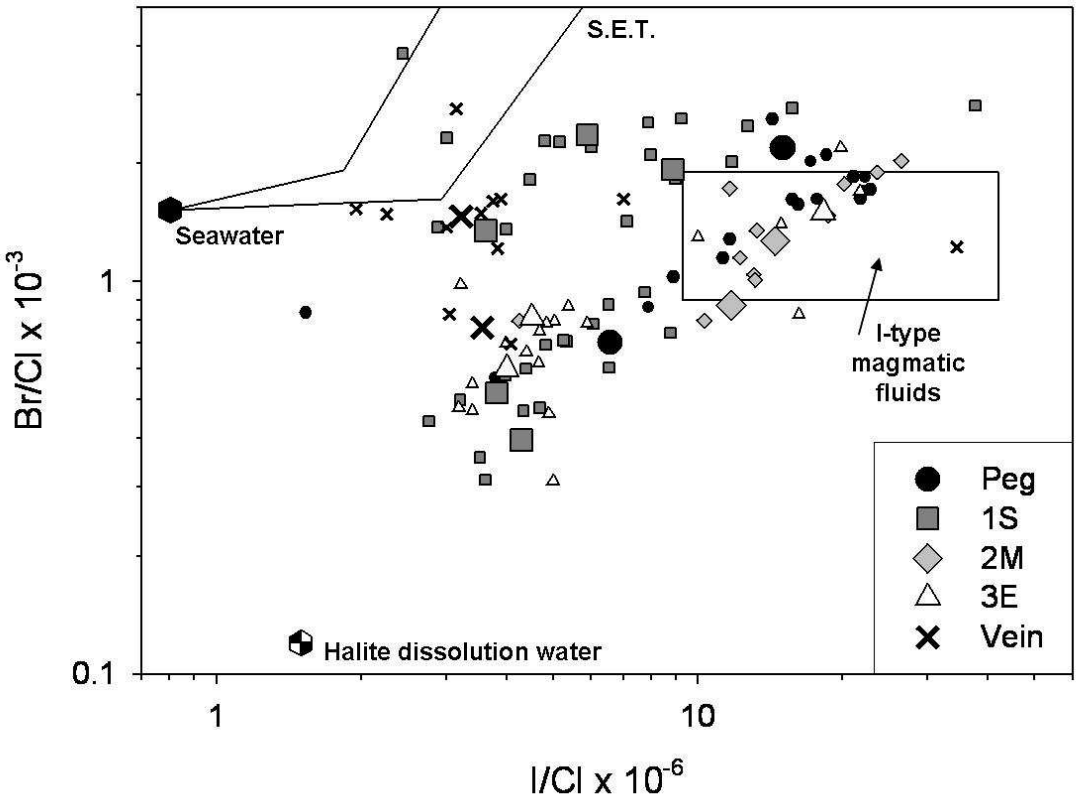

Figure 3.2. Br/Cl versus I/Cl (molar ratios). Small symbols denote individual heating steps (200-700 °C). Large symbols represent averages taken over the 500-700°C temperature steps most representative of MS fluid inclusions, however, data points may be considered to represent contributions from several different fluid inclusion populations. Osborne data for the 3E ore body from a study by Kendrick et al., (2006a) are also plotted Reference data: for Seawater Evaporation Trajectories (for Black Sea and Lake Sasky-Sivash) from Zherebtsova and Volkova, (1966); for Halite dissolution water from Böhkle and Irwin, (1992a); and for I-type magmatic fluids measured in Porphyry Copper Deposits from Kendrick et al., (2001). Errors on Br/Cl values are ~11 % for almost all steps except for the 200°C step for some samples where low volumes of gas were released and errors can be < 40 %. Errors on I/Cl values are ~20 % for almost all steps except for the 200°C step for some samples where errors can be < 60 %.

The data do not define fields that can be related to sample location. The extent of variability in the largest ore lens (1S/1SS), for which the greatest number of samples were available (Table 3.3), is similar to the variation seen throughout the entire mine (Fig 3.2). The two late vein samples have the lowest I/Cl values and intermediate Br/Cl. The two pegmatite samples have Br/Cl and I/Cl values that fall within the range measured in ore lens samples. Sample Osb40, a coarse grained pegmatite has low Br/Cl and I/Cl values that fall outside the field of I-type magmatic compositions while sample Osb852, a non-porphyritic, alkali feldspar pegmatite has higher Br/Cl and I/Cl values that lie within, and exceed, the range of I-type magmatic values (Fig 3.2).

3.3.1.1 Intra-sample variability

The samples exhibit variable behaviour during stepped heating. In most cases the lowest Br/Cl values are measured toward the top of the 200-700^{o}C temperature range. However, in sample Osb22a the fluid inclusions exhibit the opposite behaviour and the highest Br/Cl value of 3.8×10^{-3} was measured in sample Osb22a at 700^{o}C (Fig 3.3). Other samples have fluid inclusion Br/Cl values that increase to maximum values in ~400-500 °C extraction steps and then decrease to minimum values in the 700^{o}C extraction step (Fig 3.3).

The variable halogen composition of fluid inclusions in the different samples (Fig 3.2) could be partly attributed to their different abundances of LV, LVD and MS fluid inclusions (Table 3.3) with the fluids in each fluid inclusion population having different halogen ratios. However, because the highest salinity fluid inclusions are preferentially decrepitated above 500 °C in all the samples (section 3.2), and composition for each sample vary widely at this temperature and individual samples exhibit different

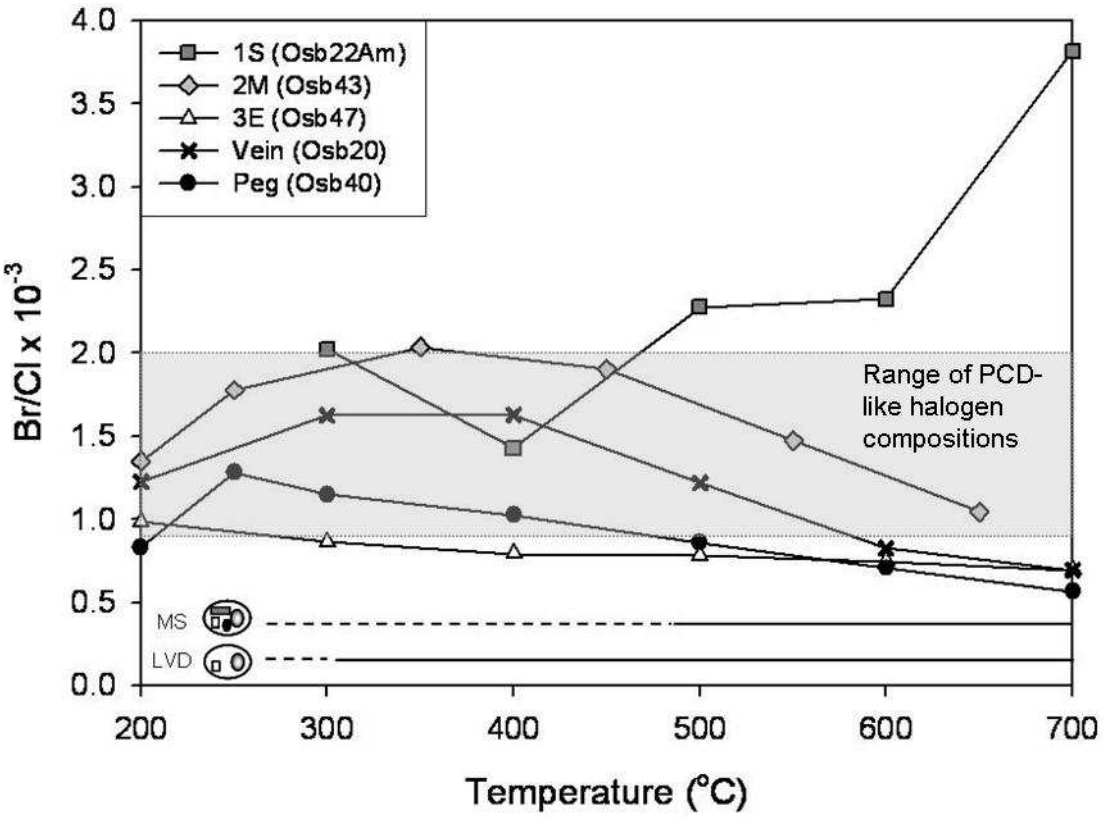

Fig 3.3: Br/Cl vs temperature. In most samples the lowest Br/Cl values are measured between 500°C and 700°C where the highest salinity fluid inclusions are inferred to decrepitate with a steady decrease in values observed over the heating range. However some samples show a peak in Br/Cl values between 300-500°C (Osb20; Osb43) and sample Osb22Am shows an increase in Br/Cl with temperature. It can be noted that at higher temperatures, the Br/Cl values for most samples shown move out of the field of I-type magmatic-like compositions.

behaviours during stepped heating (Fig 3.2 and 3.3); it can be inferred that the compositions of the different saline fluid inclusion types (LVD and MS) are as variable as the samples themselves. This is illustrated by samples Osb36B and Osb15 which have very similar fluid inclusion assemblages but quite distinct Br/Cl and I/Cl values (Tables 3.3 and 3.5).

3.3.2 Potassium and radiogenic $^{40}Ar_R$

Fluid inclusion K/Cl values in ore-related quartz and pegmatite samples, obtained from *in vacuo* crushing or low temperature extraction steps (≤500°C), range from 0.04 to 0.29 (Table 3.5). Higher K/Cl values of greater than one are obtained from three of the silica-flooding quartz samples at temperatures of >500 °C (Osb315, Osb43, Osb20; Table 3.5). These high values provide evidence for K substituted into quartz, a K-mineral impurity in either the quartz matrix, or accidentally trapped in the fluid inclusions of these samples. Small amounts of mica and feldspar have been observed within the hand samples but grain picking of quartz chips under a binocular microscope aimed to minimise these impurities in the samples analysed. Maximum K/Cl values of >0.5 measured in several other samples are also unrealistic for an ore fluid, and probably indicate the presence of a very minor K-mineral impurity in these cases. The feldspar-bearing pegmatite samples Osb40 and Osb852 have the highest K/Cl values of ~60 and 90 respectively (Table 3.5).

The sample maximum K/Cl value is not strongly correlated with its K concentration. Samples with maximum K/Cl values of <0.5 have 7-847 ppm K which overlaps the range of 13-1300 ppm K determined for samples with higher K/Cl values (Table 3.5). The lack of any clear correlation indicates that the relative abundances of mineral

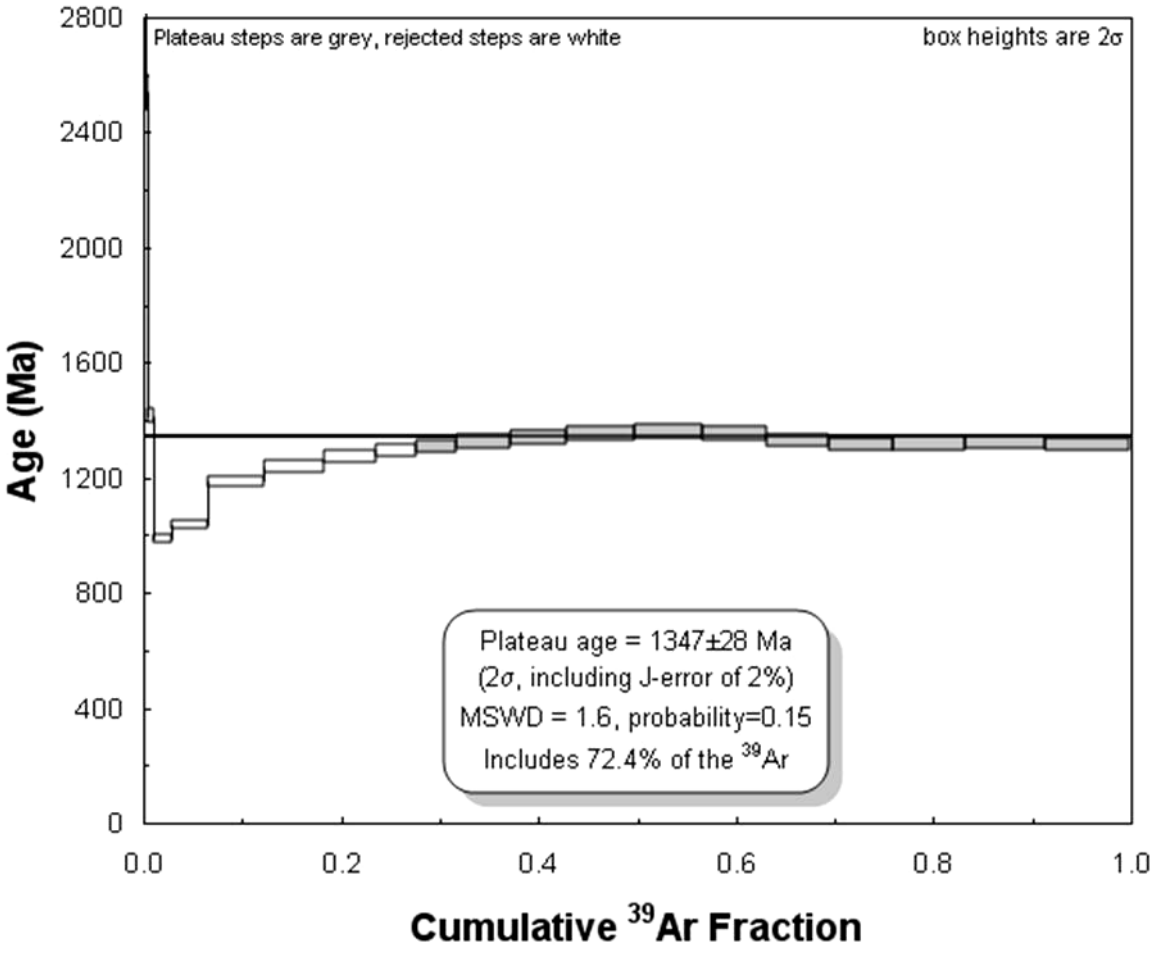

Figure 3.4: Ar-Ar plateau for sample Osb852.
The plateau defines a cooling age for the pegmatite of 1347 Ma.

Sample/ Extraction H = step heat; C = crush		$^{40}Ar/^{36}Ar$[a]		$Cl/^{36}Ar$ × 10^6	$^{40}Ar_E/Cl$ × 10^{-6}	NaCl wt.%	$[^{36}Ar]$ ppb[b]	$[^{40}Ar_E]$ ppm	Br/Cl × 10^{-3}	I/Cl × 10^{-6}	K/Cl		K ppm	U ppb
		Max Age-corrected	Sample mean (Measured)-corrected [c]	Max	Mean	MS mean (max)[d,e]			200-700 °C[f] range		FI[g] range ≤500 °C	Max	FI + Matrix	
Peg.														
Osb40	H	1665 ± 66.6	(4033) 1036 ± 332	140.07 ± 9.7	45.2 ±54.2	57 (65)	2.5 (2.9)	17.6 (20.1)	0.57-1.28	3.80-11.69	0.08-0.09	60.64	795	9
Osb852	H	1506 ± 18.1	(14642) 1206 ± 298	18.80 ± 1.4	145 ±.48.7	*57 (65)*	18.7 (21.3)	56.5 (64.4)	1.57-2.60	14.27-22.23	0.18-7.11	90.11	16601	423
IS														
Osb15	H	1015 ± 8.1	(827) 605 ±210	205.03 ± 13.3	4.1 ± 1.83	55 (64)	1.7 (1.9)	1.5 (1.8)	0.44-0.95	2.77-6.53	0.09-0.12	0.25	103	1
Osb22Am	H	870 ± 11.3	(573) 550 ±214	81.97 ± 5.5	5.2 ±.3.5	*48 (60)*	3.6 (4.5)	1.7 (2.1)	1.43-3.82	2.44-11.78	0.05-0.79	0.79	17	78
Osb27	H	775 ± 9.3	(896) 576 ±144	44.57 ± 2.9	12.3 ± 4.8	*40 (45)*	5.5 (6.2)	3.4 (3.8)	1.71-2.77	7.89-15.74	0.05-0.13	0.25	1215	75
Osb27	C	853 ± 23.9	(692) 630 ± 137	118.37 ± 8.4	8.81 ± 2.4	*40 (45)*	2.1 (2.3)	2.4 (2.7)	0.52-2.57	5.23-10.28	0.05-0.09	0.09	15	217
Osb59	H	1045 ± 16.7	(852) 784 ±266	178.23 ± 11.9	5.8 ±1.5	*50 (60)*	1.7 (2.1)	2.0 (2.4)	1.38-2.82	2.89-6.01	0.06-0.07	0.84	18	9
Osb315	H	737 ± 60.4	(1168) 527 ±140	180.96 ± 18.8	8.88 ±11.0	49 (51)	1.7 (1.7)	3.0 (3.1)	0.31-0.94	3.53-8.77	0.13-0.20	2.90	1897	3361
Osb315	C	850 ± 23.8	(690) 599 ± 179	119.95 ± 8.4	6.79 ± 3.2	49 (51)	2.5 (2.6)	2.3 (2.4)	0.52-0.74	5.23-7.86	0.09-0.10	0.10	26	695
2M														
Osb36B	H	1689 ± 109.8	(1715) 1025 ±.421	241.20 ± 15.9	7.9 ± 6.6	46 (54)	1.2 (1.4)	2.5 (2.9)	0.55-1.73	4.26-13.15	0.07-0.1	0.64	139	172
Osb43	H	1606 ± 67.5	(984) 942 ±357	141.32 ± 11.0	14.2 ± 12.6	*50 (55)*	2.2 (2.4)	4.9 (5.3)	1.04-2.04	13.08-26.50	0.07-0.16	2.23	119	106
3E														
Osb37B	H	1116 ± 24.6	(1062) 643 ±.277	468.94 ± 32.4	2.1 ± 1.1	*50 (55)*	0.7 (0.7)	0.7 (0.8)	0.45-0.83	3.18-5.89	0.08-0.11	0.72	88	419
Osb47	H	1985 ± 13.9	(1078) 938 ±.610	272.94 ± 18.0	3.5 ±.1.5	*50 (55)*	1.1 (1.2)	1.2 (1.3)	0.70-0.98	3.22-5.37	0.06-0.09	0.42	71	285
Osb47	C	1396 ± 26.0	(878) 860 ± 331	280.80 ± 19.1	3.6 ± 0.2	*50 (55)*	1.1 (1.2)	1.2 (1.4)	0.81-0.88	5.38-25.98	0.06	0.06	73	7
Late Vein														
Osb20	H	1052 ± 45.2	(1976) 795 ±.250	151.98 ± 10.5	58.5 ± 100	30 (38)	1.2 (1.5)	12 (15.2)	0.70-1.63	3.05-7.03	0.09-0.29	3.39	145	31
Osb20	C	734 ± 22.2	(813) 703 ± 21.3	59.96 ± 4.32	7.8 ± 1.0	30 (38)	3.1 (3.9)	1.6 (2.0)	1.04-1.38	5.18-6.18	0.10-0.13	0.13	19	4
Osb22Av	H	739 ± 121.9	(463) 465 ±136	91.87 ± 16.4	9.8 ± 15.1	24 (32)	1.6 (2.1)	1.6 (2.1)	1.38-2.76	1.95-2.75	0.04-0.05	0.26	9	17
Reference Values[h]														
Meteoric		295.5				0	1.6-2.7	0						
Magmatic		~30 000		~10-30	~1000	<8-?	<0.2	<100	1-2	10-70				

Table 3.5: Summary of noble gas and halogen data from stepped heating of samples

[a] Corrected for post entrapment production of radiogenic ^{40}Ar; [b] Ar concentrations are given in ppb and ppm to enable comparison with Cl and K concentrations, also given by mass. 1 ppb $^{36}Ar = 1.6\times10^3$ cm^3 cm^{-3} H_2O; 1 ppm $^{40}Ar = 1.8$ cm^3 cm^{-3} H_2O. The concentrations are based on the mean and maximum salinities of MS fluid inclusions and the $^{40}Ar_E/Cl$ or $Cl/^{36}Ar$ values tabulated; [c] The measured and age-corrected (1595 Ma) sample mean $^{40}Ar/^{36}Ar$ values; [d] MS = multi solid fluid inclusions, MS inclusions not present in Late Vein samples so salinities given are for LVD inclusions; [e] Values in italics denote mean values calculated from phase volumetric studies as decrepitation of inclusions prior to homogenisation of MS inclusions prevented experimental determination; [f] The range of Br/Cl and I/Cl values determined for uncrushed samples, in the temperature range considered most representative of fluid inclusion decrepitation (Kendrick et al., 2006a); [g] FI = fluid inclusion value; [h] Reference values in Zherebtsova and Volkova, (1966); Böhkle and Irwin, (1992b); Johnson et al., (2000); Kendrick et al., (2001)

impurities and fluid inclusions, or the proportion of high salinity K-rich fluid inclusions is quite variable between the different samples.

3.3.2.1 $^{40}Ar_R$ Correction

Fluid inclusion $^{40}Ar/^{36}Ar$ values have been corrected for post-entrapment radiogenic $^{40}Ar_R$, based on the K content of the sample and an assumed mineralisation age of 1595 Ma (Gauthier et al., 2001). The age-correction is <5-30% for most quartz sample extraction steps. Uncertainties in the deposit age of ~100 Ma correspond to a correction of <2% and will not influence the interpretation of these data.

In contrast, the correction is critical for the pegmatite samples Osb852 and Osb40 which both contain significant K. Sample Osb40 consists predominately of quartz with minor feldspar with a total K concentration of 0.07 wt % (Table 3.3; 3.5). Sample Osb852 comprises equal amounts of feldspar and quartz and has a total K concentration of 1.6 wt % (Table 3.3; 3.5). Fortunately, very little $^{39}Ar_K$ or ^{40}Ar is released from the lattices of these samples at temperatures of less than 500 °C, and the age-corrected fluid inclusion $^{40}Ar/^{36}Ar$ values are just 2-40% lower than the measured values in this temperature range. In the pegmatite samples the initial $^{40}Ar/^{36}Ar$ values determined at <500 °C, are 760-1665, which is similar to the range of values determined for fluid inclusions in the silica-flooding samples which have maximum K concentrations of 0.13 wt%, with the majority being <100ppm (Table 3.5). This agreement of age-corrected $^{40}Ar/^{36}Ar$ values in the two different sample types with over an order of magnitude difference in K concentrations provides confidence that the age-correction is accurate. The Ar released above 500 °C is dominated by the lattice Ar and because the mineral

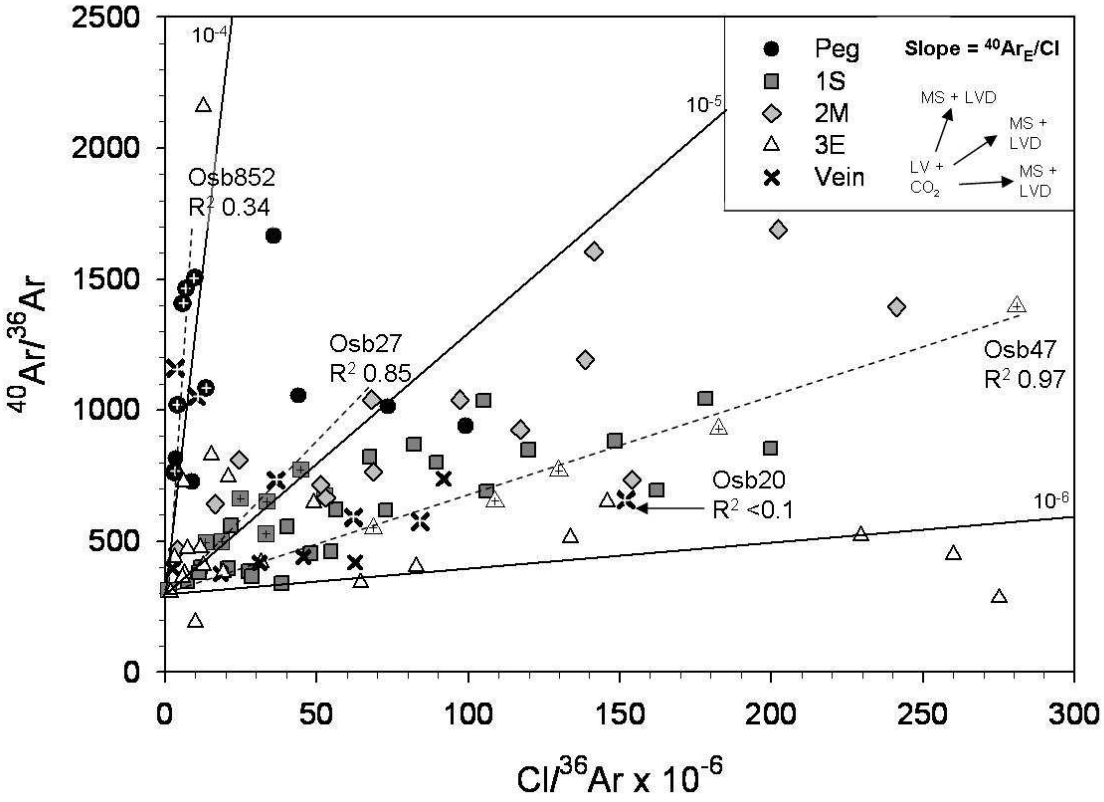

Figure 3.5: $Cl/^{36}Ar$ versus $^{40}Ar/^{36}Ar$: values measured by stepped heating between 200 and 1600°C. Sample data points define mixing arrays between extraction steps with low $Cl/^{36}Ar$ values, dominated by CO_2 and LV fluid inclusions, and extraction steps with high $Cl/^{36}Ar$ values, dominated by high salinity LVD and MS fluid inclusions (see inset). Abbreviations: LV – liquid-vapour; MS – ultra-high salinity multi-solid fluid inclusion; LVD – high salinity liquid-vapour-daughter fluid inclusion; CO_2 – liquid CO_2 fluid inclusion. Samples with indicated R^2 values are denoted by cross-hairs (see text). R^2 values for samples from the 1S ore body are >0.82 and for the 2M and 3E ore bodies fall in the range 0.55-0.97. The pegmatites and late vein samples do not show the same pattern with R^2 values below 0.34 with sample Osb20 having R^2 <0.10. The highest $^{40}Ar/^{36}Ar$ remain lower than 2000 and were measured in samples from the 2M ore body and pegmatites. The pegmatite samples show an intercept above the atmospheric value of 296 (~700).

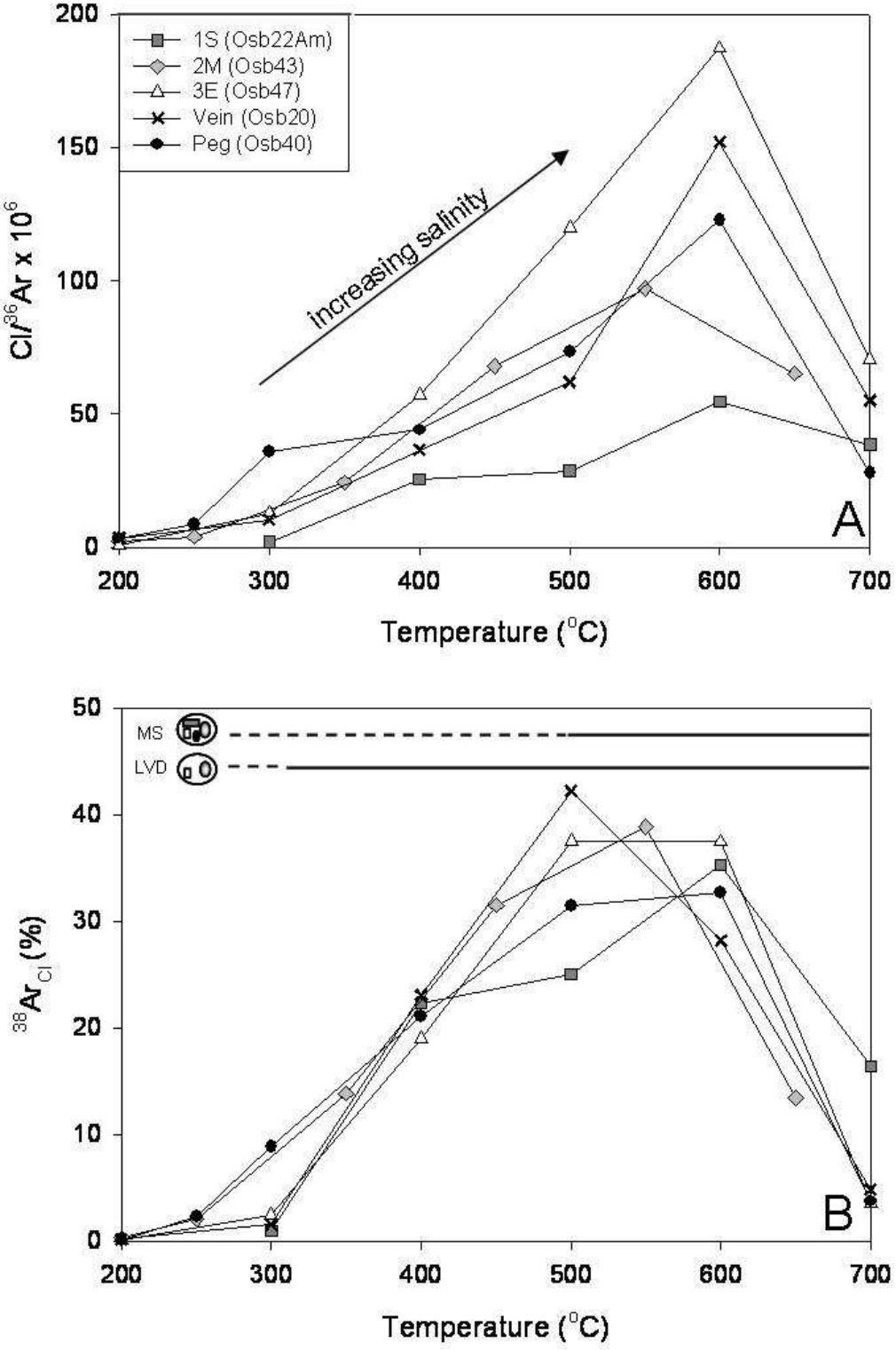

Fig 3.6: Volatile release during step heating
A: $Cl/^{36}Ar$ versus temperature. The up temperature increase in $Cl/^{36}Ar$ values (to 600 °C) is related to the preferential decrepitation of the highest salinity fluid inclusions at high temperature. The decrease above 650 °C is explained by a minor atmospheric contaminant which is more significant in low gas volume extraction steps (see b).
B: The proportion of $^{38}Ar_{Cl}$ released at 200-700 °C. In the majority of samples most fluid inclusions have decrepitated by 500-600 °C.

has an apparent age of ~1350 Ma (Fig 3.4) indicating post-crystallisation Ar-loss, an initial $^{40}Ar/^{36}Ar$ value cannot be calculated.

3.3.3 Fluid inclusion argon

Fluid inclusions in most ore-related quartz and pegmatite samples have maximum $^{40}Ar/^{36}Ar$ values of just 740-1700 (Table 3.5). The maximum $^{40}Ar/^{36}Ar$ value determined in this study, of 1983 ± 13 for an ore-related sample (Osb47), is slightly lower than the maximum value of 2236 determined for this deposit previously (Kendrick et al., 2006a; Table 3.5; Fig. 3.5). The age-corrected fluid inclusion $^{40}Ar/^{36}Ar$ values are shown plotted against $Cl/^{36}Ar$ in Fig 3.5.

The highest $Cl/^{36}Ar$ values for each sample tend to be determined in high temperature extraction steps where the high salinity LVD and MS fluid inclusions were preferentially decrepitated (Fig. 3.6a). Extraction steps dominated by Cl-poor CO_2 and LV fluid inclusions are characterised by lower $Cl/^{36}Ar$ values (Fig. 3.5; 3.6). When the high salinity fluid inclusions have the highest $^{40}Ar/^{36}Ar$ values a positive correlation results in $Cl/^{36}Ar$ versus $^{40}Ar/^{36}Ar$ space (e.g. sample Osb 47; Fig. 3.5). When the LV or CO_2 fluid inclusions have the highest $^{40}Ar/^{36}Ar$ values a negative correlation results (e.g. sample Osb20; Fig. 3.5). However, the relatively small range of $^{40}Ar/^{36}Ar$ determined for fluid inclusions in Osborne samples indicates that all of the different fluid inclusion types CO_2, LV, LVD and MS have similar $^{40}Ar/^{36}Ar$ values of less than ~2000 (Fig. 3.5).

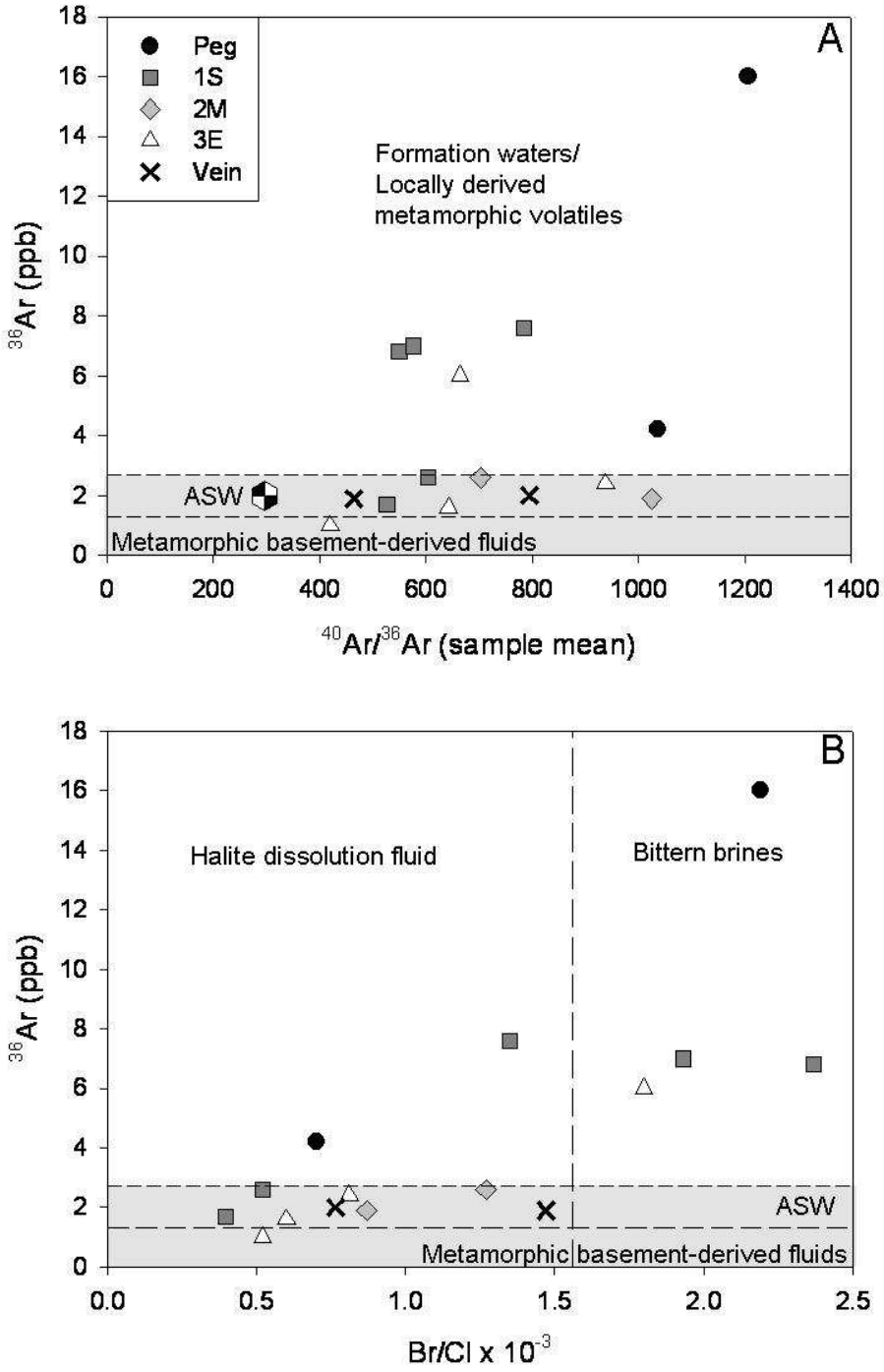

Figure 3.7: ^{36}Ar systematics in the Osborne Samples.

- *A. Lowest ^{36}Ar concentrations correlate with lowest Br/Cl signatures, further evidence that the evaporitic halogen signature is associated with a meteoric, surface derived fluid;*
- *B. Two trends are observed. The majority of data have low ^{36}Ar concentrations while a small group of samples from the 1S and pegmatite sample groups have higher ^{36}Ar concentrations which positively correlate with $^{40}Ar/^{36}Ar$ values.*

Sedimentary formation water and metamorphic fluid fields are shown for reference. Basement-derived metamorphic fluids are likely to have ASW or lower ^{36}Ar concentrations with ASW = Air Saturated Water (meteoric or seawater) with 1.3-2.7 ppb ^{36}Ar. Basement derived metamorphic fluid field based upon data from Mt Isa (Kendrick et al., 2006b).

A minor atmospheric contaminant is present in most samples and explains the decrease in $Cl/^{36}Ar$ between 600 and 700 °C shown by some samples (Fig. 3.6). This contaminant can slightly reduce measured $^{40}Ar/^{36}Ar$ values but is only significant in low gas volume extraction steps (Fig. 3.6), its main effect is to reinforce positive correlations in $Cl/^{36}Ar$ versus $^{40}Ar/^{36}Ar$ space and increase the scatter of negative correlations (Kendrick et al., 2007; i.e. Osb20 r^2 <0.1; Fig 3.5).

3.3.3.1 Argon concentrations

The ^{36}Ar concentration has been calculated from the mean salinity of MS fluid inclusions (see Chapter 2) and the sample maximum $Cl/^{36}Ar$ value (Table 3.5). Ore-related samples contain MS fluid inclusions with ^{36}Ar concentrations of 0.7 – 6.2 ppb, in most cases equal to or higher than air saturated water (ASW = 1.3-2.7 ppb; Fig. 3.7). The pegmatite sample Osb40 contains MS fluid inclusions with similar ^{36}Ar concentrations of ~2.9 ppb whereas sample Osb852 contains MS fluid inclusions with a significantly higher concentration of 21.3 ppb ^{36}Ar (Fig. 3.7). The ^{36}Ar concentration is not strongly correlated with either the $^{40}Ar/^{36}Ar$ or the Br/Cl value, although the highest ^{36}Ar concentrations are calculated for fluid inclusions with the highest Br/Cl values (Fig. 3.7).

The $^{40}Ar_E$ concentration has been calculated from the mean salinity of MS fluid inclusions and the mean $^{40}Ar_E/Cl$ values (Table 3.5). The $^{40}Ar_E/Cl$ values are given by the slopes in Fig 3.5 and range from 10^{-6} in sample Osb37B up to ~2×10^{-4} in sample Osb852. MS fluid inclusions in ore- related samples have $^{40}Ar_E$ concentrations of 0.7-15.2 ppm, while the pegmatite sample Osb852 contains fluid inclusions with elevated concentrations of 64.4 ppm $^{40}Ar_E$ (Table 3.5).

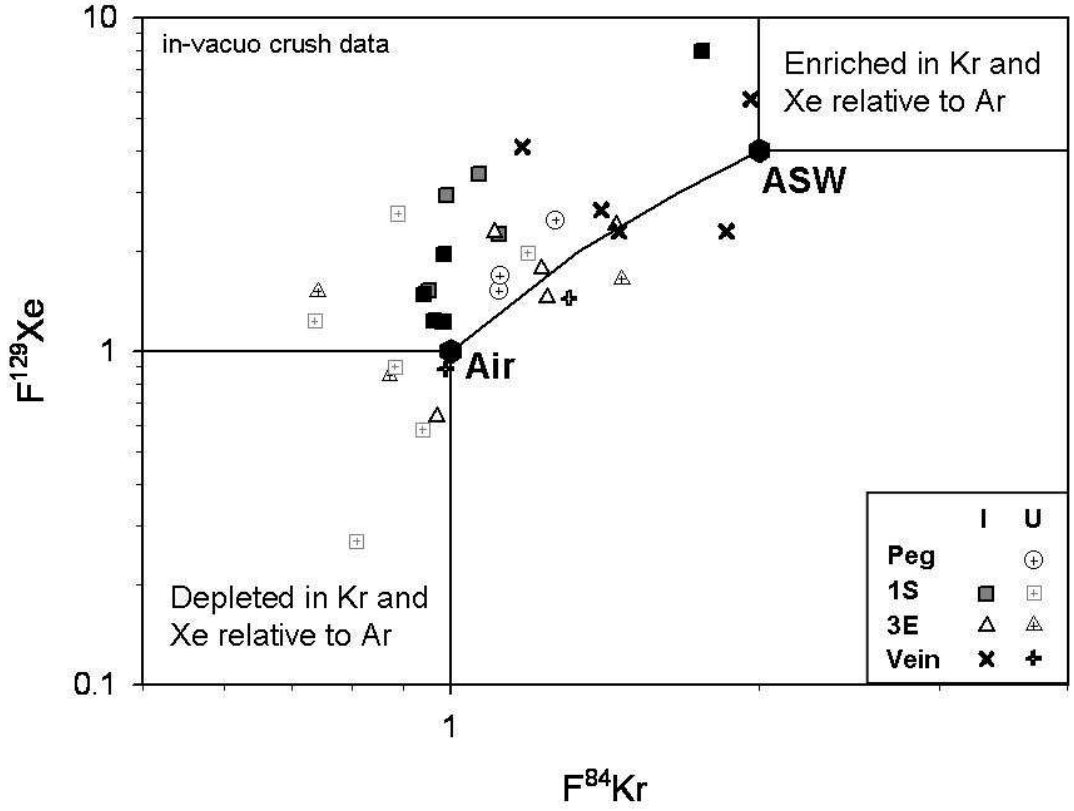

Figure 3.8: $F^{84}Kr$ versus $F^{129}Xe$ determined by in-vacuo crushing of irradiated and unirradiated samples.
The $^{84}Kr/^{36}Ar$ versus $^{129}Xe/^{36}Ar$ values are expressed as fractionation values where air has an F-value of 1. Data obtained by in-vacuo crushing of irradiated (I) and unirradiated (U) samples. The majority of data lie between the Air and air saturated water (ASW) values, consistent with mixing fluid inclusions ASW and modern air. The slightly higher F-values obtained from irradiated samples are explained by the presence of fissionogenic ^{129}Xe and to a lesser degree ^{84}Kr (see text).

3.3.4 Noble gas non-fractionation

The fluid inclusion ratios of $^{84}Kr/^{36}Ar$ and $^{129}Xe/^{36}Ar$, measured by *in vacuo* crushing irradiated and non-irradiated samples, are given relative to the atmospheric ratios as fractionation-values (F-values) in Fig. 3.8 (where air has an F value of 1). These data plot between the values of air and air saturated water (ASW) (Fig. 3.8) similar to fluids from other ore deposits and mid-crustal rocks (e.g. Drescher et al., 1998; Kendrick et al., 2001; 2002, 2007). The lack of F-values significantly outside of the air-ASW range provides little evidence for the kind of fractionation and Ar-loss that can occur during phase separation (cf. F-values from Bingham Canyon; Kendrick et al., 2001).

Fissionogenic $^{134}Xe_U$ was preferentially released during stepped heating, indicating that U present at the ppb level is hosted by the quartz matrix (Table 3.5). As a result F-values obtained by stepped heating irradiated samples are not reported here because they are elevated by fissionogenic $^{129}Xe_U$ and $^{84}Kr_U$ and can not be considered representative of the fluid composition.

3.4 Discussion

Ore-related fluid inclusions at Osborne have variable Br/Cl and I/Cl values (Fig 3.4) that are similar to regional albitisation fluids and Starra and Ernest Henry ore fluids (Williams et al., 2001; Kendrick et al., 2006b; 2007). The broad range of Br/Cl and I/Cl values, the low $^{40}Ar/^{36}Ar$ value of ~2000 and the ~1595 Ma near peak metamorphic age (Gauthier et al., 2001) of mineralisation, which predates the emplacement of the Williams-Naraku batholiths, are all inconsistent with a magmatic fluid being a

significant component of the ore forming fluids at Osborne, therefore contributions from other fluid sources must be identified and evaluated.

3.4.1 Absence of magmatic fluids

Many models for mineralisation in the Eastern Fold Belt IOCG deposits invoke a wholly magmatic origin for the high salinity and CO_2-bearing fluids observed (Perring et al., 2000; Pollard, 2001; Mark et al., 2004; Pollard, 2006) although alternative salinity sources have been considered at the Starra and Ernest Henry deposits (Williams et al., 2001; Mark et al., 2005). The $^{40}Ar/^{36}Ar$ values of 500-2000 at Osborne are similar to values measured in fluids identified as of magmatic origin in porphyry copper deposits (Kendrick et al., 2001) as well as in sedimentary formation waters (Böhkle and Irwin, 1992a; Kendrick et al., 2002).

Previous analyses of two samples from Osborne (Kendrick et al., 2006a) interpreted the similarity of $^{40}Ar/^{36}Ar$ values measured in those samples (<2200) with those found in PCD porphyry fluids as evidence for a potential magmatic fluid input at Osborne. A more recent study at the Ernest Henry IOCG deposit identified evidence for a magmatic fluid with Br/Cl values of 1-2 $\times 10^{-3}$ and $^{40}Ar/^{36}Ar$ of ~29,000 which mixed with a second fluid with lower Br/Cl values of ~ 0.4 $\times 10^{-3}$ and $^{40}Ar/^{36}Ar$ of less than 2500, interpreted as being a sedimentary formation water that had dissolved halite (Kendrick et al., 2007). Low Br/Cl values have also been measured at in ore forming fluids at Ernest Henry by PIXE, with individual fluid inclusions having molar Br/Cl values less than 1.3 $\times 10^{-3}$ and in some cases less than 0.5 $\times 10^{-3}$ (Mark et al., 2005). The highest $^{40}Ar/^{36}Ar$ value identified at Ernest Henry is an order of magnitude greater than those at

Osborne and the porphyry copper deposits and is similar to values of ~40,000 measured in MORB mantle (Burnard et al., 1997).

Porphyry copper deposits form at depths of less than 2km (Titley and Beane, 1981) while the Cloncurry district IOCG ore deposits are typically estimated to have been deposited at depths greater than 5km (Williams et al., 2005). In porphyry copper deposits mineralisation is associated with brecciated porphyritic stocks and the fluid inclusion assemblage associated with mineralisation shows evidence for phase separation; with varying degrees of vapour fill and the coexistence of high salinity brine and low density aqueous inclusions (Roedder, 1971; Nash, 1976). ^{36}Ar concentrations measured in porphyry copper deposits are as low as ~0.2 ppb (Irwin and Roedder, 1995; Kendrick et al., 2001) and $^{129}Xe/^{36}Ar$ and $^{84}Kr/^{36}Ar$ values show evidence of significant fractionation of Ar relative to Kr and Xe (Kendrick et al., 2001). Thus the low $^{40}Ar/^{36}Ar$ values measured in the fluids can be attributed to the loss of Ar from the magmatic fluids during boiling and subsequent overprinting of the $^{40}Ar/^{36}Ar$ signature by mixing with small amounts of meteoric or connate fluids (Kendrick et al., 2007).

The fluid identified as magmatic-derived at Ernest Henry has ^{36}Ar concentrations of 3-6 ppb. Therefore, the higher $^{40}Ar/^{36}Ar$ values of ~29,000 preserved in the Ernest Henry fluids are those that would be predicted for a magmatic fluid in the Cloncurry district. The Osborne fluids have low $^{40}Ar/^{36}Ar$ values of <2000 but the range of ^{36}Ar concentrations measured in the fluid inclusions is similar, 1-6 ppb, to the range measured at Ernest Henry (Kendrick et al., 2007). This suggests that the lower $^{40}Ar/^{36}Ar$ values measured at Osborne are not a product of fractionation and Ar loss, a conclusion which is supported by the fractionation values measured in the unirradiated

samples (Fig. 3.8). To date, significant fractionation of noble gas isotopes has not been identified at any Cloncurry IOCG deposit studied (Kendrick et al., 2006a; 2007). As the separation of a CO_2 phase from a carbonic brine is inferred at Osborne (Chapter 2), and has been invoked elsewhere in the Cloncurry district as a brecciation mechanism (Oliver et al., 2005), the lack of fractionation suggests that the noble gases must partition strongly into the brine phase or that the phase separation did not result in fractionation. This may be a function of the higher pressure and temperature conditions at which these processes occurred relative to those of boiling in porphyry copper systems (see Chapter 2; Roedder, 1971; Nash, 1976). There has been no examination of noble gas partitioning between brine and CO_2 phases but partitioning of noble gases between phases is a function of the density and relative volumes of the phases (Ballentine et al., 2002). So the relatively similar densities of the brine (1.0-1.3 g/cc) and carbonic phases (0.6-0.98 g/cc), as calculated from microthermometric data, may have precluded significant fractionation.

Based on the Ar data, the proportion of any fluid with a magmatic-like Ar signature that mixed with meteoric water (or high salinity halite dissolution water with atmospheric $^{40}Ar/^{36}Ar$) at Osborne can be estimated using equation 1 and the probable Ar-composition of the fluid end-members.

$$\frac{meteoric}{magmatic} = \frac{^{40}Ar/^{36}Ar_{magmatic} - 296}{^{40}Ar/^{36}Ar_{\max.measured} - 296} \times \frac{[^{36}Ar]_{magmatic}}{[^{36}Ar]_{meteoric}} \qquad \text{Eq. 1.}$$

End member 1: modern day meteoric water, $^{40}Ar/^{36}Ar$ = 296 and ^{36}Ar = 1.0-1.7×10^{-6} $cm^3cm^{-3}H_2O$. End member 2: magmatic fluid similar to that detected at Ernest Henry, $^{40}Ar/^{36}Ar$ ~29,000 and ^{36}Ar = 2.2×10^{-6} $cm^3cm^{-3}H_2O$ (Kendrick et al., 2007).

Based on these assumptions a mixing ratio of 23 parts meteoric water (or high salinity halite dissolution water) to 1 part magmatic fluid is calculated. If the $^{40}Ar/^{36}Ar$ value of the magmatic fluid end-member is reduced to an improbably low value of 10,000 (MORB mantle value is 40,000; (Burnard et al., 1997)) the calculated mixing ratio is lowered to 7:1 meteoric:magmatic.

The Ar-data and the high salinity of the magmatic-like fluid inclusions can only be reconciled with the significant involvement of a magmatic fluid if the Ar-isotope composition of the magmatic fluid at Osborne was significantly different to that of the magmatic fluid identified at Ernest Henry and used in the above calculation. A low ^{36}Ar concentration could have resulted if a magmatic fluid at Osborne had a significantly different devolatilisation history to the one identified at Ernest Henry. However, the F values are not consistent with gaseous fractionation (Fig. 3.8) with the $F^{84}Kr$ and $F^{129}Xe$ values between 1 and 10 measured at Osborne low compared with values in excess of 90 at Porphyry Copper deposits where phase separation and fractionation are documented (e.g. Kendrick et al., 2002). Furthermore, the measured ^{36}Ar concentrations do not support the substantial loss of ^{36}Ar required in the above scenario and suggest a magmatic fluid component was not significant in the Osborne ore fluids.

A simpler scenario may involve mixing of two crustal fluids in the absence of a magmatic component where one fluid would have evolved by the dissolution of halite and the other fluid would have had a composition similar to bittern brines. If these fluid end-members had recently been in equilibrium with the atmosphere and had only a short residence time in the crust, the $^{40}Ar/^{36}Ar$ values of <2000 can be accounted for without invoking a separate component of meteoric water.

3.4.2 Formation waters versus metamorphic fluid

The ore-related fluid inclusions have variable Br/Cl and I/Cl and low $^{40}Ar/^{36}Ar$ values that encompass ranges typical of sedimentary formation waters (Kelley et al., 1986; Böhkle and Irwin, 1992a; Kendrick et al., 2002). However, the halogen and argon composition of ore-related fluid inclusions is also similar to pegmatite-related fluid inclusions suggesting a local magmatic/metamorphic origin is also possible. The pegmatites formed as part of a peak-metamorphic assemblage and while they are magmatic in origin are locally derived from the melting of albitised gneisses. Thus fluids derived from them can be considered to be a metamorphic product. Alternately the pegmatite fluids may be considered to be pre-existing ore fluids that became entrained in the anatectic melts, accounting for the similarities.

The carbon dioxide fluid component that is abundant at the Osborne deposit, preserved in both CO_2 and CB inclusions (Chapter 2) could have either an igneous or metamorphic source (cf. Hollister, 1988; 1990; Xu and Pollard, 1999; Pollard, 2001; 2006). Given the apparent absence of an externally derived magmatic fluid component at Osborne the CO_2 can be inferred to be derived from metamorphic devolatisation. The CO_2 fluid phase has been interpreted as having unmixed from a carbonic brine (Chapter 2).

Therefore, the presence of a CO_2 fluid in the ore fluid inclusion assemblage can be construed as evidence for a metamorphic fluid at Osborne. Alternately the CO_2 could be derived from a sedimentary source, e.g. by interaction of acidic basinal fluids, equilibrated with clays, with carbonate-bearing sedimentary rocks (Carothers and Kharaka, 1980; Bottrell et al., 2001). Studying the noble gas and halogen systematics of the Osborne ore fluid allows evaluation of metamorphic- and sedimentary-derived components to the fluids.

Crustal fluids can have extremely variable $^{40}Ar/^{36}Ar$ values from 300-1500 in sedimentary brines in the shallow crust (Kendrick et al., 2002), up to values of 8000-15,000 or higher where they have interacted with K-rich basement rocks (Kendrick et al., 2005; 2006b). Deeper fluids are likely to have had even higher $^{40}Ar/^{36}Ar$ values because ^{40}Ar is released to the fluid more efficiently at higher temperatures and because deeper fluids tend to be older and come into contact with older basement rocks. Metamorphic dehydration fluids probably have a maximum $^{40}Ar/^{36}Ar$ value of ~100,000, as do Archean pegmatites formed during crustal anatexis (Damon and Kulp, 1958). However, they may have lower values of just thousands or tens of thousands if formed from sufficiently young rocks (Kendrick et al., 2006b).

3.4.2.1 Metamorphic $^{40}Ar/^{36}Ar$ of pegmatites

The pegmatites at Osborne both cross-cut and are overprinted by the ore zones suggesting they were emplaced over a period bracketing mineralisation and close to peak metamorphic conditions (although some of the later pegmatites may be associated with Williams-Naraku magmatism). Fluids trapped in pegmatites by anatexis have been shown to contain volatiles (N_2) which may have been derived from the protolith

metasedimentary rocks (Chapter 2), suggesting that the noble gases and halogens in the fluids can also be considered representative of locally derived volatiles. The pegmatite samples have $^{40}Ar/^{36}Ar$ values of ~1500 and ^{36}Ar concentrations of 2.5 – 21.3 ppb. A study of the Mt Isa Cu deposit, in the Western Fold Belt, identified a fluid with $^{40}Ar/^{36}Ar$ of ~20,000 which is interpreted as being a metamorphic fluid derived from 'dry' basement rocks (Kendrick et al., 2007).

The high concentrations of ^{36}Ar (~1–6 ppb) measured at Osborne are typical of sedimentary formation waters but could also be consistent with a metamorphic fluid that evolved from a pre-existing pore fluid, or derived its ^{36}Ar content from the devolatisation of sedimentary rocks with high ^{36}Ar. The much lower $^{40}Ar/^{36}Ar$ values at Osborne are not consistent with a basement derived metamorphic fluid (see discussion above). But a metamorphic fluid could still be a significant component of the Osborne ore fluids if the fluids were derived from the local metasedimentary rocks. Fluid inclusion microthermometry indicates silica flooding took place at a minimum depth of 7km and at temperatures of 500-600 ºC, above the Ar-closure temperature of all crustal minerals.

Mineralisation at the Osborne deposit is hosted by the 1685 Ma Mt Norna Quartzite, part of the Soldiers Cap Group, which comprises amphibolites, feldspathic psammites, cummingtonite-rich schists and banded ironstones (see Chapter 1, section 1.4.2). Whole rock XRF studies suggest the psammites have an average K content of 2 wt% (~5×10^{-4} mol g^{-1}; Adshead, 1995). If the protoliths had a ^{36}Ar concentration of 1.5-5$\times 10^{-12}$ mol g^{-1} which is equivalent to the median ^{36}Ar concentration of subaerial sedimentary rocks (~3×10^{-12} mol g^{-1}; Ozima and Podosek, 2002) and assuming an age of 1700 Ma an

average $^{40}Ar/^{36}Ar$ value of 1000-2000 would be expected for fluids derived from local metamorphic devolatilisation. A calculation based on a modified form of the K-Ar decay equation (equation 2) indicates that the maximum measured $^{40}Ar/^{36}Ar$ value of ~1500 in pegmatite fluid inclusions (Table 3.5) is realistic for a metamorphic fluid formed from either the Soldiers Cap Group or the Corella Formation at 1595 Ma.

$$\left(\frac{^{40}\mathrm{Ar}}{^{36}\mathrm{Ar}}\right)_{fluid} = 296 + \frac{(\mathrm{K\ mol\ g^{-1}})_{rock}}{\left(^{36}\mathrm{Ar\ mol\ g^{-1}}\right)_{rock}} \cdot (^{40}K/K) \cdot (\lambda_e/\lambda) \cdot (e^{\lambda t_{1685\,Ma}} - e^{\lambda t_{1595Ma}}) \qquad \text{Eq. 2}$$

The lowest $^{40}Ar/^{36}Ar$ ratios measured in Osborne fluids (<2200; Figure 3.7) are similar to values measured at Eloise and in parts of the Ernest Henry IOCG deposit (Kendrick et al., 2006ab; Kendrick et al., 2007). These values are strong evidence for a surface derived fluid component for the argon. Furthermore, the fact that the many of $^{40}Ar/^{36}Ar$ values are less than half the calculated rock value (<1000), suggests that a surficial fluid must have infiltrated the deep crust without equilibration with the surrounding host rocks.

3.4.2.2 Mixed fluids

The 'early', near peak-metamorphic, timing of mineralisation at Osborne implies fluid/volatile reservoirs would have been different to those available during post-peak mineralisation in other IOCG or the unrelated Mt Isa copper deposit (see Kendrick et al., 2006ab; 2007). For example, 1) sedimentary pore-fluids could have been present in the protoliths and 'metamorphic fluids' are likely to have comprised a mixture of: i) pre-existing pore fluid; and ii) volatiles derived during dehydration. 2) Sedimentary rocks have higher ^{36}Ar concentrations than crystalline metasedimentary rocks (Ozima

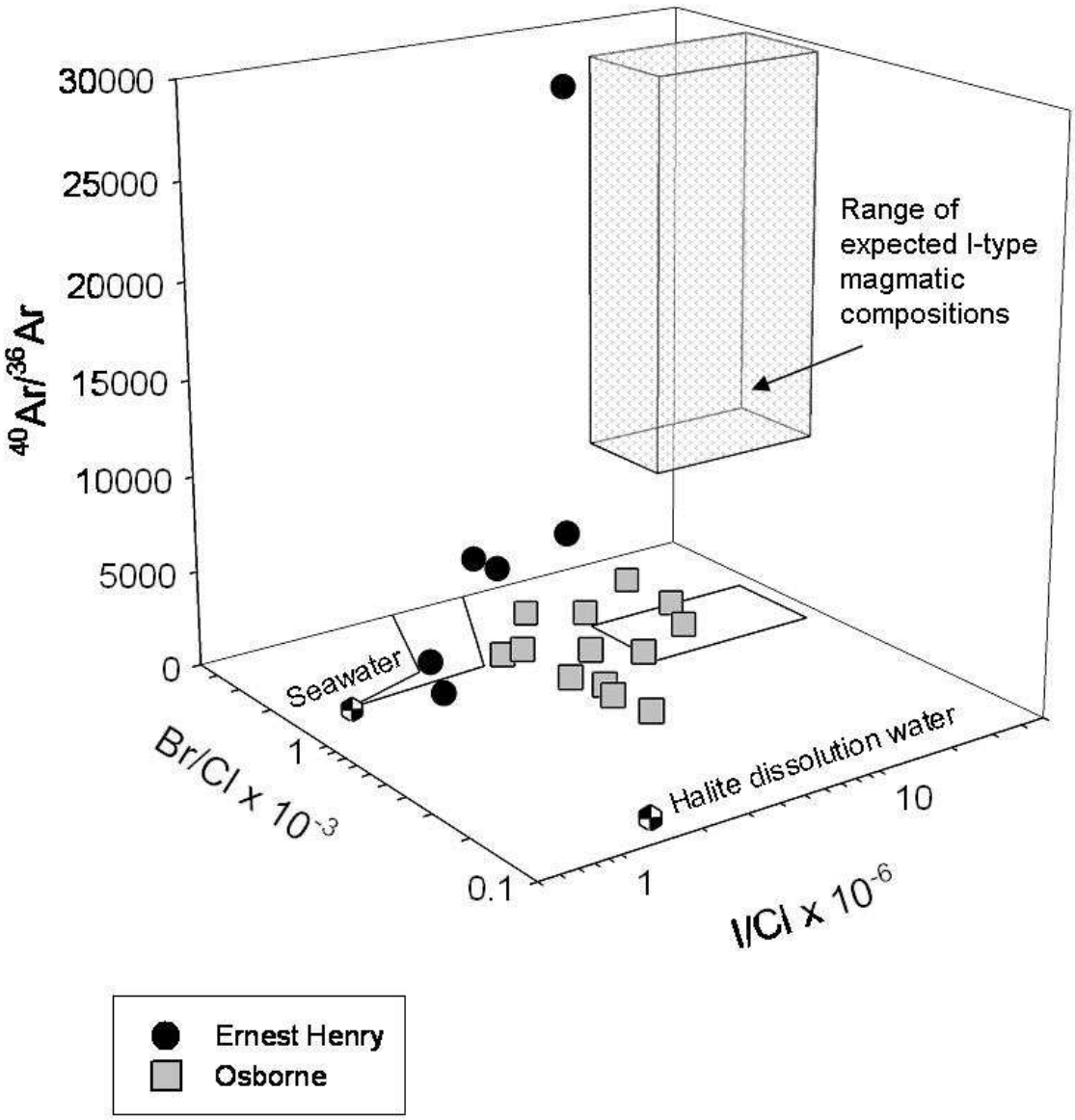

Figure 3.9: Comparison of Osborne and Ernest Henry halogen and noble gas data.
The range of Br/Cl and I/Cl values measured at Ernest Henry is similar to that at Osborne. However the much higher $^{40}Ar/^{36}Ar$ values (2500-29,000) measured at Ernest Henry are indicative of a magmatic fluid component.

and Podosek, 2002). 3) Volatiles such as CO_2 could have been easily sourced from carbonate lithologies and much of the halite in the meta-evaporitic Corella Formation was probably removed in solution.

The Br/Cl and I/Cl values determined in this study form a mixing array similar to that observed at Ernest Henry (Fig 3.9); with a low Br/Cl and I/Cl end-member that is best explained by the dissolution of halite and a second end-member that has higher Br/Cl and variable I/Cl values that are consistent with a modified seawater. The lowest Br/Cl and I/Cl values measured in the Osborne samples are slightly above those measured in a halite-dissolution fluid (Böhkle and Irwin, 1992a) and encompass a similar range to those measured in the Eloise and Ernest Henry IOCG deposits (Kendrick et al., 2006a; Kendrick et al., 2007). In all of these deposits the low Br/Cl and I/Cl values can be explained by dissolution of evaporitic rocks; interaction with halite can produce Br/Cl values of ~0.1×10^{-3} but higher values could be achieved if interaction with sylvite was significant (Fontes and Matray, 1993; McCaig et al., 2000). The coincidence of low Br/Cl and low I/Cl values at Osborne is strong evidence for interaction with evaporites and dissolution of halite is favoured as the most likely cause of low Br/Cl values at Osborne because of the proximity of the meta-evaporite bearing Corella and Staveley Formations.

The semi-bulk methodology of the combined noble gas and halogen analyses means that multiple populations of fluid inclusions are analysed at each heating step and thus it must be considered that the spread in Br/Cl and I/Cl values can be attributed to mixing between the fluids entrapped in the MS and LVD inclusions. However, examination of the data suggests this is not the case. Firstly, the intra- and inter-sample variability

(discussed in section 3.3.1.1) show distinct variation in Br/Cl and I/Cl ratios between samples even where the fluid inclusion assemblages are very similar. Secondly the ultra-high salinity of the MS inclusions mean that their compositions would dominate the measured halogens. Furthermore, fluid mixing has previously been indicated by oxygen isotope studies (Adshead, 1995). The spread in oxygen isotope values at Osborne was interpreted as being produced by mixing between metamorphic and meteoric fluids; a similar scenario to that implied by the halogen data collected in this study.

Alternative explanations for the lower Br/Cl values such as halogen fractionation due to interaction with biotite and amphibole are not favoured (see Chapter 4, section 4.4.5, for detailed discussion). Metamorphic hydration reactions can increase fluid salinity by adsorbing OH (e.g. Yardley et al., 2000; Yardley and Graham, 2002; Gleeson et al., 2003). Br/Cl variation in high grade metamorphic terranes can be a product of lowered $a H_2O$ leading to incorporation of Cl into hydrous minerals (Svensen et al., 2001). However, the upper amphibolite conditions reached during peak metamorphism would result in dehydration reactions, and even under hydration conditions because Cl can substitute for OH preferentially relative to Br or I, this process would lead to an increase in fluid Br/Cl and I/Cl values (Svensen et al., 2001) meaning it could not account for the lowest values measured at Osborne ($\sim 0.3 \times 10^{-3}$). Typical devolatisation fluids at high metamorphic grades would have a much lower salinity than measured at Osborne (e.g. Kullerud and Erambert, 1999; Kendrick et al., 2006b). A chlorine isotope study of ore fluids in IOCG deposits in the Norbotten Province of Sweden showed significant fractionation of chlorine isotopes during mineralisation ($\delta^{37}Cl$ -0.99 to -5.63) which was interpreted as resulting from the formation of Cl-rich mineral phases such as

scapolite, biotite and amphibole. However, it was noted that as Br/Cl ratios of mariolitic scapolite closely reflect the halogen content of co-existing fluids (Pan and Dong, 2003), this fractionation process would be unlikely to affect Br/Cl signatures in the hydrothermal fluids (Smith and Gleeson, 2005).

Yardley and Graham (2002) have shown that in many cases the salinity of metamorphic fluids is independent of metamorphic grade, but rather is a function of the Cl content of the protolith, due to salinity being inherited from pore fluids present prior to metamorphism. The range of Br/Cl values observed at Osborne indicates that halogen ratios may also be inherited.

The potential for remnant pore fluids and their halogen signatures to be incorporated into fluids derived from metamorphic devolatisation is called into question by studies which show several metasomatic events occurring at Osborne prior to peak metamorphism, resulting in extensive local albitisation (Rubenach, 2005b; Rubenach et al., in press). Pore fluids present in the sedimentary rocks during these metasomatic events would be expected to become entrained in the circulating fluids. Thus any contribution from pore fluids to the Osborne ore fluids would not be representative of connate sedimentary fluids, but would reflect the earlier metasomatic fluids, although it is possible that the earlier metasomatic fluids were the connate fluids.

3.4.3 Circulation of fluids at mineralisation depths

Interpretation of mineral assemblages and fluid inclusion trapping conditions suggests that the Osborne mineralisation occurred at depths greater than 7km (Chapter 2; Adshead, 1995; French, 1997). Early studies of fluid origins in the Cloncurry district relied on oxygen stable isotope data and indicated the presence of magmatic and

metamorphic fluids in the majority of IOCG deposits (Adshead, 1995; Baker, 1996; Mark et al., 2004; Marshall et al., 2006; see Chapter 1). However, it has been suggested that resetting of oxygen isotopes could have modified the original fluid signatures and that the use of isotopes of less reactive elements (e.g. noble gases) may reveal the true source of the fluids (Haynes, 2000).

The noble gas data from combined noble gas and halogen analysis indicates that at least one component of the Osborne ore fluids had a surficial origin. The 1595 Ma age of mineralisation (Gauthier et al., 2001) means that the high salinity surface derived fluids at Osborne must have infiltrated to the depth of mineralisation under conditions similar to those at the peak of metamorphism. Fluid inclusion studies give depth estimates for mineralisation of greater than 7 km. This depth is greater than 6km which is generally considered to be the limit of convective circulation (Wood and Walther, 1986).

Fluid pressure in a sedimentary basin will follow the hydrostatic pressure gradient until the collapse of the interconnected pore system causes the fluid pressure to increase until it approaches the lithostatic gradient (Wood and Walther, 1986; Fig. 3.10). The depth at which the transition from hydrostatic pressure to lithostatic pressure takes place varies substantially between basins, but generally occurs above 6km (Rubey and Hubbert, 1959). In prograde metamorphic environments fluid flow occurs due to (1) metamorphic dewatering and upward fluid flow; or (2) circulation of sedimentary formation waters or metamorphic pore fluids (Wood and Walther, 1986). In the zone where fluid pressure is under hydrostatic conditions, typically < 3km, fluids can convect and circulate, resulting in potentially high fluid:rock ratios, whereas in the zone where

fluid pressure approaches the lithostatic pressure it is thought that convection will not take place and fluid flow will be a 'single pass' event (Wood and Walther, 1986).

Kendrick et al., (in press), suggested that the saline and carbonic fluids observed regionally across the Cloncurry district were produced by metamorphic dewatering and devolatisation of the carbonate- and evaporite-bearing Corella Formation. A similar argument can be made for at least one of the fluids identified at Osborne with either the Corella or Staveley Formations potential sources of fluids and ligands. Prograde metamorphism of pelites, which are the dominant component of the Soldiers Cap Group, has been shown to produce approximately 2 moles of fluid per kilogram of rock (Walther and Orville, 1982) so locally derived metamorphic fluids could also contribute to the Osborne ore fluids. However, as evidenced by the presence of the pegmatites, Osborne is within a zone that experienced anatexis during peak metamorphism, and partial melting would be expected to have removed all the water from the system, drying out the crust, unless the melt produced was not able to migrate out of the region. This further supports the need for a fluid sourced from the pegmatites.

The naturally occurring noble gas isotopes, particularly the $^{40}Ar/^{36}Ar$ ratios, are consistent with a surface derived fluid component. While fluids with a metamorphic origin, discussed above could be considered to have flowed through the host rocks in a 'single pass' fluid pulse, convective circulation of fluids is unlikely to have occurred at the depth and pressure of mineralisation. Therefore, the presence of fluids with a surficial argon signature requires a conduit to permit fluid flow to depth, such as movement along faults or shear zones, and a mechanism for rapid circulation of surface fluids down to the depths of mineralisation must be identified. Deep drilling and

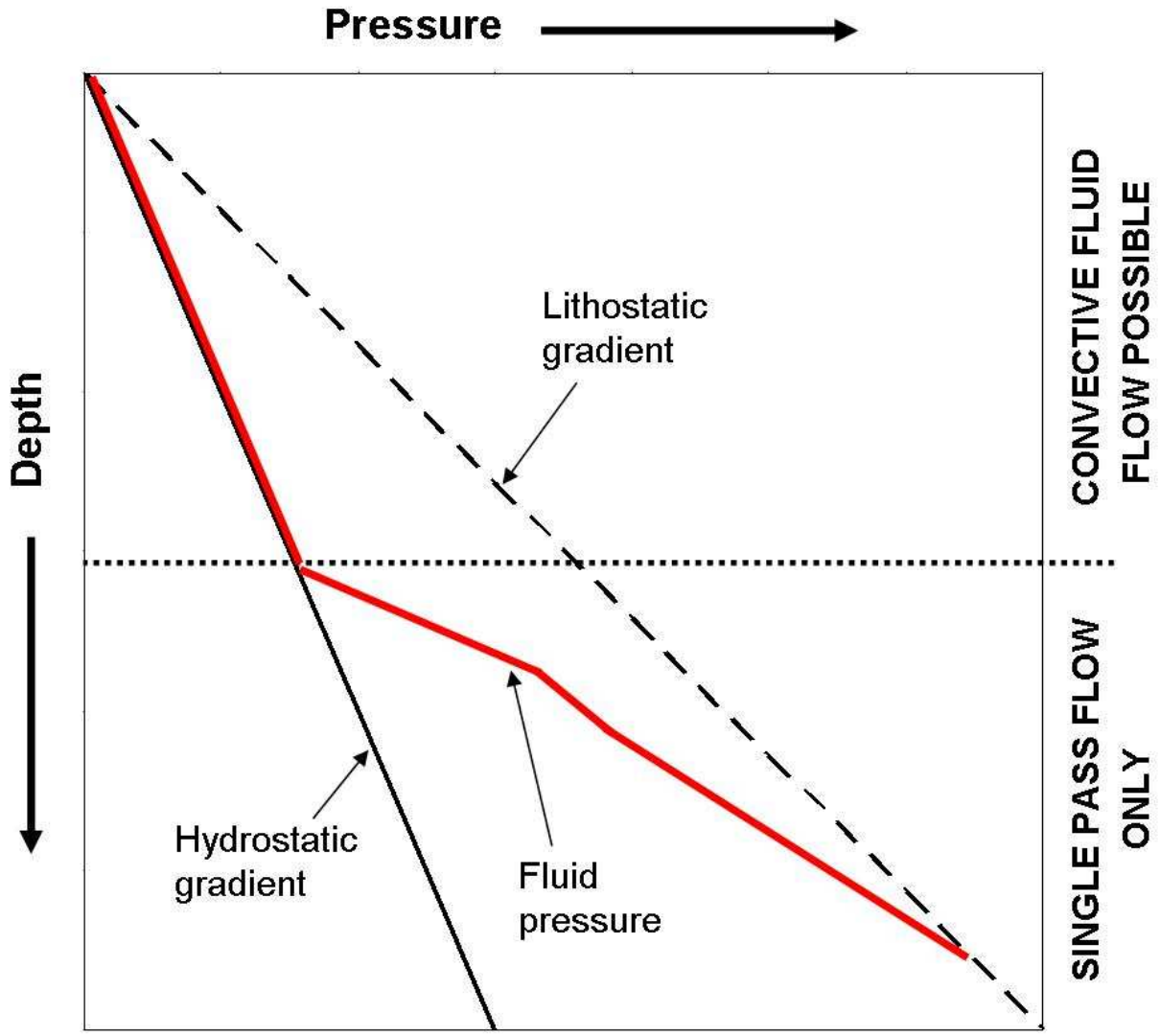

Figure 3.10: Fluid pressure as a function of depth in a sedimentary basin.
As interconnected pore systems collapse the fluid pressure moves from a hydrostatic pressure towards the lithostatic gradient. In the zone of hydrostatic pressure convective fluid flow is possible while at lithostatic pressures only 'single pass' flow is possible (after Gregory and Backus, 1980).

oxygen isotope studies have shown that surficial fluids can penetrate to depths of up to 10km in the crust. This infiltration of fluids has been documented in shear zones, around metamorphic complexes and magmatic intrusions (Möller et al., 1997; Stober and Bucher, 1999; Taylor, 1990; Wickham et al., 1993). The flow of surficial fluids to mid-crustal level and their expulsion upwards through shear zones has been documented in retrograde metamorphic environments by oxygen isotopic evidence (McCaig et al., 1990; Cartwright and Buick, 1999). More recently basinal brines have been shown to penetrate into crystalline basement with the hotter basement rocks recording episodic flow triggered by seismic events (Gleeson et al., 2003). The localisation of the Osborne deposit has been shown to be structurally controlled with the ore bodies situated in space created by dextral movement on a shear zone (McLellan, 2000). This shear zone would create pathways for fluid movement, both up and down, promoting fluid mixing.

3.5 Conclusions

The halogen and Ar data indicates at least two fluids were present during mineralisation at the Osborne deposit, with fluid mixing implicated as a potential ore deposition mechanism. A high salinity evaporite dissolution fluid is favoured as the most significant source of high salinity brines while a second fluid component is interpreted as a formation water or metamorphic brine with a bittern brine-like halogen signature. The low I/Cl signature measured in late stage quartz veins may be the result of the involvement of a third fluid or the evolution/fractionation of a mixing product.

The uniformly low $^{40}Ar/^{36}Ar$ values measured in Osborne samples are consistent with crustal fluids of surface origin that penetrated to mineralisation depths rapidly and

without equilibration with wall rocks. The low $^{40}Ar/^{36}Ar$ values are also consistent with fluids derived from metamorphism of local metasedimentary rocks.

If any fluids present had a magmatic origin it is required that Osborne lost most of its magmatic $^{40}Ar/^{36}Ar$ signature during an early phase of devolatilisation, and there is no evidence for this in noble gas ratios. The most interesting aspect of the combined Ar and halogen dataset is that a magmatic fluid is not favoured, indicating that a magmatic fluid is not an essential component of IOCG-forming systems.